Institut für Neurowissenschaften
Fakultät für Medizin der Technischen Universität München
Medical Graduate Center der TUM Graduate School

A potential cerebellar circuit and synaptic mechanism of acoustic startle response-modulation in mice revealed by harmaline-induced cerebellar tremor

Thomas Christopher Wegehaupt

Vollständiger Abdruck der von der Fakultät für Medizin der Technischen Universität München
zur Erlangung des akademischen Grades eines
Doktors der Medizinischen Wissenschaft (Dr. med. sci.)
genehmigten Dissertation.

Vorsitzender: Prof. Dr. Thomas Misgeld

Prüfer der Dissertation:
1. Prof. Dr. Arthur Konnerth
2. Prof. Dr. Markus Ploner

Die Dissertation wurde am 21.03.2019 bei der Technischen Universität München eingereicht und durch die Fakultät für Medizin am 17.07.2019 angenommen.

Institut für Neurowissenschaften
Fakultät für Medizin der Technischen Universität München
Medical Graduate Center der TUM Graduate School

A potential cerebellar circuit and synaptic mechanism of acoustic startle response-modulation in mice revealed by harmaline-induced cerebellar tremor

by
Thomas Christopher Wegehaupt

Meiner Familie gewidmet
Traugott, Isabella, Oliver

Synopsis

Significance statement

The acoustic startle response (ASR) is an important model for sensorimotor gating and habituation in mammals. Habituation is one of the most fundamental forms of implicit learning. Both the ASR and its habituation are impaired in schizophrenia, autism and other neuropsychiatric disorders. In the present thesis, a potential circuit and synaptic mechanism was identified in the cerebellum for habituation-alike ASR-modulation by harmaline-induced cerebellar tremor.

Major findings

1. Global dendritic calcium transients of Purkinje neurons co-occur with their climbing fibre synapse-evoked somatic complex spike responses
2. Acoustic startle stimulation evokes climbing fibre synapse-driven global dendritic calcium responses in Purkinje neurons of the cerebellar vermis
3. Acoustic startle stimulation-evoked calcium responses persist throughout the process of acoustic startle response habituation and despite startle suppression
4. The acoustic startle response is suppressed under harmaline-induced cerebellar tremor
5. Harmaline increases climbing fibre synapse-driven complex spikes and simultaneously suppresses parallel fibre synapse transmission-associated simple spikes in Purkinje cells
6. Acoustic startle stimulation-evoked calcium responses persist during harmaline-induced cerebellar tremor

Key words

Acoustic startle response (ASR), ASR modulation, ASR habituation, cerebellum, vermis, Purkinje neuron, harmaline, tremor, complex spike, simple spike, dendritic calcium signal, two-photon calcium-sensitive microscopy, single-cell electrophysiology, *in-vivo* stimulation

Abstract

The acoustic startle response (ASR) constitutes a defensive reaction to threatening stimuli vastly abundant across animal species. Multiple neuroanatomical structures have been identified as modifiers by acting on the basic neuronal startle pathway. The cerebellar vermis has been reported to be one of them. Particular focus has been given to its role in startle habituation. Habituation is one of the most fundamental forms of non-associative learning. So far, however, no specific ASR-modulating cerebellar mechanism has been suggested.

The present thesis assessed whether acoustic startle stimulus-evoked signals are present in Purkinje neurons, the sole output of the cerebellar cortex, and how they change during the process of startle habituation. Moreover, effects of harmaline-induced cerebellar tremor on ASR behaviour and Purkinje cell neurophysiology were analysed, since harmaline disrupts intact cerebellar neurophysiology.

Using cutting-edge two-photon calcium-sensitive microscopy in awake, behaving mice, synaptically-evoked global dendritic calcium responses in Purkinje neurons could be effectively elicited by auditory stimulation both during the ASR as well as throughout the entire process of its habituation. Neuronal output, monitored by combined in-vivo single-cell electrophysiology and dendritic calcium imaging, confirmed their climbing fibre synapse-derived origin by co-occurrence of characteristic complex spikes. Remarkably, harmaline-induced cerebellar tremor suppressed the ASR at comparable levels as previous 1Hz-high-frequency stimulation-induced habituation. Harmaline-associated changes in Purkinje neuron activity were increased complex spike count with simultaneous suppression of parallel fibre-associated simple spikes. Dendritic calcium signals evoked by auditory stimulation, however, persisted under harmaline-induce cerebellar tremor.

In summary, persistence of sound-evoked climbing fibre-input together with impaired parallel fibre-transmission has been identified as a potential circuit and synaptic mechanism for habituation-alike ASR-modification. These are significant novel findings considering the importance of ASR-modulation as a model for sensorimotor gating and habituation in mammals. Moreover, these results might have clinical implications on diseases with cerebellar affection and ASR-deviations like schizophrenia or autism spectrum disorder. Future work ought to elucidate the underlying circuit and synaptic processes in further depth.

Table of contents

List of figures

List of tables

Unit and unit prefix directory

Units

Ω	ohm
°C	degrees celsius
A	ampere
bpm	beats per minute
B	Bel
g	gram
h	hour
Hz	hertz (cycles per second)
l	litre
m	metre
min	minute
M	molar
Pa	pascal
s	second
V	volt
W	watts

Prefixes (Metric prefixes of the International System of Units)

G	giga	10^{9}
M	mega	10^{6}
k	kilo	10^{3}
d	deci	10^{-1}
c	centi	10^{-2}
m	milli	10^{-3}
µ	micro	10^{-6}
n	nano	10^{-9}
p	pico	10^{-12}
f	femto	10^{-15}

Abbreviations

5-HT	5-hydoxytryptamine, serotonin
ACh	Acetylcholine
ACSF	Artificial cerebrospinal fluid
AMPA	α-Amino-3-hydroxy-5-methyl-4-isoxazolepropionic-acid
AMPA-R	α-Amino-3-hydroxy-5-methyl-4-isoxazolepropionic-acid receptor
ASR	Acoustic startle response
BAPTA	1,2-bis(2-aminophenoxy)ethane-N,N,N',N'-tetraacetic acid
BG	Background
BW	Body weight
$C_4H_8N_3Na_2O_5P$	Phosphocreatine disodium salt
$C_6H_{11}KO_7$	Potassium gluconate
$C_6H_{12}O_6$	Glucose
Ca^{2+}	Calcium
$CaCl_2$	Calcium chloride
Cal520AM	Cal520 acetoxymethyl ester
CF	Climbing fibre
CO_2	Carbon dioxide
CS	Complex spike
DCN	Deep cerebellar nuclei
ER	Endoplasmic reticulum
DNA	Deoxyribonucleic acid
GABA	γ-aminobutyric acid
GABA-R	γ-aminobutyric acid receptor
GC	Granule cell
GECI	Genetically encoded calcium indicator
GL	Granular layer
H_2O	Ultrapure water
HEPES	4-(2-Hydroxyethyl)-1-piperazineethanesulfonic acid
IO	Inferior olive, inferior olivary body, inferior olivary complex
i.p.	Intraperitoneally
IP3	Inositol triphosphate
IP3-R	Inositol triphosphate receptor
ISI	Inter-stimulus-interval
K_d	Dissociation constant
KCl	Potassium chloride
LTH	Long-term habituation
MAO	Monoamine oxidase
MF	Mossy fibre
MgATP	Adenosine triphosphate magnesium salt
$MgCl_2$	Magnesium chloride
mGlu-R	Metabotropic glutamate receptor
ML	Molecular layer
MLI	Molecular layer interneuron
Na_2GTP	Guanosine triphosphate sodium salt
nACh-R	Nicotinic acetylcholine receptor
NaCl	Sodium chloride
NaH2PO4	Sodium dihydrogen phosphate
NaHCO3	Sodium hydrogen carbonate
NMDA	N-methyl-D-aspartate
NMDA-R	N-methyl-D-aspartate receptor
NRPC	Nucleus reticularis pontis caudalis
n.s.	Not significant (p-value > 0.05)
NXC	Sodium-calcium exchanger
O_2	Oxygen
OGB-1 6k	Oregon Green 488 BAPTA-1 hexapotassium salt

OGB-5N	Oregon Green 488 BAPTA-5N	**s.e.m**	Standard error of the mean
OPA	Operational amplifier	**SERCA**	Sarco-/endoplasmic reticulum calcium
PC	Purkinje cell, Purkinje neuron		ATPase
PCL	Purkinje cell layer	**SG**	Spiral cochlear ganglion
PF	Parallel fibre	**SS**	Simple spike
pH	Potentia hydrogenii	**STH**	Short-term habituation
PMCA	Plasma membrane calcium ATPase	**TRPC**	Transient receptor potential channel
PN	Precerebellar neuron	**VGCC**	Voltage-gated calcium channel
ROI	Region of interest	**vol/vol**	Percentage by volume
Ry-R	Ryanodine receptors	**%**	Percent
S_0	Ground energy state	*****	P-value < 0.05
S_1	Excited energy state	******	P-value < 0.01
s.c.	Subcutaneously	*******	P-value < 0.001
s.d.	Standard deviation		

1. Introduction

1.1 Motivation – the emergent diversity of cerebellar function

The unique geometric structure of the cerebellum and its regular circuitry have fascinated neuroscientists ever since the beginning of detailed descriptions on its gross anatomy 1776 by Vincenzo Malacarne and the subsequent descriptions on its cytoarchitecture 1837 by Jan Evangelista Purkinje as well as in more detail 1894 by Ramón y Cajal (Glickstein, Strata et al. 2009). Owing to its uniformity, both in terms of cellular architecture as well as in terms of connectivity, many features of cerebellar physiology are already well-established compared to other brain structures. This makes it an excellent model for neuroscientific research. Its influence, nonetheless, reaches out ranging from theories on general neuronal computation to algorithms on supervised learning (Ito 2006, Swain, Kerr et al. 2011, Raymond and Medina 2018).

Compared to the cerebral cortex regarding function, however, the cerebellum has mainly been considered as of minor importance. It has been seen as primarily being concerned with motor tasks, such as motor control, motor coordination, motor learning and timing (Manto, Bower et al. 2012). Among the most extensively discussed (sensori-)motor tasks in the literature are control of voluntary limb movement (Ebner, Hewitt et al. 2011), timing and synchronization of motor behaviour (Harrington, Lee et al. 2004, Diedrichsen, Criscimagna-Hemminger et al. 2007), oculomotor control (Kheradmand and Zee 2011), classical conditioning of eye blink (Thompson and Steinmetz 2009), control of motor speech (Spencer and Slocomb 2007) and control of grip force (Anens, Kristensen et al. 2010).

Nonetheless, growing body of evidence from the past decades of research suggests considerable involvement in non-motor tasks (Buckner 2013). Although these functions might appear subtle, the cerebellum is reported to participate in the regulation and modulation of perceptual, behavioural, autonomic, cognitive and affective processes (Strick, Dum et al. 2009, Koziol, Budding et al. 2014).

Among the rather non-prominent functions of the cerebellum, it has been suggested to play a role in the modulation of the acoustic startle response (Leaton and Supple 1986). This will be one of the main topics of the present thesis (see section 1.3 for more information on the acoustic startle response and its habituation and chapter 2 for the scope of the present thesis).

Not surprisingly, besides well-known motor deficits following cerebellar dysfunction, e.g. in spinocerebellar ataxia or stroke, there is an increasing number of reports on further cerebellar disturbances (Bodranghien, Bastian et al. 2016). This is appreciated, for instance, in the nosology of the cerebellar affective cognitive syndrome (Schmahmann 2004). Moreover, recent evidence suggests cerebellar involvement in neuropsychiatric disorders like autism spectrum disorder (Fatemi, Aldinger et al. 2012, Shakiba 2014) or schizophrenia spectrum disorder (Shakiba 2014, Baumann, Borra et al. 2015). Future research on cerebellar physiology and function, thus, inherits the promise to shed new light on the potentially underrated complexity of this unique neuronal structure and its role in health and disease.

The present thesis assessed cerebello-cortical neurophysiology, more precisely, Purkinje neuron physiology, in context of the acoustic startle response (ASR), its habituation and its modification under harmaline-induced cerebellar tremor. In doing so, changes in ASR behaviour ought to be traced down to changes in neuronal circuits, neurons and synapses. The upcoming sections of the introduction address cerebellar neuroanatomy and neurophysiology, the ASR and its modulation, harmaline-induced cerebellar tremor as well as biophysical principles of two-photon calcium-sensitive fluorescent microscopy. This is meant to set the theoretical foundations for the presentation of results in chapter 4 and their discussion in chapter 5. The objectives and central questions are formulated in chapter 2, before introducing the *in-vivo*-methodology in chapter 3.

1.2 Basics of cerebellar neuroanatomy and neurophysiology

The cerebellum (Latin for “small brain”) is a neuroanatomical structure present in all vertebrates (Voogd and Glickstein 1998). Lying within the posterior fossa of the cranium in mammals, connection to the rest of the nervous system is made via the cerebellar peduncles which attach the cerebellum to the brainstem. From a gross anatomy point of view, the mammalian cerebellum may be divided into distinct anatomical substructures. Regularly classified, it consists most basically of two hemispheres, which are interconnected by the central vermis and its surrounding paravermal (intermediate) region. In brief, these structures, again, are subdivided into lobes and lobules via fissures. Further common categorisations relate either to the phylogenetic evolution of the cerebellum or to its crude afferent connectivity. Characteristically, the surface of the cerebellum is intensely folded in a transversely-parallel manner, shaping the so-called “folia et fissurae cerebelli” (Latin for “leafs and clefts of the cerebellum”). Underneath the meningeal surface, a grey substance is found, constituting the cerebellar cortex. Further below the cortex, a strongly-branching body of white matter represents the afferent and efferent connections to and from the cortex, shaping the so-called cerebellar “arbor vitae” (Latin for “tree of life”). Finally, within the white matter, the deep cerebellar nuclei (DCN) are embedded. Figure 1A displays an illustration of the mouse brain including the cerebellum (left panel) and the general structure of cerebellar layers (middle panel). (Voogd and Glickstein 1998, Voogd 2003, Roostaei, Nazeri et al. 2014)

Besides the basic gross anatomy, mammals - and in particular among those rodents - share a common basic cytoarchitecture (Voogd and Glickstein 1998). In general, afferent and efferent connections of the cerebellum run via the three cerebellar peduncles. The diversity of origins aside, two characteristic afferent pathways to the cerebellum may be distinguished.

Firstly, there is the climbing fibre (CF) pathway, almost exclusively originating from neurons in the inferior olivary complex (IO) within the brainstem. Secondly, there is the mossy fibre (MF) pathway, either providing signals from a multitude of extra-cerebellar sources in the brainstem and spinal cord, or feeding back signals from deep cerebellar nuclei from within the cerebellum. Neurons of the IO receive input from large parts of the central nervous system. Among others, these are neurons from the spinal cord and brainstem (e.g. from the reticular formation), but also major projections from neocortical areas. Sources of MFs originating from the brainstem include the vestibule nuclei, the reticular formation, the raphe nuclei, the nuclei ruber as well as pontine nuclei which, notably, relay information from several areas of the neocortex forming the cerebro-pontocerebellar pathway. (Voogd and Glickstein 1998, Ruigrok, Sillitoe et al. 2015)

CF as well as MF inputs transduce information to both the cerebellar cortex - in case of CFs directly, in case of MFs indirectly via parallel fibres (PFs) of granule cells, as such, forming the mossy fibre-parallel fibre pathway - and via collaterals to DCN. At DCN, the signal coincides with inhibitory Purkinje neuron (PC) projections, which constitute the sole computational output of the cerebellar cortex (detailed description below). In addition, a third pathway may be seen in modulatory monoaminergic, cholinergic and peptideric fibres reaching the cerebellum. (Voogd and Glickstein 1998, Ruigrok, Sillitoe et al. 2015)

Projections from DCN constitute the cerebellar output, with direct inhibitory projections of PCs onto vestibule nuclei being the sole exception. Whereas most connections of DCN are excitatory, projections back to the IO are usually inhibitory. Apart from the IO, DCN target large parts of the central nervous system. These include several brainstem regions, notably, abovementioned sources of MFs (e.g. pontine nuclei), but also thalamic nuclei, eventually relaying information back to neocortical areas. (Voogd and Glickstein 1998, Ruigrok, Sillitoe et al. 2015)

Taking the relation of afferent and efferent structures into account, several loops and circuits may be identified on different levels. For instance, there are feedback loops within the cerebellum among neighbouring PCs and among DCN and the cerebellar cortex. Besides, there are loops involving extra-cerebellar regions (Voogd and Glickstein 1998, Ruigrok, Sillitoe et al. 2015). One example is the olivo-cerebellar circuit, comprising of projections from the IO onto the cerebellar cortex, from the cerebellar cortex onto DCN and from there back to the IO (Chen, Kovalchuk et al. 2010, Ruigrok, Sillitoe et al. 2015). Other circuits may also involve the neocortex, as was shown for humans (Buckner 2013). Taken together, these loops might represent important regulatory units in information processing (Benagiano, Rizzi et al. 2018).

As described above, signals reaching the cerebellum via mossy and climbing fibres are processed within the cerebellar cortex. The cerebellar cortex may be divided into three distinct layers. Densely packed next to one another, somata of Purkinje cells (PC) form the shallow Purkinje cell (mono-) layer (PCL). PCs constitute the sole cerebellar cortical output. They synapse onto DCN using the inhibitory transmitter gamma-aminobutyric acid (GABA). Additionally, cell bodies of Bergmann glia are located in the PCL. (Voogd and Glickstein 1998, Ruigrok, Sillitoe et al. 2015)

Above the PCL, there is the molecular layer (ML). It consists of the planar, spiny dendritic trees of PCs, orientated parasagittal. Besides, CFs terminate in the ML. They form glutamatergic, excitatory synaptic connections with six up to ten different PC dendritic trees in the parasagittal direction. In contrast, PFs in the ML, originating from granule cells (see below), run in a transversal direction (parallel to the long axis of folia). They form a total of several hundred thousand glutamatergic excitatory synapses with neighbouring PCs. In doing so, each parallel fibre only synapses once or twice onto an individual PC. Moreover, the ML is home to GABAergic inhibitory molecular layer interneurons (MLIs), commonly separated into stellate cells and basket cells.

Together, they form an inhibitory network around PCs. Whereas stellate cells are mostly found in the upper half of the ML, where they make synaptic connections to multiple PC dendrites and other interneurons, basket cells are located rather in the lower half of the ML and closely to the somata of PCs. There, they built basket-shaped axonal connections around PC cell bodies which terminate at the PCs' initial segments (so-called "pinceaux"). Major input for interneurons derives from excitatory PF synapses. Again, dendrites and axonal processes of MLIs extend rather parasagittal. The number of MLIs, however, is estimated to exceed the number of PCs tenfold. (Voogd and Glickstein 1998, Ruigrok, Sillitoe et al. 2015)

Beneath the PCL, the granular layer (GL) comprises the vast number of small granule cells (GC). GCs impressively represent an estimated 50-80% of all neurons in the central nervous system. PFs, the axonal processes of GCs, ascend from the GL and bifurcate in the ML (see above). As such, PFs relay mossy fibre input which, again, is received in a rather parasagittal manner. Besides GCs, several interneurons may be found in the GL, such as Golgi cells, unipolar brush cells, Lugarno cells and Candelabrum cells. Figure 1B illustrates a simplified synopsis of cerebellar neuroanatomy. (Ruigrok, Sillitoe et al. 2015)

Notably, the seemingly uniform cerebellar architecture is suggested to be contrasted by differences in discrete (functional) input-output relations, by subtle differences in cortical microcircuitry as well as by differences in molecular markers and gene expression patterns. Ultimately, these could give rise to distinct organisational and functional units. For instance, input and output projections are reciprocally restricted to particular subdivisions of DCN, cerebellar cortical areas and extra-cerebellar regions (e.g. the IO), respectively. These interconnected structures are suggested to shape so-called "functional modules" (Ruigrok 2011, Witter and De Zeeuw 2015). Besides, afferent mossy and climbing fibre inputs are reported to share congruent zonal distribution in the cerebellar

cortex (Eccles, Sabah et al. 1972, Ekerot and Larson 1980). Further microzonal organisation is reported on the level of heterogeneous cerebello-cortical microcircuitry, possibly allowing for subtle differences in information processing (Cerminara, Lang et al. 2015). Finally, multiple molecular markers, such as zebrin II, characterise an additional form of zonal organisation of the cerebellar cortex (Brochu, Maler et al. 1990).

Since it is the sole output of the cerebellar cortex, the PC holds a special role in cerebellar neuroanatomy. One PC receives afferent excitatory input from only one CF, but from several hundred thousand different PFs. Both these inputs use the neurotransmitter glutamate. Besides, GABAergic inhibitory input comes from MLIs, which in turn, receive their input mostly via excitatory glutamatergic PF synapses. A simplified scheme of functional connectivity within the cerebellar cortex may be found in Figure 1A (right panel). While climbing up the proximal dendritic branches of a PC, the CF repeatedly forms synapses (several hundred), thus, creating a powerful synaptic connection. Indeed, the CF-PC synapse is one of the most powerful synapses known. Therefore, synaptic CF-input always results in a strong PC membrane depolarisation followed by a prolonged after-depolarisation. This leads to a so-called complex spike output response of the PC. In contrast, normal output responses of PCs, the so-called simple spikes, are regarded as the computational result of PF-PC synapse transmission, mostly at the distal spiny dendrites. (Eccles, Llinas et al. 1966, Ruigrok, Sillitoe et al. 2015)

There are several forms of functional plasticity present in the cerebellar cortex. This is especially true at the level of synaptic connections onto PCs, such as the PF-PC synapse, the CF-PC synapse and the MLI-PC synapse (Gao, van Beugen et al. 2012, Ruigrok, Sillitoe et al. 2015). Relevant types of synaptic plasticity regarding the present thesis are addressed in 5.4.2.

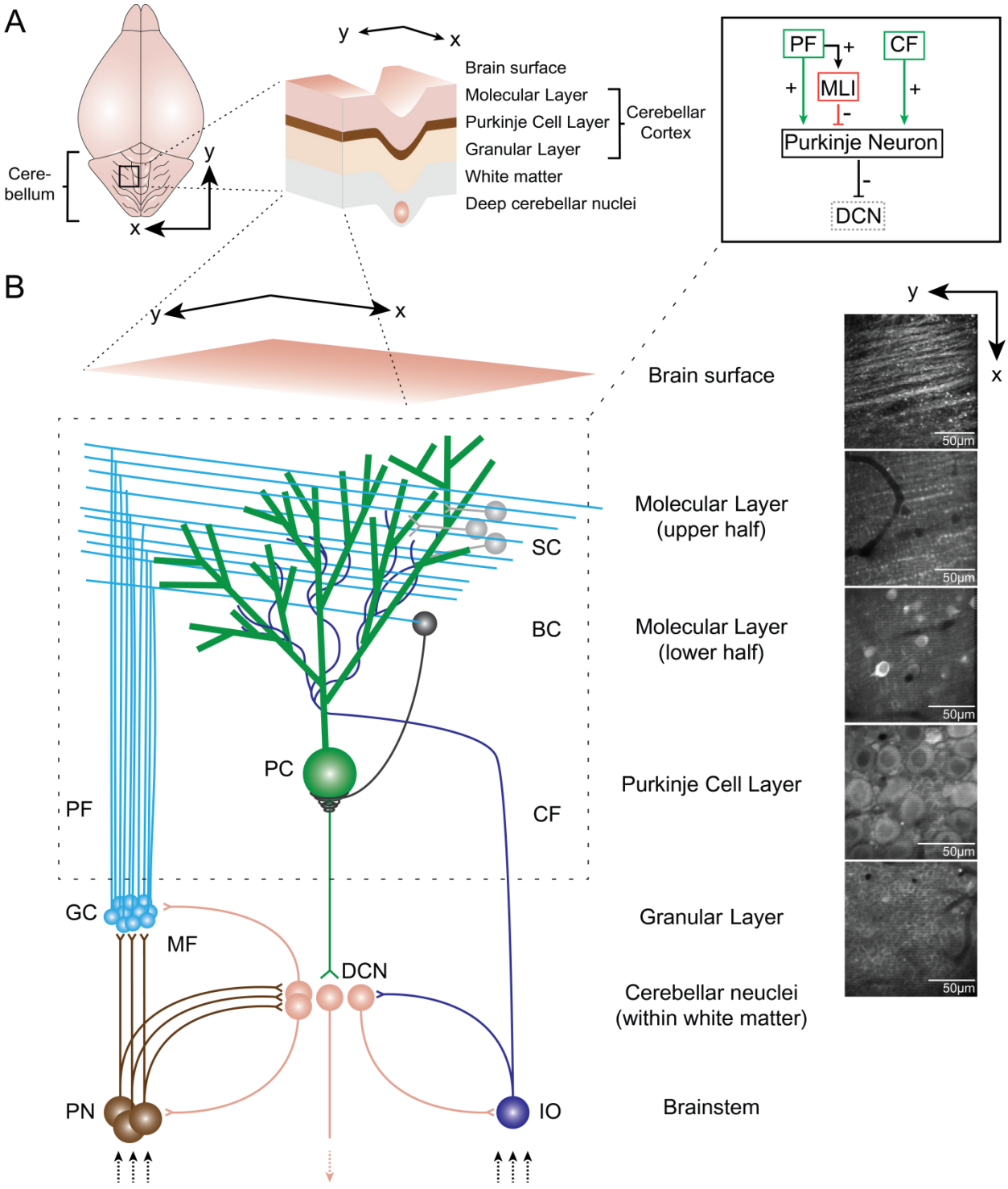

Figure 1: Basic cerebellar neuroanatomy and neurophysiology (after Ruigrok, Sillitoe et al. 2015). (A) Left: Illustration of a mouse brain from dorsal. Top: Rostral. Bottom: Caudal. Middle: Standard classification of cerebello-cortical layers. Right: Simplified scheme on functional connectivity of Purkinje neuron input and output. Parallel fibre (PF). Climbing fibre (CF). Molecular layer interneuron (MLI). Deep cerebellar neuclei (DCN). (B) Left: Schematic illustration of stereotypic cerebellar neuroanatomy. Purkinje neuron (PC). Granule cell (GC). Inferior olive (IO). Stellate cell (SC). Basket cell (BC). Precerebellar neuron (PN). Rest as in (A). Right: Representative images (xy-plane) of each cerebello-cortical layer obtained from recordings during calcium-sensitive microscopy experiments after multi-cell bolus loading.

1.3 The acoustic startle response and its modulation

The acoustic startle response (ASR) is a short-latency, defensive reaction vastly present in animals including rodents and primates (Prosser and Hunter 1936, Landis and Hunt 1939, Yeomans and Frankland 1995, Koch and Schnitzler 1997, Koch 1999, Davis, Antoniadis et al. 2008). Following an unexpected, intense and potentially harmful auditory stimulus, it is suggestive to serve for protection of vulnerable body parts by immediate eye-lid closure, stiffening of facial, neck and skeletal muscles, vegetative alert and arrest of ongoing behaviour as well as to prepare for subsequent flight or fight (Koch 1999, Yeomans, Li et al. 2002). In addition to auditory stimulation, the startle response may be evoked by several other stimuli, such as tactile, visual and olfactory (Pfeiffer 1962, Koch 1999). Besides its physiologic importance, the ASR is a widely-used, popular behavioural paradigm in basic biomedical and clinical research (Koch 1999). It has an intrinsic modulation-dependent appearance which, moreover, is susceptible for extensive experimental manipulation (Glowa and Hansen 1994, Koch and Schnitzler 1997, Koch 1999). Besides, it displays alterations under pathophysiological conditions (Braff, Grillon et al. 1992, Koch 1999, van den Buuse 2010). For instance, ASR-associated parameters are found to be altered in schizophrenia spectrum disorder (Ludewig, Geyer et al. 2003) and autism spectrum disorder (Erturk, Korkmaz et al. 2016).

As shown in rats, the suggested basic neuronal startle pathway comprises of an oligosynaptic network located in the lower brainstem projecting, eventually, to cranial and spinal motor neurons (Davis, Gendelman et al. 1982, Lingenhohl and Friauf 1994, Yeomans and Frankland 1995). Since under identical stimulation parameters equal responses are observable in both rats and humans, it is suggested that the neuronal startle pathway may be generalised from rats to humans (Koch 1999).

More precisely, the basic neuronal startle pathway consists of sensory cochlear hair cells which are connected to spiral ganglion cells whose axons form the auditory nerve transmitting information to the cochlear nuclei. Subsequently, latter pass signals on to (giant) neurons of the ventrocaudal part of the nucleus reticularis pontis caudalis (NRPC) of the reticular formation, as possibly do in a parallel fashion, several other nuclei from primary central auditory pathways. From there, cranial motor neurons, motor neurons of the brainstem as well as of the spinal cord are targeted, e.g., via the reticulospinal tract in the medial longitudinal fasciculus. Finally, these motor neurons form neuromuscular junctions with effector muscles. Additionally, spinal interneurons may be interposed. (Davis, Gendelman et al. 1982, Yeomans and Frankland 1995, Koch 1999)

Notably, multiple structures extrinsic to the basic startle pathway project onto the NRPC (Lingenhohl and Friauf 1994). Therefore, the NRPC is regarded as a sensorimotor interface susceptible for modulation (Lingenhohl and Friauf 1994). Figure 2 summarises the fundamental acoustic startle pathway (left box).

Interestingly, the ASR magnitude in mammals has a none-zero-baseline, i.e., its response amplitude is plastic and may be modulated positively or negatively depending on environmental or experimental conditions (Koch 1999). For example, fear-potentiation and sensitisation increase the startle magnitude (Koch and Schnitzler 1997, Koch 1999). In contrast, the startle response is reduced by pre-pulse-inhibition, pleasure-attenuation and different types of habituation (Koch and Schnitzler 1997, Koch 1999). In this respect, several neuroanatomical structures have been suggested as mediators of ASR-modulation by acting on the basic neuronal startle pathway. For example, extrinsic ASR-modulation is reported for the amygdala (Koch and Ebert 1993, Fendt, Koch et al. 1994), the inferior (Leitner and Cohen 1985, Li and Yeomans 2000) and superior colliculi (Fendt, Koch et al. 1994, Li and Yeomans 2000), the periaqueductal grey (Borszcz,

Cranney et al. 1989), cortical areas (Groves, Wilson et al. 1974) and the medial cerebellum (Leaton and Supple 1986). Importantly, these extrinsic structures might project to the NRPC which has been suggested to serve as the central integrator within the startle pathway in this context. Among its extrinsic afferents are axonal projections from deep cerebellar nuclei (DCN), which means, the cerebellum has a potential anatomic connection to the startle pathway (Teune, van der Burg et al. 2000). Notably, besides external modulation, the ASR is also regulated intrinsically, as is described further below (Weber, Schnitzler et al. 2002, Simons-Weidenmaier, Weber et al. 2006, Zaman, De Oliveira et al. 2017). For the purpose of the present thesis, a focus will be primarily given to the negatively-modulating effect of habituation.

Habituation is the most fundamental form of non-associative, procedural learning during which an organism reduces or ceases an initial response to a specific stimulus after repetitive stimulus occurrence, hence, allowing for adaption and selective attention to biologically relevant information (Harris 1943, Thompson and Spencer 1966, Koch 1999). Besides response decrement, several other important features characterise habituation, such as spontaneous recovery upon stimulus withdrawal or the phenomenon of dishabituation upon stimulus deviations (Thompson and Spencer 1966). In 2009, the definition of habituation was revised and was extended to a total of ten characteristics (Rankin, Abrams et al. 2009). Notably, the dual-process theory (Groves and Thompson 1970) supposes two opposing mechanisms independently occurring at the same time to the given stimulus, i.e., habituation and sensitisation. Effective habituation is, thus, understood as a net result of both processes. Being important for sensory filtering and, thus, for attention and cognition, disturbances of habituation are associated with neuropsychiatric disorders like schizophrenia spectrum disorder (Ludewig, Geyer et al. 2003).

Extensive investigation on the neuronal basis of habituation has been carried out in invertebrates, such as in the sea slug *Aplysia* (Castellucci, Pinsker et al. 1970, Kandel 2001). Whereas many aspects of habituation have been addressed in invertebrates, much of the neuronal basis of habituation in mammals is still largely unsolved. It is commonly anticipated to rely on forms of plasticity in complex polysynaptic circuits, for instance, synaptic plasticity like N-methyl-D-aspartate-receptor-mediated long term potentiation (Bliss and Gardner-Medwin 1973, Bliss and Collingridge 1993, Malenka and Nicoll 1993, Koch and Schnitzler 1997). The identity of habituation-specific circuits and mechanisms, however, remained mainly unknown (Ramaswami 2014). Therefore, models of habituation in mammals accessible both in terms of experimental manipulability and in terms of interpretational potential based on known underlying neuronal circuitry are rare, yet all the more, availability is of major interest (Koch and Schnitzler 1997).

Habituation of the ASR is a prototypic behaviour in mammals which might fulfil these needs (Lingenhohl and Friauf 1994, Koch and Schnitzler 1997). It embraces the reduced startle response amplitude to repeated auditory stimuli that is not otherwise attributed to effector muscle fatigue or adaptation of sensory receptor responsiveness (Prosser and Hunter 1936, Harris 1943, Koch 1999). Frequently, short-term habituation (sometimes simply termed “habituation”), i.e., a decline of startle to repetitive stimulation within one test session is contrasted to long-term habituation, a pronounced decrease over the course of multiple sessions which can last for days, weeks or even longer (Koch 1999).

Synaptic depression intrinsic to the basic startle pathway is considered to account for the process of short-term habituation (Lingenhohl and Friauf 1994, Pilz and Schnitzler 1996, Koch 1999, Weber, Schnitzler et al. 2002, Simons-Weidenmaier, Weber et al. 2006, Zaman, De Oliveira et al. 2017) . For the process of long-term habituation several structures extrinsic to the startle pathway

have been suggested to be relevant. These include the ventral periaqueductal grey (Borszcz, Cranney et al. 1989), the mesencephalic reticular formation (Jordan and Leaton 1983), different cortical regions (Groves, Wilson et al. 1974) and the cerebellar vermis (Leaton and Supple 1986, Lopiano, de'Sperati et al. 1990, Leaton and Supple 1991).

Taken together, the cerebellar vermis is suggested to be a relevant neuronal structure in context of ASR-modulation. On the one hand, it is a promising candidate since there are neuroanatomical interconnections manifest among (para-)vermal areas and central auditory pathways. For instance, cerebellar regions, such as lobule VI of the vermal cortex and deep cerebellar nuclei (DCN), reive signals from neurons in the cochlear nuclei, the inferior colliculi and other central auditory sites (Snider and Stowell 1944, Altman, Bechterev et al. 1976, Huang, Liu et al. 1982, Huang and Liu 1985). In turn, DCN synapse on neurons of the basic acoustic startle pathway, such as on neurons of the NRPC (Teune, van der Burg et al. 2000), a major site of sensorimotor integration in this pathway, as described above. On the other hand, functional imaging studies additionally confirm an auditory task-associated activation of cerebellar cortical areas, again including the vermis (Petacchi, Laird et al. 2005, Pastor, Vidaurre et al. 2008, Baumann and Mattingley 2010). Moreover, previous lesion-studies suggest an involvement of the cerebellum particularly in the long-term habituation of the ASR (Leaton and Supple 1986, Lopiano, de'Sperati et al. 1990, Leaton and Supple 1991). Although once again mostly drawing special attention to the cerebellar vermis, the specific intra-cerebellar processes remain unclear. While many authors emphasise a role in long-term habituation, the exact function of the cerebellum in ASR-modulation might be, however, more elusive. Different Manifestations of ASR habituation and possible functions of the cerebellar vermis in modulating the ASR are addressed again in chapter 5. The hypothetical integration of a

modulating cerebellar circuit into a more extensive acoustic startle pathway is illustrated in figure 2 (right box).

Measurements of the ASR are easily feasible and may be performed by a variety of means, e.g., by electromyography of individual muscles or as accelerometric whole-body measurements. As such, the ASR magnitude is regularly displayed in ballistograms. For more information on the method of whole-body measurements see section 3.3. The characteristic temporal shape of a whole-body ASR measurement consists of a short-latency steep incline, followed by a variable oscillation falling back to the baseline. (Koch 1999, Valsamis and Schmid 2011)

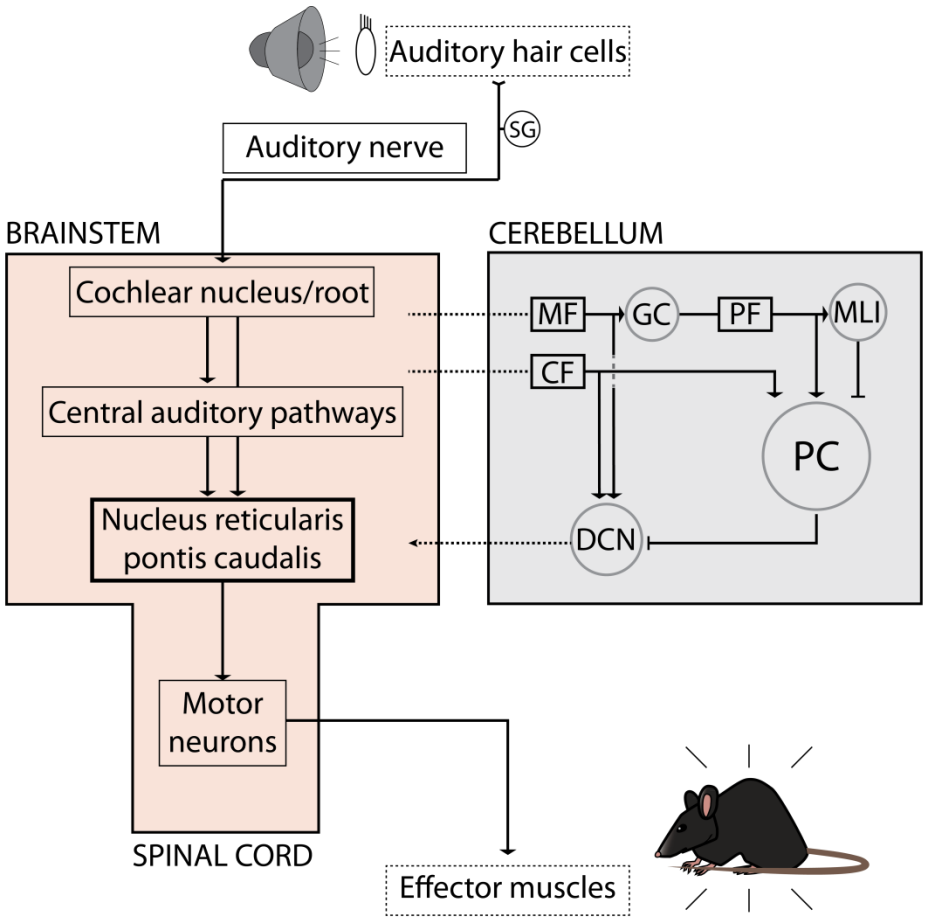

Figure 2: Schematic illustration of the basic acoustic startle pathway (left box, after Koch 1999) and hypothetical integration of a modulating cerebellar circuit (right box). Spiral cochlear ganglion (SG). Mossy fibre (MF). Granule cell (GC). Parallel fibre (PF). Molecular layer interneuron (MLI). Climbing fibre (CF). Purkinje neuron (PC). Deep cerebellar nuclei (DCN).

1.4. Harmaline-induced cerebellar tremor

Tremor is defined phenomenologically as an involuntary, rhythmic, sinusoidal oscillatory movement of any body part at varying frequencies, amplitudes and distributions (Deuschl, Bain et al. 1998, Govert and Deuschl 2015). Although there is a physiological form, tremor has to be considered being pathologic and is thought to either appear as a monosymptomatic entity on its own or symptomatic of a primary disease (Hallett 2014, Govert and Deuschl 2015). Prominent diseases associated with symptomatic tremor are Parkinson's disease or dystonia (Elias and Shah 2014, Hallett 2014). Tremor can be distinguished based on several characteristics, for instance, its presence at rest or at activity. Activity tremor may be further divided into postural, kinetic, task-specific, isometric and intention tremor (Elias and Shah 2014). Besides its diverse clinical appearance, aetiological considerations are an important part of the classification of tremor syndromes (Govert and Deuschl 2015).

A prominent type of tremor, cerebellar tremor, is found in accordance with cerebellar affection, such as lesions or genetic variants (Gemba, Sasaki et al. 1980, Bonnet, Apartis et al. 2012). The prototypic appearance of cerebellar tremor is called intention tremor. It is characterised by an increase of tremor amplitude when approaching a target and may be triggered, for example, by the finger-to-nose-test (Deuschl, Bain et al. 1998). Depending on the underlying cerebellar affection, it may be accompanied by other typical cerebellar motor symptoms, such as nystagmus, slurred speech (as such together forming Charcot's neurologic triad) or ataxia (Deuschl, Bain et al. 1998, Elias and Shah 2014). Furthermore, a general pathophysiologic involvement of the cerebellum is suggested for some other types of tremor, predominantly for essential tremor (Jenkins, Bain et al. 1993, Louis, Shungu et al. 2002, Hallett 2014).

As such, reports propose deviations in the olivo-cerebellar circuit as a possible cause (Batini, Buisseret-Delmas et al. 1979, Hallett and Dubinsky 1993, Hallett 2014).

In this context, harmaline is a well-known substance to induce cerebellar tremor (Ahmed and Taylor 1959, Lamarre and Mercier 1971, Llinas and Volkind 1973). Harmaline (1-methyl-7-methoxy-3,4-dihydro-β-carboline) is one amongst several representatives of the group of harmala alkaloids (Herraiz, Gonzalez et al. 2010). The harmala alkaloids, particularly harmine and harmaline, are naturally found as components of several plants, such as *Peganum harmala* (L), from whom they can be extracted (Khan, Maalik et al. 2013). Due to their beta-carboline backbone the harmala alkaloids are part of the group of bioactive indole alkaloids. Many other well-known natural substances are part of the indole alkaloid group, including tryptophan as well as the neurotransmitter and tryptophan-derivative serotonin (5-hydoxytryptamine; 5-HT). The pharmaceutical effects of harmaline described further below may be considered in view of these chemical characteristics of harmala alkaloids. Figure 3A shows the chemical structure of harmaline (PubChem Compound Database).

Different pharmacological interactions and biological effects of harmaline regarding DNA, enzymes and receptors have been reported (Cao, Peng et al. 2007, Handforth 2012). Upon application, effects of harmaline range from being vasoactive and antimicrobial to being neuro- and psychotropic (Cao, Peng et al. 2007, Khan, Maalik et al. 2013). One of the striking characteristics of harmaline, however, is its aforementioned tremorgenic effect, making it a well-used model of essential tremor and tremor in general (Miwa 2007, Handforth 2012). Upon administration, an acute kinetic and postural tremor of the trunk, head, tail and limbs, hence, of the entire body musculature is induced (Handforth 2012).

In doing so, harmaline is known to exert a rather specific effect on neurons of the inferior olivary complex (IO), inducing enhanced climbing fibre (CF) mediated input to the cerebellar cortex and deep cerebellar nuclei (DCN) (Lamarre and Mercier 1971, Llinas and Volkind 1973). The tremorgenic effect is not elicited by direct application of harmaline to the cerebellar cortex or to Purkinje neurons (Chen, Kovalchuk et al. 2010). However, dissection of CFs and lesions of the IO suppress tremor (Llinas and Volkind 1973, Simantov, Snyder et al. 1976). Interestingly, elimination of Purkinje neurons does not reduce tremor, suggesting that DCN are key mediators of tremor (Llinas and Volkind 1973, Milner, Cadoret et al. 1995). The resulting, stark augmented cerebellar output is supposed to promote tremor via brainstem nuclei and spinal motor neurons (Llinas and Volkind 1973).

Although the underlying cause of harmaline-induced tremor is suggested to be found in its effect on neurons of the IO, the exact physiological mechanism is not entirely clarified as of now. Harmaline and other beta-carbolines are reported to facilitate rhythm-generating ionic conductance, accountable for the synchronous and oscillatory rhythmic activity of the electronically coupled IO neurons (Llinas, Baker et al. 1974, Llinas and Yarom 1981, Llinas and Yarom 1986). This effect seems to be restricted to the caudal parts of the medial and dorsal accessory nuclei of the IO projecting to vermal regions of the cerebellum and DCN (De Montigny and Lamarre 1975). In this regard, γ-aminobutyric acid (GABA) A receptor-controlled gap junctions and 5-HT afferents to the IO are considered important mediators and modulators of electronic coupling, hence, also on output-generation (King, Ho et al. 1984, Pazos, Cortes et al. 1985, Sotelo, Gotow et al. 1986).

Several interactions of harmaline have been reported which are of potential relevance in this context. Harmaline is stated to be a potent reversible selective monoamine oxidase A (MAO-A) inhibitor (Kim, Sablin et al. 1997, Herraiz, Gonzalez et al. 2010) and monoamine-uptake inhibitor (Airaksinen, Svensk et al. 1980) which leads to increased monoamine levels, in doing so, affecting the serotoninergic system. Besides, a direct interaction with 5-HT-receptors has been described (Sugihara, Lang et al. 1995). Like other beta-carbolines, harmaline also interacts with the benzodiazepine site of GABA-A-receptors (Robertson 1980, Weiss, Buldakova et al. 1995). However, there is controversy on the exact physiology and relevance (Deecher, Teitler et al. 1992). Another important target is the T-type calcium channel, which is involved in subthreshold oscillatory rhythm-generation in neurons of the IO (Llinas and Yarom 1986, Park, Park et al. 2010). Besides, a number of additional targets and interactions have been reported, such as, with the N-methyl-D-aspartate receptor, opiate receptors, voltage-dependent sodium and calcium channels, sodium-dependent transport processes as well as further interactions in GABAergic and dopaminergic systems (Smart 1981, Airaksinen, Saano et al. 1984, Deecher, Teitler et al. 1992, Handforth 2012). The resulting enhanced output activity of IO neurons, however, leads to an increase of characteristic complex spike responses in Purkinje neurons through activation of CF synapses in the cerebellar cortex (Eccles, Llinas et al. 1966, De Montigny and Lamarre 1973).

In summary, the rather specific effect on neurons of the inferior olive make harmaline a potent tool for experimental manipulation of CF input to the cerebellar cortex of the vermis under conditions of harmaline-induced cerebellar tremor. Therefore, harmaline was deployed in the present thesis as a pharmaceutical intervention to increase CF input of Purkinje neurons. Figure 3B illustrates the effects of harmaline on the olivo-cerebellar circuit. See section 1.2 for more details on the neuroanatomy and neurophysiology of the cerebellum including the olivo-cerebellar circuit.

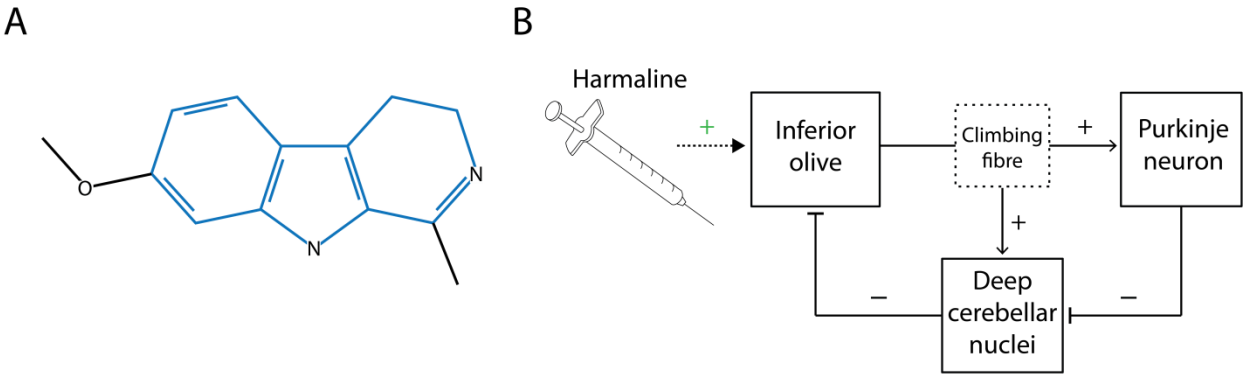

Figure 3: The chemical structure of harmaline and its effect on the olivo-cerebellar circuit. (A) Chemical structure of harmaline. Blue: Beta-carboline backbone (after PubChem Compound Database). (B) Harmaline-induced increase of climbing fibre activity within the olivo-cerebellar circuit (after Chen, Kovalchuk et al. 2010).

1.5. Biophysical principles of two-photon calcium-sensitive fluorescent microscopy

This section introduces the biophysical foundations for two-photon calcium-sensitive fluorescent microscopy, one of the *in-vivo* methods used in the present thesis.

1.5.1. The role of calcium and relevant sources for calcium-sensitive microscopy

Calcium plays a critical role in biological processes and in the physiology of organisms. Its functions are extraordinarily diverse, ranging from regulating gene expression, the cell cycle, apoptosis and enzyme activity to signal transduction, structural formation, cell migration and muscle contraction (Berridge, Lipp et al. 2000, Berridge, Bootman et al. 2003, Dulhunty 2006, Verkhratsky 2007, Lyons and West 2011, Humeau, Bravo-San Pedro et al. 2018).

In this context, calcium acts as an intracellular messenger, cofactor of enzymes, structural component and contributes to the electrochemical gradient of the membrane potential (Krauss 2001, Berridge, Bootman et al. 2003). This is why it is not surprising, that disturbances in the calcium homeostasis are in turn correlated with a multitude of dysfunctions, for instance neurologic disorders like cerebellar syndromes (Matilla-Duenas, Ashizawa et al. 2014) or Alzheimer's disease (Busche, Eichhoff et al. 2008, Sanabria-Castro, Alvarado-Echeverria et al. 2017).

Prerequisite for its function is the high diversity of calcium concentrations amongst distinct compartments (Berridge 2006). For example, at resting membrane conditions of most neurons cytosolic concentration of calcium is typically around 100nM and approximately 1-2mM extracellularly (Berridge, Lipp et al. 2000). If channels allow for transmembrane conduction, this results in a powerful influx of calcium ions following their electrochemical gradient into the cell. During activity, a localised and transient increase in calcium concentration of 10 to 100 fold is possible (Berridge, Lipp et al. 2000). Eventually, all functions of calcium are mediated by temporal and spatial summation of changes in calcium concentration in defined cellular domains or other specific compartments (Berridge and Dupont 1994, Bootman, Lipp et al. 2001, Jia, Rochefort et al. 2010).

In the nervous system, calcium plays a vital role particularly in general neuronal activity, plasticity mechanisms and during development (Lohmann, Finski et al. 2005, Zheng and Poo 2007, Kwan 2008, Yasuda 2017). As such, calcium is involved, for instance, in establishing electric excitability, membrane signal generation and conduction as well as in synaptic transmission by neurotransmitters vesicle release and post-synaptic signal transduction (Berridge, Lipp et al. 2000, Krauss 2001, Neher and Sakaba 2008). Since changes in intracellular calcium concentration and

electrical activity are strongly correlated, calcium is a valuable surrogate to observe neuronal activity (Tsien and Tsien 1990, Smetters, Majewska et al. 1999, Stosiek, Garaschuk et al. 2003, Kerr, Greenberg et al. 2005, Kitamura and Kano 2013, Grienberger, Chen et al. 2015). Since calcium acts as an intracellular messenger, however, this is frequently connected with secondary processes (Berridge, Lipp et al. 2000). To make calcium signals visible, specific calcium sensitive fluorescent indicators are used, which fluoresce upon calcium-binding. For more details on fluorescence see the following section, for calcium sensitive fluorescent indicators see section 3.6.1.2.

Observation of changes in calcium concentration allow for the investigation of neuronal activity on different scales - from neural networks and populations to single neurons or even subcellular structures (Grienberger and Konnerth 2012). In doing so however, the origin of the detected signal has to be taken into account for an accurate interpretation, i.e., underlying structures, such as cell somata, dendritic branches or presynaptic axonal terminals. Again depending on the cell type and subcellular structure involved, the exact composition of calcium sources contributing to the signal may differ significantly and has to be appreciated. (Grienberger and Konnerth 2012, Grienberger, Chen et al. 2015)

Sources may be classified in those leading to extracellular calcium influx and those leading to release from intracellular stores. Extracellular calcium influx is mediated mainly by different types of voltage-gated calcium channels (VGCC), but also by transient receptor potential channels (TRPC) or different calcium permeable receptors. These are, for instance, ionotropic glutamate receptors, most importantly the N-methyl-D-aspartate (NMDA) receptor or to a (much) lesser degree the α-amino-3-hydroxy-5-methyl-4-isoxazolepropionic-acid (AMPA) receptor.

Besides, other receptors like the nicotinic acetylcholine receptor (nACh-R) have to be considered. Intracellular calcium release form the endoplasmic reticulum (ER) is mediated, for instance, by inositol triphosphate (IP3) receptors via IP3 generated by metabotropic glutamate receptors (mGlu-R), or by calcium-induced calcium release via ryanodine receptors (Ry-R). Again, additional sources exist. Cytosolic calcium is either buffered temporarily by calcium-binding proteins, stored in the ER via the sarco-/endoplasmic reticulum calcium ATPase (SERCA), or removed to the extracellular space via sodium-calcium exchangers (NXCs) and the plasma membrane calcium ATPase (PMCA). (Grienberger and Konnerth 2012)

At resting membrane conditions, there is a dynamic equilibrium between the involved parties. At activity, the equilibrium is altered as calcium-permeable channels and/or receptors mediate changes in calcium conductance, resulting in changes in calcium concentration (Berridge, Lipp et al. 2000, Berridge, Bootman et al. 2003). Figure 4 generally outlines important calcium sources for calcium-sensitive microscopy in neurons and the cellular pathways of calcium turnover, neither taking into consideration their specific spatial distribution, nor their distinct occurrence in different cell types or subcellular compartments.

The temporal dynamics of changes in calcium concentration at neuronal activity lead to a characteristic shape of the detected calcium signal - the so called calcium transient. It usually comprises of a steep signal incline as rapid calcium influx to the cytosol appears following its electrochemical gradient. Subsequently, a slower, inverse-exponentially decay ensues, mainly representing the efflux of cytosolic calcium via pumps and transporters. Besides physiological properties and current cellular calcium levels, the exact kinetics of the calcium transient depend on the features of the calcium-sensitive indicator deployed. For calcium-sensitive fluorescent indicators consider section 3.6.1.2.

In this context, the most important calcium source regarding *in-vivo* calcium-sensitive fluorescent microscopy of Purkinje neuron dendrites is found in high-threshold P-type VGCCs which are activated by suprathreshold dendritic voltage, i.e., primarily by climbing-fibre input (Usowicz, Sugimori et al. 1992, Westenbroek, Sakurai et al. 1995, Kitamura and Kano 2013, Roome and Kuhn 2018). Several other sources have been described, particularly, at parallel fibre-synapses of dendritic spines, however as for now, mostly *in-vitro* (Eilers, Augustine et al. 1995, Kitamura and Kano 2013).

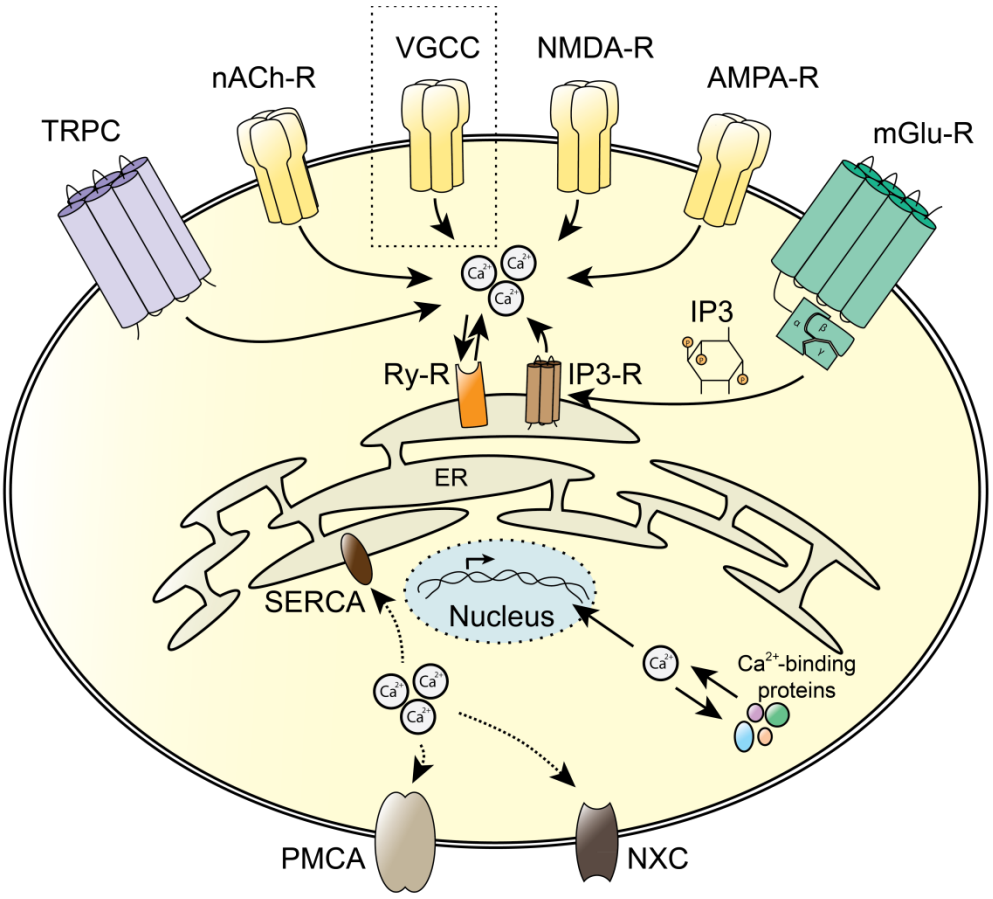

Figure 4: Schematic illustration of relevant calcium sources and cellular calcium turnover regarding calcium-sensitive microscopy (after Grienberger and Konnerth 2012).
Voltage-gated calcium channel (VGCC), N-methyl-D-aspartate receptor (NMDA-R) , α-amino-3-hydroxy-5-methyl-4-isoxazolepropionic-acid receptor (AMPA-R) , nicotinic acetylcholine receptor (nACh-R), transient receptor potential channel (TRPC), metabotropic glutamate receptor (mGlu-R), inositol triphosphate (IP3), inositol triphosphate receptor (IP3-R), ryanodine receptor (Ry-R), sarco-/endoplasmic reticulum calcium ATPase (SERCA), plasma membrane calcium ATPase (PMCA), sodium-calcium exchanger (NXC), endoplasmic reticulum (ER). Box: VGCCs are the most important calcium source in Purkinje neurons regarding *in-vivo* calcium-sensitive fluorescent microscopy.

1.5.2. Two-photon fluorescence excitation

In brief, fluorescence is based on the capability of a fluorophore to absorb photons containing a specific amount of energy, in other words, photons of a fluorophore-specific wavelength spectrum, defining the so-called excitation spectrum. (Lichtman and Conchello 2005, Nemoto, Kawakami et al. 2015)

These photons are able to shift orbital electrons of the fluorophore from their ground energy state S_0 to an excited state S_1. Hence, the photons' energy must be at least equivalent to the energy gap between the energy states of the fluorophore. Shortly afterwards, the excited electrons fall non-radiatively into the lowest energy level within the excited energy state S_1. Now, fluorescence occurs as the fluorophore's orbital electrons shift back from the S_1 state to the S_0 ground energy state, emitting luminescent photons. Again, there is a fluorophore-specific wavelength spectrum, now, for emission. Usually, only the peak excitation and emission wavelength are stated for a given fluorophore. (Lichtman and Conchello 2005, Nemoto, Kawakami et al. 2015)

In case of single-photon absorption, the emitted photons' wavelength spectrum, however, is longer than the one of the absorbed photons, that is, the photon energy is now lower. Simplified, the loss of energy, respectively, the change in wavelength is due to the energy difference between the initial level of the excited energy state and the lowest level of the excited energy state being termed Stokes shift (Lichtman and Conchello 2005). This interrelation is demonstrated in figure 5A.

The phenomenon of fluorescence is usually visualised in a so called Jablonski diagram, named after Polish physicist Aleksander Jablonski. In figure 5B on the left, a Jablonski diagram is shown for one-photon absorption of a fluorophore, whereas on the right, a Jablonski diagram is illustrated for two-photon excitation of a fluorophore.

The foundation of two-photon excitation microscopy is the principle of two-photon absorption. The proposal of the physical theory of two-photon absorption dates back to the first half of the twentieth century (Göppert-Mayer 1931). Unlike one-photon excitation, the energy needed to shift the fluorophore into the excited energy state is achieved by the effectively simultaneous excitation of two photons within an approximate femtosecond to picosecond time range (Helmchen and Denk 2005, Nimmerjahn, Theer et al. 2008). Under normal light conditions, two-photon absorption is a highly unlikely phenomenon. Whereas the probability of one-photon absorption is linear to the photon flux density, the rate of two-photon absorption is proportional to the square of it (Helmchen and Denk 2005, Svoboda and Yasuda 2006). Thus, prerequisite for the occurrence of two-photon excitation is the presence of high photon flux density (Diaspro, Bianchini et al. 2006). This is regularly achieved by high-power lasers. For further information on the method and devices needed for two-photon excitation microscopy see section 3.6.

Importantly, devices of the experimental setup have to be carefully adjusted according to excitation and emission spectra of the fluorescent indicators used.

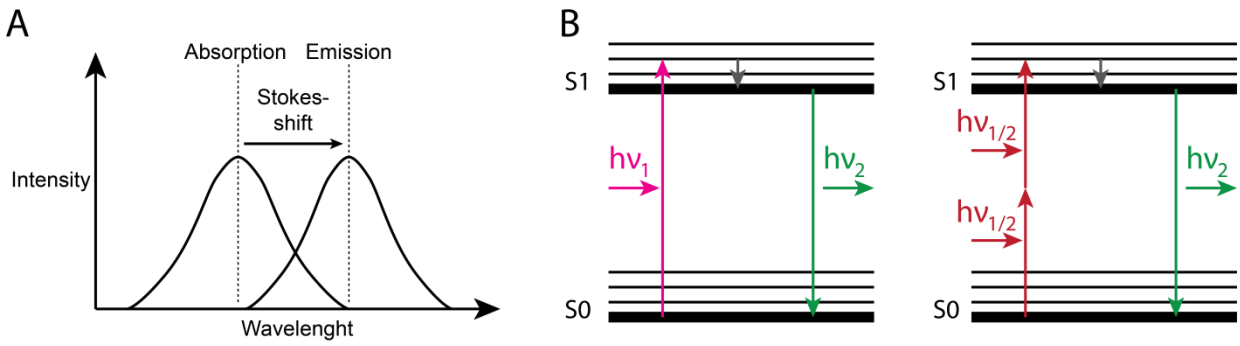

Figure 5: Biophysical principles of fluorescence. (A) Schematic illustration of the so-called Stokes-shift between the absorption and emission wavelength of a photon (after Lichtman and Conchello 2005). (B) Schematic illustrations of the Jablonski diagrams for one-photon excitation (left) and two-photon excitation (right) of a fluorophore (after Helmchen and Denk 2005). Planck's constant (h). Photon frequency (ν).

2. Hypotheses, objective and scope

As reviewed in section 1.3, previous studies suggest that the cerebellar vermis is involved in the modulation of the acoustic startle response (ASR). In particular, lesion studies in rats draw attention to its role in the habituation of the ASR. However, an explanatory mechanism has not been postulated. In this context, the present study addressed the overall hypothesis that the cerebellum is effectively involved in the modulation of the acoustic startle response. More precisely, the objective was to address several central questions (predictions) hypothetico-deductively derived from the overall hypothesis. Together, these formed the scope of this study. Questions guiding the process of the study were formulated as follows:

1. Assuming the cerebellar vermis is generally involved in processing information following acoustic startle stimulation, do respective signals or signal changes occur in the cerebellar cortex of the vermis in line with this proposition?
2. Supposing the cerebellar cortex is furthermore involved in the habituation of the ASR, are there changes in signals during the process of habituation and if yes of what kind?
3. Do pharmaceutical interventions affecting cerebellar neurophysiology, i.e. harmaline-induced cerebellar tremor in case of this study, alter the ASR behaviour?
4. If yes, what are associated physiological changes in the cerebellar cortex?
5. What could be a potential mechanism of cerebellar ASR-modulation in this context?

The Purkinje neuron (PC) represents the sole computational output of the cerebellar cortex. Since, thus, being a strategic “bottleneck” in the stream of information processing within the cerebellum, it has been chosen as a promising target to detect respective signals. Especially PCs of the (upper) vermis seem viable candidates, for this area is reported to receive auditory inputs as reviewed in section 1.3. These may be considered additional hypotheses.

In brief, the outline of the project agenda was bipartite and structured as follows:

In the beginning of the first part, behavioural studies on the ASR and its habituation were conducted. A habituation protocol was established which critically reduced the ASR, termed “startle suppression”, and allowed for controlled experimental stages in later investigations on head-fixed animals during calcium-imaging experiments. Secondly, deploying *in-vivo* electrophysiology and *in-vivo* calcium-sensitive microscopy, different signals of PC activity were analysed, characterised and correlated. This allowed for interpretation of directly observed dendritic calcium signals in awake, behaving mice both during single acoustic startle stimulation as well as throughout the entire startle suppression protocol by combined behavioural testing and *in-vivo* calcium-imaging.

In the beginning of the second part, transiently-induced cerebellar tremor by harmaline-application was characterised. Secondly, ASR behaviour was analysed under harmaline-induced cerebellar tremor. Subsequently, changes in electrophysiology and calcium signalling of PCs following harmaline-application were assessed. Finally, calcium signals of PCs evoked by acoustic startle stimulation were investigated during harmaline-induced cerebellar tremor in awake, behaving mice.

In summary, the present thesis aimed at elucidating the modulatory role of the cerebellum in context of the acoustic startle response and its habituation in further detail. Focus was given to *in-vivo* analysis of Purkinje neurons in the mouse cerebellar vermis. Derived from alterations during harmaline-induced cerebellar tremor a potential mechanism might be conceptualised.

3. Materials and methods

This chapter states as well as describes in detail all methods, materials, devices and experimental protocols used in the present thesis. The first two sections focus on the experimental animal model and the substance harmaline, which was used for pharmaceutical interventions in different experimental settings. The subsequent sections cover these different experimental settings, respectively. These are behavioural experiments, *in-vivo* single-cell electrophysiology and *in-vivo* two-photon calcium-sensitive microscopy. Each section introduces the respective methodology, lists all materials, devices and reagents used, displays the experimental setup as well as describes the experimental protocols. In section 3.4, preparatory steps prior to *in-vivo* experiments are explained.

3.1 Animal model

Male mice of the C57BL/6 strain were deployed as *in-vivo* model organism throughout all experiments in the present thesis. This strain dates back to the first half of the twentieth century (Jackson and Little 1933, Murray and Little 1935) and is a commonly used animal model in biomedical research. Mice of this inbred strain are considered genetic background controls. They are frequently used for tests on the acoustic startle response (Shnerson and Willott 1980, Willott, Kulig et al. 1984, Parham and Willott 1988, Willott and Carlson 1995, Carlson and Willott 1998, Shoji and Miyakawa 2018). Age of mice ranged between 35 to 42 days (5 to 6 weeks) post-partum. Mice were obtained from the in-house animal breeding facility. They were group-housed under a 12h-light/dark-cycle per day and had access to food and water *ad libitum*. Experiments were conducted during light cycle. Animal breeding, keeping and procedures were carried out according to institutional animal welfare regulations and approved by the government of Upper Bavaria (person responsible: thesis supervisor).

3.2 Harmaline

The indole alkaloid harmaline was used as a pharmaceutical intervention to increase climbing fibre input specifically from neurons of the caudal parts of the medial and dorsal accessory nuclei of the inferior olive which project to vermal Purkinje neurons (see figure 1B and 3B). At the same time, it prompted harmaline-induced cerebellar tremor. For more information on harmaline and harmaline-induced cerebellar tremor, see section 1.4. Throughout all experiments, harmaline was administered intraperitoneally at a dose of 3mg/kgBW, after being previously diluted in a standard sodium chloride solution to a concentration of 0.6mg harmaline/ml solution. See table 1 for reagents and the composition of the harmaline solution.

Name	**Provider/Stock keeping unit**
Harmaline hydrochloride dihydrate	Sigma-Aldrich Chemie GmbH/H1392
Isotonic sodium chloride solution (0.9% NaCl in pure water)	B. Braun Melsungen AG
Name	**Composition**
Harmaline solution	0.6mg harmaline hydrochloride dihydrate, 1ml isotonic sodium chloride solution

Table 1: Reagents of the harmaline solution and its composition

3.3 Behavioural experiments

Behavioural experiments have been carried out as a global test of the acoustic startle response (ASR) under different experimental conditions. This section describes the method, lists all devices and reagents used, illustrates the experimental setup as well as states the experimental protocol.

3.3.1 Accelerometric whole-body measurements of the acoustic startle response

As described in section 1.3, there are several approaches to measure the acoustic startle response. One of these methods is the accelerometric whole-body measurement, making use of the kinetic energy contained in the startle movement. In order to transduce mechanic forces into a detectable signal, accelerometers may be used. In case of the present thesis this was a piezoelectric sensor, converting dynamic changes in pressure acting vertically on the sensor into electric currents based on the piezoelectric effect. For a maximum in signal acquisition, animals were put into a startle chamber mounted on the sensor to capture the entire whole-body startle.

3.3.2 Experimental setup and devices

Animals were placed in a costume-made plastic box (length: 8.5cm, width: 8.5cm, height: 5cm), which was mounted on a base plate (length: 12cm, width: 12cm). A piezoelectric accelerometer (MP100 Pulse Transducer, ADInstruments) was positioned centrally underneath the plate. The recorded signal was fed via an analogue-digital-converter (PowerLab 4/25, ADInstruments) to an analysis-computer (Celsius M, Fujitsu Siemens).

Both the acoustic stimulation (95dB white noise, 100ms, near-instant rise time), applied via a costume-built amplifier and a speaker (G25FFL 8Ω, Visaton) as well as the background noise (60dB white noise), applied via an amplifier (ED1 Electrostatic Speaker Driver, Tucker Davis Technologies) and a speaker (ES1 Electrostatic Speaker, Tucker Davis Technologies), were controlled centrally by this computer. Bandwidth of white noise ranged from 0-50kHz. The inter-stimulation-interval was set and the respective acoustic stimulation executed by a pulse generator (Master-8, A.M.P.I.). On one experimental condition, harmaline (Sigma-Aldrich, 3mg/kgBW) was administered intraperitoneally. The experimental setup for behavioural testing is displayed in figure 6.

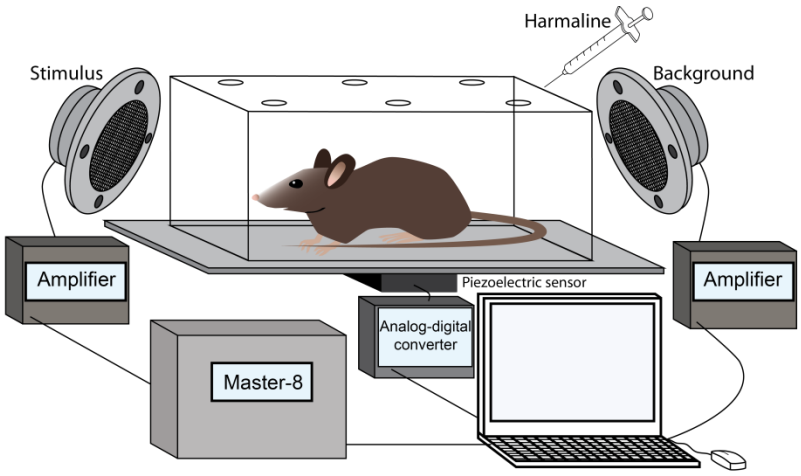

Figure 6: Schematic illustration of the setup for accelerometric whole-body measurements of the acoustic startle response.

3.3.3 Reagents, pharmaceuticals and solutions

For reagents and the composition of the harmaline solution please consider section 3.2. Provider of isoflurane for short-term anaesthesia was CP-Pharma Handelsgesellschaft mbH.

3.3.4 Experimental protocol

The behavioural protocol based on pre-existing parameters and paradigms on habituation (Davis 1970, Valsamis and Schmid 2011). However, it was modified as stated below to accommodate the needs discussed in the results (sections 4.2 and 4.9).

The acoustic startle response (ASR) was evoked by white noise of 95dB and 100ms over a continuous 60dB white noise background (see also 3.3.2). As the ASR is distorted by animal behaviour like grooming and exploratory movement, the animal underwent an acclimation period of 10min prior to the respective experiment to adapt to the environment and the background noise after placement in the box. Recordings were started once the animal calmed down and remained still in a steady position. For both experimental settings, control conditions comprised of 1.5min at an inter-stimulus-interval (ISI) of 15s (a total of 6 stimuli).

In case of experiments on habituation of the ASR ("ASR suppression"), control conditions were followed by 5min of 1Hz-high-frequency stimulation for induction and maintenance of habituation. The experiment was completed by a stage of 5min at an ISI of 15s during recovery. The protocol is illustrated in figure 15 in section 4.2.

In case of experiments on the ASR under harmaline-induced cerebellar tremor, control conditions were followed by immediate i.p. administration of harmaline (3mg/kgBW) under short-term isoflurane anaesthesia, delivered via a mildly isoflurane-soaked cotton ball. After a 30min break, recordings were taken over 1.5min at 15s ISIs under visually-identifiable tremor. After a second break (approximately 120min after injection) when tremor had visually ceased, another recording of 1.5min at ISIs of 15s followed. An illustration of the protocol may be found in figure 27 in section 4.9. It grounded on previous reports (Pellet, Weiss et al. 1983) and was adapted based on observations from own experiments (see section 4.8).

3.4 Preparations for in-vivo electrophysiology and in-vivo two-photon fluorescent microscopy

3.4.1 Artificial cerebrospinal fluid, internal solution and external buffer solution

Artificial cerebrospinal fluid (ACSF) is a solution applied to exposed brain tissue for buffering and for maintaining osmolarity at physiological levels (Stosiek, Garaschuk et al. 2003). ACSF was applied as of the time after implementation of the craniotomy for *in-vivo* electrophysiology and *in-vivo* tow-photon calcium sensitive microscopy to guarantee for a continuous perfusion of brain tissue. For the surgical procedure see 3.4.2, for electrophysiology see 3.5 and for two-photon calcium sensitive microscopy see 3.6. In case of mere behavioural experiments no ACSF was needed. For behavioural experiments see 3.3.

ACSF was gas-flushed with carbogen (5% carbon dioxide and 95% oxygen) to establish a pH of 7.4. Reagents and the composition of the ACSF solution may be found in table 2.

Reagent	**Provider/Stock keeping unit**
Sodium chloride (NaCl)	Merck KGaA/106404
Potassium chloride (KCl)	Merck KGaA/104936
Sodium hydrogen carbonate ($NaHCO_3$)	Merck KGaA/106329
Sodium dihydrogen phosphate (NaH_2PO_4)	Sigma-Aldrich Chemie GmbH/S9638
Calcium chloride ($CaCl_2$)	AppliChem GmbH/131232
Magnesium chloride ($MgCl_2$)	AppliChem GmbH/A4425
Glucose ($C_6H_{12}O_6$)	Merck KGaA/108342
Ultrapure water (H_2O)	Millipore/Milli-Q® Direct 8 Water Purification System
Carbogen (95% O_2 and 5% CO_2)	Sauerstoffwerk Friedrichshafen GmbH
Solution	**Composition**
Artificial cerebrospinal fluid (ACSF)	125mM NaCl, 4.5mM KCl, 26mM $NaHCO_3$, 1.25mM NaH_2PO_4, 2mM $CaCl_2$, 1mM $MgCl_2$, 20mM $C_6H_{12}O_6$ in H_2O

Table 2: Reagents of artificial cerebrospinal fluid and its composition

Internal solution was needed for the preparation of the calcium-sensitive indicator solution containing Oregon Green BAPTA-1 488 hexapotassium salt (OGB-1 6k) before performing indicator loading via electroporation. For the preparation of the OGB-1 6k solution see 3.4.3, for calcium-sensitive indicators 3.6.1.2 and for indicator loading procedures 3.6.4. Reagents and the composition of internal solution may be found in table 3.

Reagent	**Provider/Stock keeping unit**
Potassium gluconate ($C_6H_{11}KO_7$)	AppliChem GmbH/A3133
HEPES	Sigma-Aldrich Chemie GmbH/H3375
Potassium chloride (KCl)	Merck KGaA/104936
Phosphocreatine disodium salt ($C_4H_8N_3Na_2O_5P$)	Sigma-Aldrich Chemie GmbH/P7936
Adenosine triphosphate magnesium salt (MgATP)	Sigma-Aldrich Chemie GmbH/A9187
Guanosine triphosphate sodium salt (Na_2GTP)	Sigma-Aldrich Chemie GmbH/G8877
Ultrapure water (H_2O)	Millipore/Milli-Q® Direct 8 Water Purification System
Solution	**Composition**
Internal solution	168.75mM $C_6H_{11}KO_7$, 12.5mM HEPES, 5mM KCl, 12.5mM $C_4H_8N_3Na_2O_5P$, 5mM MgATP, 0.375mM Na_2GTP in H_2O

Table 3: Reagents of the internal solution and its composition

External buffer solution was a component of the calcium-sensitive indicator solution containing Cal520 acetoxymethyl ester (Cal520AM) used for dye loading via multi-cell bolus loading. For preparation of the Cal520AM dye solution see 3.4.3, for calcium-sensitive indicators and dye loading procedures see 3.6. Reagents and the composition of external buffer solution may be found in table 4.

Reagent	Provider/Stock keeping unit
Sodium chloride (NaCl)	Merck KGaA/106404
Potassium chloride (KCl)	Merck KGaA/104936
HEPES	Sigma-Aldrich Chemie GmbH/H3375
Solution	**Composition**
External buffer solution	150mM NaCl, 2.5mM KCl, 10mM HEPES

Table 4: Reagents of the external buffer solution and its composition

3.4.2 Surgical procedure

Mice underwent prior surgical craniotomy when *in-vivo* electrophysiology and/or *in-vivo* calcium-sensitive fluorescent microscopy were performed (for electrophysiology see 3.5, for two-photon calcium sensitive microscopy see 3.6). Surgery followed in accordance with an established protocol (Stosiek, Garaschuk et al. 2003, Garaschuk, Milos et al. 2006). In case of mere behavioural experiments no preparatory steps, i.e., surgery needed to be taken (for behavioural experiments see 3.3).

Surgery was carried out under anaesthesia with isoflurane (CP-Pharma Handelsgesellschaft mbH, 0.8-1.2% (vol/vol) in pure 0_2), delivered to the mouse by an evaporator for inhalative anaesthetics (Vapor 19.3 for Isoflurane, Drägerwerk Ag & Co. KGaA) and through a costume-made tube and mask system. Analgesia was achieved by a combination of metamizole (bela-pharm GmbH & Co. KG, 200mg/kgBW), meloxicam (Boehringer Ingelheim GmbH & Co. KG, 1.5mg/kgBW), both administered systemically s.c. into the animal's flanks, and approximately 50µl of 2% lidocaine (AstraZeneca GmbH) in an isotonic sodium chloride solution (0.9% NaCl in ultrapure water, B. Braun Melsungen AG), applied locally s.c. to the dorsal head. At the same time the subcutaneous-application of diluted analgesics accounted for sufficient fluid supply during procedures. Depth of anaesthesia and effectiveness of

analgesia was regularly assessed by absence of eyelid reflexes, absence of reflective movements to painful stimulation and continuous monitoring of sufficient heart and respiration rates of around 500bpm and 80-130bpm, respectively, and was adjusted if necessary. Heart and respiration rates were controlled using a pressure sensor (Spirometer Pod ML311, ADInstruments) placed underneath the animal and was connected via an analogue-digital-converter (PowerLab 4SP, ADInstruments) to a computer (Precision T5500, Dell).

After previous implementation of anaesthesia and analgesia, mice were transferred onto a warming plate (DIGI 35, Voltcraft), securing a constant body temperature of 37-38°C throughout the entire surgical procedure. Temperature was monitored with a rectal probe of a digital thermometer (K101 Digital Thermometer, Voltcraft). Application of eye protection lotion (Bepanthen) prevented desiccation of the animal's eyes.

Surgical section, removal of skin and tissue as well as subsequent drying of the exposed bone was performed under binocular stereoscopic microscopy assistance (Stemi SR, Carl Zeiss AG) using standard surgical instrumentation.

A custom-made circular recording chamber of 35mm in diameter (Stosiek, Garaschuk et al. 2003, Garaschuk, Milos et al. 2006) with a central opening of 3mm in diameter was securely attached to the dried scull by applying an adhesive (OptiBond All-In-One, Kerr GmbH) and dental cement (Tetric EvoFlow, Ivoclar Vivadent GmbH), finally hardened under UV-light. The chamber allowed both for fixation of the head in a custom-made holder during the craniotomy and later during recordings as well as for appropriate perfusion of exposed brain tissue with carbogen gas-flushed artificial cerebrospinal fluid (ACSF) at 37°C as of the time after implementing the opening as described below (see figure 7B, for ACSF see 3.4.1).

At 2.5mm posterior to lambda and 0.5mm left-lateral to the midline an opening of the scull, 1 to 2mm in diameter, was created using a dental drill (C2 Master, Schick GmbH), hence being located above the left part of the cerebellar vermis. This area is susceptible for auditory inputs as described in section 1.3. Coordinates were determined by considering a mouse brain atlas (Paxinos and Franklin 2001). Figure 7C illustrates how the site for craniotomy was identified by using the coordinates. Using a syringe (20 Gauge BD Microlance, Becton Dickinson GmbH) residual bone was carefully removed from the brain tissue and an opening in the dura mater was cut remotely off the designated recording site, allowing for subsequent tension-free penetration of pipettes for dye loading and electrophysiological recordings. Apart from that, the dura was left intact, especially, above the designated recording site for subsequent calcium-sensitive fluorescent microscopy.

After establishing the craniotomy animals were transferred immediately to the respective recording setup. Analgesia, monitoring and support of abovementioned vital parameters were maintained until the end of experimentation. To minimize tissue pulsation and to stabilize recording conditions, agarose (2% agarose in ACSF, Sigma-Aldrich Chemie GmbH) was applied on the opening at the setup before starting experiments. Experiments in awake animals (= close to zero anaesthesia) were performed after prior acclimation-training of mice to the setup. Surgery and experiments were conducted under supervision by the thesis supervisor. Figure 7B shows the craniotomy after agarose application as it is also found during experiments. Figure 7A outlines the central components from the setup for surgical craniotomy. Table 5 lists all reagents, pharmaceuticals and solutions used during surgery.

Reagents	Provider/Stock keeping unit
Agarose	Sigma-Aldrich Chemie GmbH/A9793
Pharmaceuticals	**Provider**
Isoflurane	CP-Pharma Handelsgesellschaft mbH
Metamizole	bela-pharm GmbH & Co. KG
Meloxicam	Boehringer Ingelheim GmbH & Co. KG
Lidocaine	AstraZeneca GmbH
Solutions	**Composition**
Artificial cerebrospinal fluid (ACSF)/Carbogen	See section 3.4.1
Agarose solution	20mg agarose in 1ml ACSF

Table 5: Reagents, pharmaceuticals and compositions of solutions used during craniotomy

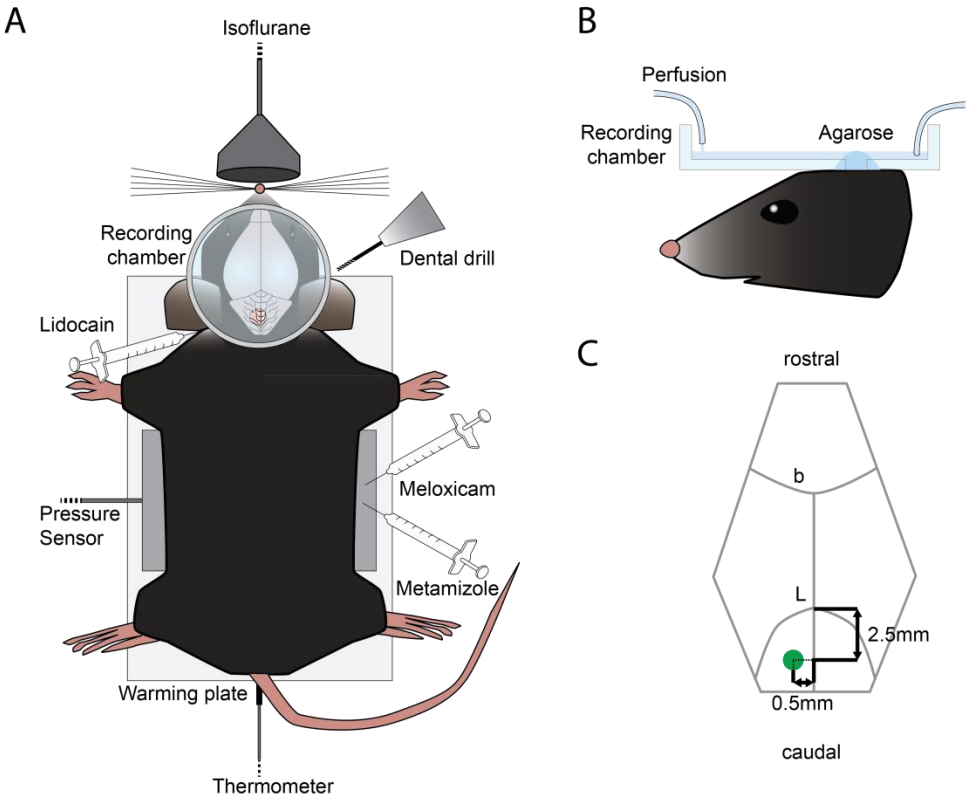

Figure 7: Illustration of the surgical procedure for craniotomy. (A) Illustration of the setup and the procedure. The mouse brain is projected transparently onto the head to demonstrate the location of the craniotomy. (B) Magnification of the mouse head after recording chamber fixation, craniotomy and agarose-application. (C) Illustration of the coordinates for craniotomy in respect to lambda. Green spot indicates location of the craniotomy. Bregma (b). Lambda (L).

3.4.3 Preparation of calcium-sensitive indicators, fluorescent dye solution and micropipettes

Two types of calcium-sensitive fluorescent indicators and a standard fluorescent dye were deployed during the experiments. This section describes the procedures to prepare the indicator and dye solutions as well as the procedure to prepare micropipettes. For more details on the role of calcium see 1.5.1, for biophysical principles of fluorescence see 1.5.2, for calcium-sensitive fluorescent indicators see 3.6.1.2 and for calcium indicator loading procedures see 3.6.4.

To prepare Cal520 acetoxymethyl ester (Cal520AM) calcium indicator solution, 50µg of Cal520AM (AAT Bioquest) were dissolved in 4µl of a detergent solution facilitating transmembrane diffusion which comprised of 20% Pluronic F-127 in dimethyl sulfoxide (Thermo Fisher Scientific). Additionally, 76µl extracellular buffer solution was added (for buffer solution see 3.4.1). The solution was filtered (Ultrafree-MC UFC30HV25, Merck Millipore) and subsequently stored on ice.

For Oregon Green 488 BAPTA-1 hexapotassium salt (OGB-1 6k) calcium indicator solution, 500µg of OGB-1 6k (Molecular Probes) were mixed with 10µl ultrapure water and 40µl internal solution (for internal solution see 3.4.1). The solution was filtered (Ultrafree-MC UFC30HV25, Merck Millipore) and subsequently stored on ice.

Alexa 488 fluorescent dye solution was prepared by adding Alexa Fluor 488 Dye (Molecular Probes) to external solution (for external solution see 3.4.1), achieving a final molar concentration of 50µM. The solution was vortexed before utilisation.

In table 6, all reagents as well as the compositions of calcium-sensitive indicator and dye solutions are stated.

Reagent	Provider
Cal520 acetoxymethyl ester (Cal520AM)	AAT Bioquest
Pluronic F-127 (20% in dimethyl sulfoxide)	Thermo Fisher Scientific
Oregon Green 488 BAPTA-1 hexapotassium salt (OGB-1 6k)	Molecular Probes
Ultrapure water (H_2O)	Millipore/Milli-Q® Direct 8 Water Purification System
Alexa Fluor 488 Dye	Molecular Probes
Solution	**Composition**
External buffer solution	See 3.4.1
Internal solution	See 3.4.1
External solution (ACSF)	See 3.4.1
Cal520AM solution	50µg Cal520AM, 4µl Pluronic F-127 (20% in dimethyl sulfoxide), 76µl external buffer solution
OGB-1 6k solution	500µg OGB-1 6k, 10µl H_2O, 40µl internal solution
Alexa Fluor 488 Dye solution	50µM in external solution

Table 6: Reagents and compositions of calcium indicator and fluorescent dye solutions

Micropipettes for calcium-sensitive indicator loading and for electrophysiology were produced immediately before the respective experiment by pulling a borosilicate glass capillary (Clark Electromedical Instruments) using a heat-based pipette puller (Model PC-10, Narishige). Pipette opening resistances ranged from approximately 2-3MΩ for multi-cell bolus loading, 5-5.5MΩ for electroporation to approximately 6-6.5MΩ for electrophysiology.

3.5 In-vivo electrophysiology

In-vivo single-cell electrophysiological recordings have been used in the present thesis to detect bioelectric signals of vermal Purkinje neurons at their somata, before, during and after harmaline-administration. This section introduces the method, illustrates the experimental setup, lists all devices and reagents used as well as states the experimental protocol. Basic biophysical principles of cellular neurophysiology are not explicitly addressed and are assumed to be known.

3.5.1 Single-cell electrophysiological recordings

One particularly fruitful method to investigate bioelectric activity of neurons is the so-called patch-clamp technique. Application of different configurations of this technique allows for the recording of electrochemical properties from several up to one single ion channel in the membrane of a neuron. General principle of this method is the combination of a micropipette, containing an electrode within an electrolyte solution, and an effective amplifier, being able to pick up even small ionic currents in the range of picoamperes. (Sakmann and Neher 1984, Neher and Sakmann 1992)

By placing the micropipette in the immediate proximity of a membrane patch from a neuron, measurements of current flowing through ion channels in its membrane are possible. Precondition is the formation of a seal between the membrane patch and the edge of the pipette tip. This is achieved by generating negative pressure within the pipette via suction. The result is an electrically-isolated membrane patch, which means, currents passing the membrane may now be recorded via the electrode within the pipette. At the same time, the established high seal resistance guarantees for low leakage and background currents, thus,

offering excellent signal-to-noise recordings. This is one of the major advantages of the patch-clamp technique compared to other electrophysiological methods. The first configuration established in this manner, is called cell-attached recording. Depending on the strength of the seal, this configuration is performed either with a loose seal resistance in the kΩ to MΩ range, the so-called loose-patch cell-attached configuration, or with a tight seal resistance in the GΩ range, usually referred to as giga-seal cell-attached configuration (giga from GΩ). Pipette-retraction from the tight seal cell-attached configuration causes the patch to dislocate from the membrane. This leads to the so-called inside-out configuration. In contrast, further suction in the tight seal cell-attached configuration breaks the membrane. As a result, the cytosol is now in continuity with the inside of the pipette. This configuration is called whole-cell recording. Again, pipette-retraction from the whole-cell configuration leads to the dislocation of the membrane patch, however now forming the so-called outside-out configuration. Each configuration enables new experimental approaches, such as different targeting of pharmaceutical interventions as well as different modifications or recordings of current and voltage properties. (Sakmann and Neher 1984)

In the so-called voltage-clamp mode the potential between the electrode in the micropipette and the reference electrode is hold (‘clamped’) at a fixed value in order to be able to measure solely the changes of ionic currents. These currents, in turn, are merely proportional to the membrane conductance representing the ionic flux through channels and transporters. The clamping is achieved by detecting differences in the potential to a pre-defined value and their correction through compensating currents via negative feedback. These currents are equal, yet, opposite to the ionic currents passing the membrane and can be recorded. (Cole 1949, Hodgkin, Huxley et al. 1952, Numberger and Draguhn 1996)

In case of cell-attached recordings, the potential between the extracellular patch at the tip of the pipette and the bath-electrode is hold in voltage-clamp. In case of whole-cell recordings, the transmembrane potential is hold (Sakmann and Neher 1984).

The general set-up for electrophysiology consists of a silver chloride electrode within a glass micropipette, a reference electrode in the bath solution, an operational amplifier together with a feedback-resistor located in the so-called headstage usually mounted directly on the pipette holder and, finally, a recording amplifier. The analogue signal from the amplifier is fed via an analogue-digital converter to a computer. The recording set-up up until the headstage should be placed inside of a Faraday cage for protection of electromagnetic disturbances and on a vibration isolation table. (Numberger and Draguhn 1996)

Recording of ionic currents as well as voltage-clamping via a single micro-electrode is possible using a current-to-voltage amplifier. It mainly consists of an operational amplifier and a feedback-resistor. Briefly, if there is a difference at the input of the operational amplifier (OPA) between the command potential and the potential at the electrode tip in the pipette, a strongly amplified potential proportional to the input is generated at the output of the OPA. The resulting potential difference leads to a current, fed back into the pipette electrode via the feedback resistor and proportional to the potential difference. Precondition is an extremely high input resistance of the OPA. The current flow stops as soon as the potential difference at the input of the OPA is compensated. The recording amplifier detects and displays the generated compensating current. (Numberger and Draguhn 1996)

In the present thesis the loose-patch cell-attached voltage-clamp configuration was deployed, since it is excellently suitable for mere action potential detection, while causing no harm to the integrity of the recorded cell (Perkins 2006). The recorded somatic currents of Purkinje neurons reflect back-propagating action potentials, which derive from the initial segment of the axon, that is, their neuronal output following suprathreshold activation (Davie, Clark et al. 2008, Palmer, Clark et al. 2010).

3.5.2 Experimental setup and devices

The mouse was head-fixed via the recording chamber into a holder centrally to the set-up. Analgesia, anaesthesia via the isoflurane-evaporator-tube-mask-system, monitoring and supply of vital parameters were maintained throughout the experiments identical to the prior surgical procedure (for the surgical procedure see 3.4.2). Continuous perfusion with fresh and carbogen gas-flushed artificial cerebrospinal fluid at 37°C was guaranteed by a pump (IPS-8, Ismatec). The inner core of the setup was mounted on a motorised positioner (table and controller 8SMC1-USBhf, Standa), which allowed for the exact positioning of the mouse under the microscope.

The equipment for electrophysiology consisted of a silver chloride electrode within a glass micropipette (for pipette preparation see 3.4.3), a bath electrode, an amplifier system (EPC10 USB Quadro, HEKA Elektronik) and a modular electronic platform, the PXI-unit (PXIe-1082, National Instruments) feeding the signal to the setup computer (Think Centre, Lenovo). The micropipette was controlled via a micro-manipulator (Junior, Luigs & Neumann) and a manipulator control panel (SM5, Luigs & Neumann). Electrodes were regularly inspected and freshly chlorinated at least once a week. On one experimental condition harmaline (Sigma-Aldrich, 3mg/kgBW) was administered intraperitoneally.

Electrophysiology was performed under two-photon microscopy-guidance. Moreover, in a set of experiments, electrophysiology was combined with calcium-sensitive microscopy. The equipment for microscopy consisted of a tuneable, mode-locked, high-peak-power, femtosecond-pulsed Ti:Sapphire-crystal laser with a repetition rate of 80MHz, a pulse width at peak of 140fs and an average power >2.5W (Chameleon Vision, Coherent Chameleon Laser Systems), a shutter (Uniblitz Electronic Shutter, Vincent Associates) with a shutter driver (Uniblitz VCM-D1 Shutter Driver, Vincent Associates), a Pockels cell (Model 350-50,

conoptics) with a Pockels cell driver (Model 302, conoptics) for modulation of laser intensity, a set of mirrors (BB1-E03, ThorLabs) for direction of the optical pathway, an optical beam expander (BE02-05-B, ThorLabs), a scanning system (12KHz CRS resonant scanner and 6215H galvanometer scanner, Cambridge Technology) with a scanning lens (AC254-150-B-ML, ThorLabs), an upright microscope (BX51WI, Olympus) with a water-immersion objective (40X/0.80NA/3.5mmWD, Nikon), a drive for remote-controlled focusing (SM4, Luigs & Neumann) and a photomultiplier tube (H7422P-40, Hamamatsu) for photon detection, positioned after a dichroic mirror (T 795 LPXRXXT, AHF analysetechnik AG via Chroma Technology Corp.). The signal was fed via the PXI-unit (PXIe-1082, National Instruments), to the setup computer (Precision 690, Dell). The entire setup was mounted on an optical table (table RS4000 and stabilizer I-2000, Newport). Laser wavelength was set to 925nm. This is in the proximity of the two-photon excitation spectrum optima fluorescent dyes deployed. Average power measured under the objective ranged between 23-73mW and was kept as low as possible for dye and tissue protection. For more details on two-photon calcium-sensitive microscopy, see 3.6. The setup for electrophysiology is illustrated in figure 8.

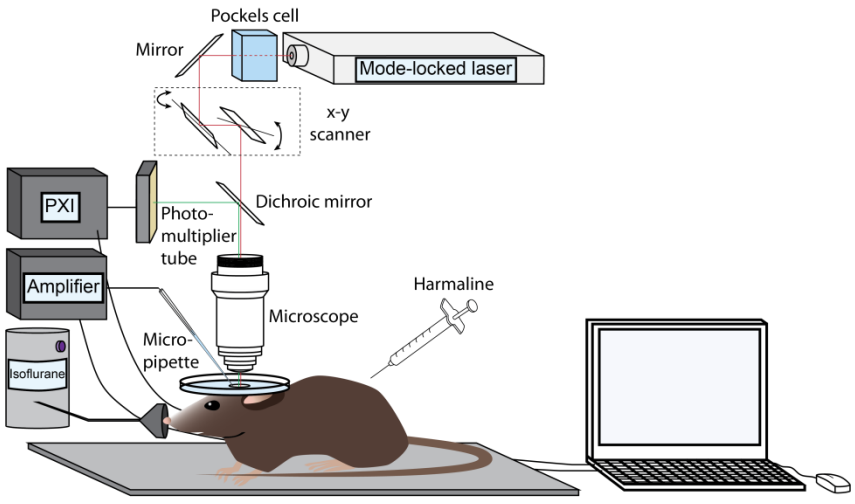

Figure 8: Schematic illustration of the setup for microscopy-guided *in-vivo* single-cell electrophysiology.

3.5.3 Reagents, pharmaceuticals and solutions

Table 7 lists all solutions used during the *in-vivo* electrophysiology experiments. For the reagents and compositions of each solution, kindly consult the respective section mentioned in the table. For anaesthesia and analgesia during electrophysiology see section 3.4.2.

Solution	Composition
Artificial cerebrospinal fluid (ACSF)/Carbogen	See 3.4.1
Alexa Fluor 488 Dye solution	See 3.4.3
Harmaline solution	See 3.2

Table 7: Solutions used during electrophysiology

3.5.4 Experimental protocol

In-vivo cell-attached recordings were established under anaesthesia and by the shadow-patching approach (Kitamura, Judkewitz et al. 2008), using the fluorescent dye Alexa Fluor 488 for two-photon fluorescent microscopy-guidance. In this approach, somata of Purkinje neurons could be identified and targeted by visualising their silhouettes as a negative image, or so-called “shadow”, when ejecting dye from the pipette in the expected penetration depth within the cerebellar cortex.

Firstly, a newly-pulled micropipette was filled with 5µl Alexa Fluor 488 Dye solution and immersed in the bath solution, sustaining light positive pressure. After correction for the offset potential, pipette resistance was calculated using a test pulse. Resistance was around 6-6.5MΩ. The micropipette resistance was compensated and the potential between the microelectrode and the bath electrode was set to 0mV and clamped.

The tip of the pipette was guided to the soma of a Purkinje cell in the Purkinje cell layer under two-photon microscope surveillance. An increase of resistance and the formation of a fluorescent dye-filled dimple indicated immediate contact to the cell membrane. Now, negative pressure via suction led to the formation of the patch seal between the edge of the pipette tip and the cell membrane. Seal resistance ranged between 40-80MΩ. A two-photon fluorescent microscopy image of a Purkinje neuron soma just before patch-formation with a dye-filled micropipette in the shadow-patching approach is shown in figure 9.

After formation of the loose-patch cell-attached configuration, spontaneous activity could be recorded. In case of pharmaceutical interventions, spontaneous control recordings were followed by intraperitoneal application of harmaline at 3mg/kgBW. After a break of 30min, recordings were obtained under harmaline. Onset of the harmaline effect was confirmed by presence of tremor when anaesthesia was briefly reduced. Recordings for harmaline wash-out were acquired 120min after harmaline-injection. Figure 28 in section 4.10 displays the experimental protocol of the harmaline intervention. The protocol based on previous experimental findings (see section 4.9). For one set of experiments, *in-vivo* electrophysiology was performed simultaneously to *in-vivo* single-cell two-photon calcium-sensitive microscopy. This is described in the following section.

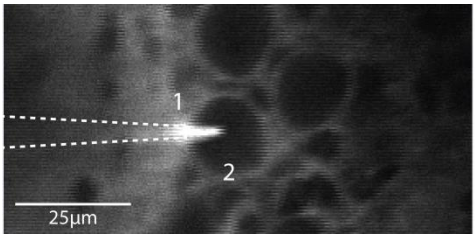

Figure 9: Image (xy-plane) taken from microscopy-guided patch-formation in the shadow-patching approach for *in-vivo* single-cell electrophysiology. (1) Tip of the fluorescent dye-filled micropipette. Dashed lines indicate its shape. (2) Purkinje neuron soma.

3.6 In-vivo calcium-sensitive fluorescent microscopy

In-vivo two-photon excitation laser-scanning calcium-sensitive fluorescent microscopy has been used in the present thesis to observe dendritic calcium signals from vermal Purkinje neurons in awake, behaving mice under different experimental conditions. Besides, it was partly used in combination with simultaneous *in-vivo* single-cell loose-patch cell-attached somatic recordings. This section introduces the method, illustrates the experimental setup, lists all devices and reagents used, describes the indicator dye loading procedure as well as states the experimental protocols. For biophysical principles of the method see section 1.5.

3.6.1 Two-photon excitation laser-scanning calcium-sensitive fluorescent microscopy

3.6.1.1 Two-photon excitation laser-scanning microscopy

As introduced in section 1.5.3, prerequisite for induction of two-photon absorption is high photon flux density. This is achieved by the combination of mode-locked, high-peak-power pulsed lasers and high numerical aperture lenses, mediating photon beam focusing (Denk and Svoboda 1997, Piston 1999). As a consequence, effective photon flux density for two-photon excitation may be established in a small focus volume (Helmchen and Denk 2005, Svoboda and Yasuda 2006). Figure 10 opposes linear one-photon excited fluorescence and non-linear two-photon excited fluorescence. For microscopy of lager structures, such as nerve cells or nerve cell ensembles, the small focus volume is continuously run in a two-dimensional array via an optical deflection system, for example scan mirrors, in order to scan the specimen (Fan, Fujisaki et al. 1999).

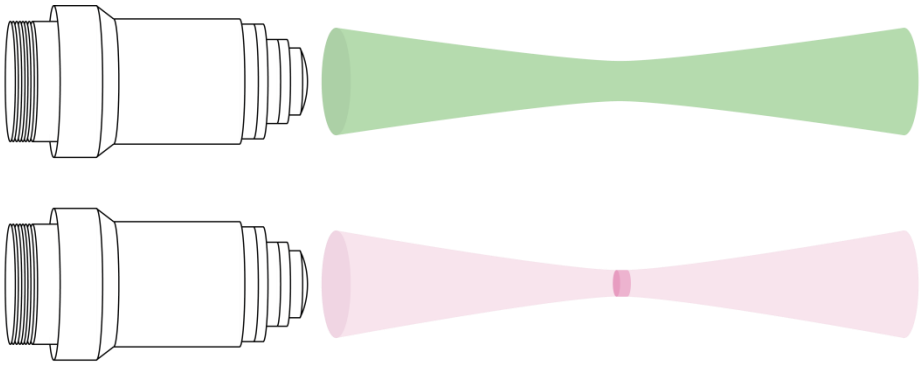

Figure 10: Schematic illustration of linear excited fluorescence in one-photon microscopy (upper) and localised non-linear excited fluorescence in two-photon microscopy (lower) (after Helmchen and Denk 2005).

Other than one-photon excitation, two-photon excitation is a non-linear phenomenon. Two-photon excitation spectra differ from the theoretically calculated spectra based on one-photon excitation. These aspects have to be taken into account regarding arrangement of the experimental setup. (Helmchen and Denk 2005)

There are major advantages of two-photon excitation laser-scanning microscopy over methods of one-photon excitation microscopy. In this context, it is in particular photon scattering within the tissue increasing with specimen thickness, which leads to several issues. On the one hand, it limits penetration depth of photons for effective excitation. On the other hand, emitted photons reaching the optical detection system cannot be attributed back unambiguously to their emission origin due to scattering. This results in weakening of contrast and resolution. One way to compensate for the negative effects of scattering is the utilisation of spatial filters. For example, pinhole optical systems reduce the loss of contrast, however, at the expense of excluding most of the emitted photons from detection. (Helmchen and Denk 2005)

Another way to address scattering is the usage of two-photon effect-based microscopy. Scattering (S) is inversely proportional to the fourth power of the wavelength (λ) (Helmchen and Denk 2005):

$$S \sim \frac{1}{\lambda^4}$$

On the one hand, penetration depth is increased since two-photon excitation allows for longer wavelengths. Moreover, since two-photon excitation is known to occur only within a small focus volume which may be controlled via the scanning process, it is possible to trace back all emitted photons reaching the detector without using any further spatial filters. This boosts photon yield to a maximum and results, eventually, in comparably bright and high contrast optical recordings. (Piston 1999, Helmchen and Denk 2005, Svoboda and Yasuda 2006)

Additionally, in contrast to one-photon microscopy, no unintended excitation occurs outside the focus volume, causing reduced bleaching of the fluorescent dye, less thermal damage inside the tissue and lower phototoxicity (Piston 1999, Helmchen and Denk 2005). In this context, phototoxicity terms the generation of harmful substances, such as oxygen radicals. The continuous scanning additionally supports the tissue protective feature of two-photon excitation (Stephens and Allan 2003, Fischer, Wu et al. 2011).

3.6.1.2 Calcium-sensitive fluorescent indicators

Calcium-sensitive fluorescent indicators are used to visualize changes in calcium concentration. For information on the physiological role of calcium and biophysical principles of fluorescence, kindly consult section 1.5. Indicators regularly consist of a molecular domain for calcium-binding and a fluorophore-domain. A fluorescence peak of these indicators at the detected wavelength, however, only occurs when calcium ions are bound and induce structural changes. (Tsien 1989, Paredes, Etzler et al. 2008)

In case of so called ratiometric indicators, these changes lead to a shift in the excitation or emission spectrum of the indicator (spectral shift). In case of so called non-ratiometric indicators, the fluorescence intensity of the indicator increases at the given wavelength (intensity shift). (Grynkiewicz, Poenie et al. 1985, Paredes, Etzler et al. 2008)

The advantage of ratiometric indicators is the possibility to establish a certain ratio between the calcium-binding and the non-binding portion of indicator. This is done if the fluorescent dye is excited or detected at both wavelengths, at the one of the initial structural state as well as at the one after the calcium-induced structural change (Grynkiewicz, Poenie et al. 1985, Paredes, Etzler et al. 2008). The calculated ratio is independent of several possible experimental confounders, e.g. the dye loading success (uneven dye loading), different loading behaviours of cells, dye bleaching, dye leaking, changes in laser intensity, changes in cell volume or focal plane discrepancies of recordings. The disadvantage, though, is the technical and experimental execution. (Grynkiewicz, Poenie et al. 1985)

Both types of indicators, however, enable the dynamic detection of relative changes in calcium concentration over time.

Indicators differ in several further characteristics, most importantly: their excitation and emission spectra, their binding-affinity to calcium, i.e., their binding-kinetics, the way the indicator is loaded into the cell as well as if the localisation of the indicator may be controlled (Paredes, Etzler et al. 2008).

The affinity of an indicator is expressed in the dissociation constant K_d. Put simply, it indicates at which calcium concentration half of the indicator is bound. Importantly, one should keep in mind that besides the indicator, K_d also depends on pH, temperature, viscosity, ionic strength, protein binding and the presence of other ions, such as in the case of calcium, that is magnesium (Cossart, Ikegaya et al. 2005). Unlike low-affinity indicators (e.g. OGB-5N), high-affinity indicators (e.g. OGB-1) may already detect small signal changes, however, their dissociation kinetics are slower due to their calcium-buffering effect. For this reason, low-affinity indicators may be more suitable for high-frequency signals. The dissociation constant of an indicator should be chosen, e. g., according to signal intensity, signal-to-noise-ratio, signal frequency and desired signal resolution. Besides, the buffering-capabilities of the indicator and their physiological consequences have to be taken into account. (Tsien 1989, Paredes, Etzler et al. 2008)

In respect of indicator loading and controllability of localisation, one may differentiate two major types: Synthetic calcium indicators and genetically encoded calcium indicators (GECIs) (Grienberger and Konnerth 2012, Looger and Griesbeck 2012). Regarding the loading procedure, there are two important methods: Manually loading of synthetic indicators and cellular expression of genetically-encoded indicators (Grienberger and Konnerth 2012). Making use of distinct promoters, the possible cell-type specific or even organelle-specific

expression is most certainly a major advantage of GECIs. This allows for precisely controlled localization of the indicator. (Rehberg, Lepier et al. 2008, Grienberger and Konnerth 2012) For more details on the loading procedures used in the present thesis, see section 3.6.4.

Besides calcium-sensitive fluorescent indicators, there are plenty of indicators for other ions or substances, such as sodium, magnesium, glutamate or even indicators for changes in voltage (Tsien 1989). One of the major advantages of calcium-sensitive fluorescent indicators, nonetheless, is the excellent signal-to-noise-ratio and their fast kinetics due to the vast transmembrane concentration gradient of calcium (Putney, Eichberg et al. 2006).

In the present thesis, the synthetic non-ratiometric, high-affinity calcium sensitive indicators Oregon Green 488 BAPTA-1 (OGB-1), with an excitation maximum at 488nm and an emission maximum at 520nm (Paredes, Etzler et al. 2008), as well as Cal520, with an excitation maximum at 492nm and an emission maximum at 514nm (Tada, Takeuchi et al. 2014), have been used. Both these indicators base on the calcium-specific chelator 1,2-bis(2-aminophenoxy)ethane-N,N,N',N'-tetraacetic acid (BAPTA). They are well-suited for two-photon microscopy of relative changes in calcium concentration and feature an excellent signal-to-noise quality (Paredes, Etzler et al. 2008, Tada, Takeuchi et al. 2014).

The recorded global dendritic calcium signals of vermal Purkinje neurons *in-vivo* mainly reflect voltage gated calcium channel-mediated calcium-influx, frequently induced upon excitatory climbing fibre synapse activation (Westenbroek, Sakurai et al. 1995, Kitamura and Kano 2013).

3.6.2 Experimental setup and devices

The mouse was head-fixed via the recording chamber into the holder centrally in the set-up. A piezoelectric accelerometer (MP100 Pulse Transducer, ADInstruments) was positioned centrally under a base plate (length: 12cm, width: 12cm) underneath a costume-made treadmill for the mouse. The recorded signal was fed via an analogue-digital-converter (PowerLab 4/25, ADInstruments) to an analysis-computer (Celsius M, Fujitsu Siemens). Both the acoustic stimulation (95dB white noise, 100ms, near-instant rise time) via a costume-built amplifier and a speaker (G25FFL 8Ω, Visaton) as well as the background noise (60dB white noise) via an amplifier (ED1 Electrostatic Speaker Driver, Tucker Davis Technologies) and a speaker (ES1 Electrostatic Speaker, Tucker Davis Technologies) were controlled centrally by this computer. White noise had a bandwidth of 0-50kHz. The inter-stimulation-interval was set and the acoustic stimulation executed by a pulse generator (Master-8, A.M.P.I.). On one experimental condition, harmaline (Sigma-Aldrich, 3mg/kgBW) was administered intraperitoneally. The inner core of the setup was mounted on a motorised positioner (table and controller 8SMC1-USBhf, Standa), which allowed for the exact positioning of the mouse under the microscope. The exposed brain tissue was perfused continuously with fresh and carbogen gas-flushed artificial cerebrospinal fluid at 37°C using a pump (IPS-8, Ismatec).

The microscopy setup consisted of a tuneable, mode-locked, high-peak-power, femtosecond-pulsed Ti:Sapphire-crystal laser with a repetition rate of 80MHz, a pulse width at peak of 140fs and an average power greater than 2.5W (Chameleon Vision, Coherent Chameleon Laser Systems), a shutter (Uniblitz Electronic Shutter, Vincent Associates) with a shutter driver (Uniblitz VCM-D1 Shutter Driver, Vincent Associates), a Pockels cell (Model 350-50, conoptics) with a Pockels cell driver (Model 302, conoptics) for modulation of laser intensity, a set of mirrors (BB1-E03, ThorLabs) for direction of the optical pathway, an optical

beam expander (BE02-05-B, ThorLabs), a scanning system (12KHz CRS resonant scanner and 6215H galvanometer scanner, Cambridge Technology) with a scanning lens (AC254-150-B-ML, ThorLabs), an upright microscope (BX51WI, Olympus) with a water-immersion objective (40X/0.80NA/3.5mmWD, Nikon), a drive for remote-controlled focusing (SM4, Luigs & Neumann) and a photomultiplier tube (H7422P-40, Hamamatsu) for photon detection, positioned after a dichroic mirror (T 795 LPXRXXT, AHF analysetechnik AG via Chroma Technology Corp.). The recorded signal was fed via a modular electronic platform, the PXI-unit (PXIe-1082, National Instruments), to the setup computer (Precision 690, Dell). The entire setup was mounted on an optical table (table RS4000 and stabilizer I-2000, Newport). The laser wavelength was set to 925nm, being in the proximity of the two-photon excitation spectrum optima of the two deployed calcium-sensitive indicators. Average power measured under the objective ranged between 23-73mW and was kept as low as possible for dye and tissue protection. An overview of the experimental setup is displayed in figure 11.

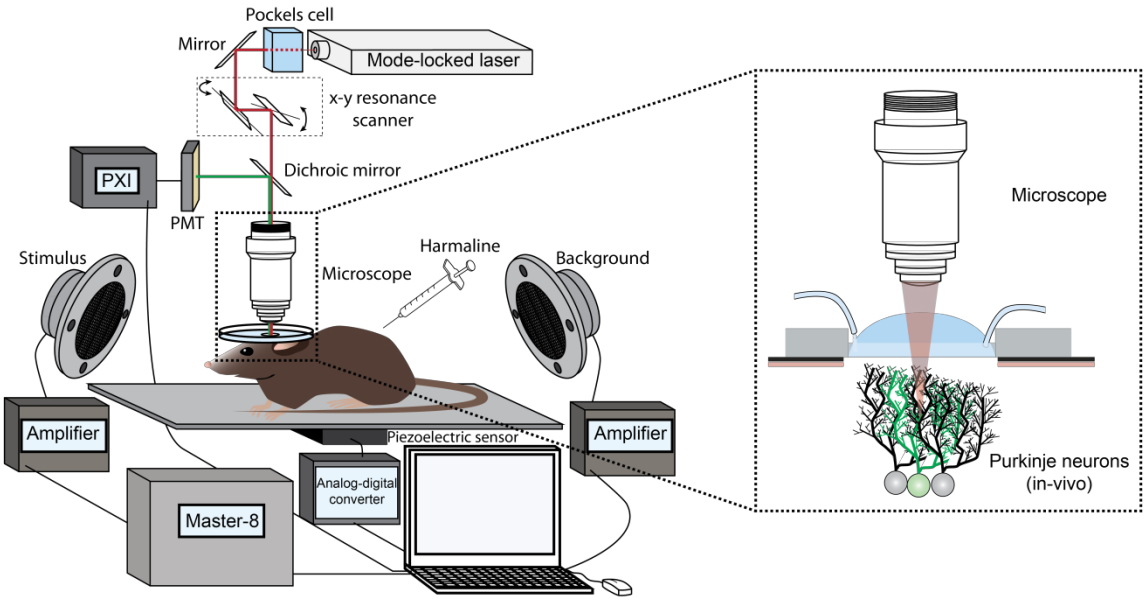

Figure 11: Schematic illustration of the setup for *in-vivo* two-photon calcium-sensitive fluorescent microscopy.

3.6.3 Reagents, pharmaceuticals and solutions

Solutions for *in-vivo* two-photon calcium-sensitive microscopy experiments are listed in table 8. For the reagents and compositions of each solution, kindly consult the respective section mentioned in the table. For anaesthesia and analgesia, which was maintained during loading procedures as well as during combined *in-vivo* single-cell electrophysiological recordings and calcium-sensitive fluorescent microscopy, see section 3.4.2.

Solution	Composition
Artificial cerebrospinal fluid (ACSF)/Carbogen	See 3.4.1
Cal520AM solution	See 3.4.3
OGB-1 6k solution	See 3.4.3
Harmaline solution	See 3.2

Table 8: Solutions used during two-photon excitation calcium-sensitive microscopy

3.6.4 Loading procedure for calcium-sensitive indicators

There are several techniques available for loading calcium-sensitive indicators (Grienberger and Konnerth 2012). This section describes the methods used in the present thesis, i.e., multi-cell bolus loading for Cal520AM and single-cell electroporation for OGB1-6k. For details on the preparation of calcium-sensitive indicators and micropipettes, see 3.4.3. For more information on fluorescent indicators, see 3.6.1.2.

As a lipophilic acetoxymethyl ester derivative, Cal520AM is capable of permeating cell membranes passively through diffusion. Once inside the cell, the ester group, however, is hydrolysed by intracellular esterases. As a result, the indicator is subsequently trapped inside of the cell. (Tsien 1981)

Multi-cell bolus loading is a loading procedure which makes use of acetoxymethyl ester derivatives of different indicators (Stosiek, Garaschuk et al. 2003). It stains all cellular structures within the proximity of the distributed indicator. These are cell somata of neurons and glia cells as well as the neuropil, which consists of dendritic branches, axons, presynaptic boutons and glial processes (Kerr, Greenberg et al. 2005). This has to be taken into account when interpreting the recorded signals.

In contrast, the polar, hydrophilic salt OGB-1 6k is loaded into the cell via a process called electroporation. Electroporation may be used for single-cell loading as well as for staining of smaller cell arrays (Grienberger and Konnerth 2012). A short-lasting electromagnetic pulse disrupts the integrity of the cell membrane by creating pores, through which the dye is subsequently driven. Shortly after, the cell membrane restores its integrity with the dye now being trapped inside of the cell. (De Vry, Martinez-Martinez et al. 2010)

For loading procedures, animals were head-fixed via the recording chamber into a holder centrally in the set-up after surgery. In case of dye bolus loading, a freshly-pulled pipette (2-3MΩ) was filled with 5µl Cal520AM indicator solution and low positive pressure was applied. The pipette was directed into the characteristic Purkinje cell layer within the designated recording site (approximately 150µm from the surface). Until final placement of the pipette, this procedure was performed under microscopy-guidance. Subsequently, positive pressure was raised to 12.5kPa. After 1min, the pipette was retracted to the surface in a total of 4 steps of equal distance (approx. 25µm), at each step pausing for 1min, respectively. At the end of the last step, positive pressure was terminated and the pipette was removed entirely. As a result, staining was established in an area of several hundred µm in extent. Recordings were started 1.5h after loading.

In case of electroporation, a freshly-pulled pipette (5-5.5MΩ) was filled with 5µl OGB-1 6k indicator solution and low positive pressure was applied. Under microscopy-guidance, the pipette was directed into the Purkinje-cell layer and a single cell was selected using the shadow-patching approach (for more details on this approach see 3.5.4.). In the immediate proximity of the designated cell, one or a maximum of two pulses of 2.5µA at 50ms were delivered to the soma via a microelectrode within the pipette and the dye was driven into the cell. This was done by using a pulse stimulator (Model 2100 Isolated Pulse Stimulator, A-M Systems). Recordings were started 1.5h after recording.

Pipettes for multi-cell bolus loading and electroporation were guided using a micro-manipulator (Junior, Luigs & Neumann) together with its manipulator control panel (SM5, Lugis & Neumann).

Figure 12 illustrates the methods used for indicator loading in the present thesis. Additionally, it shows images of a Purkinje neuron before and after electroporation. In figure 1 of section 1.2, the layers of the cerebellar cortex are shown stained after multi-cell bolus loading.

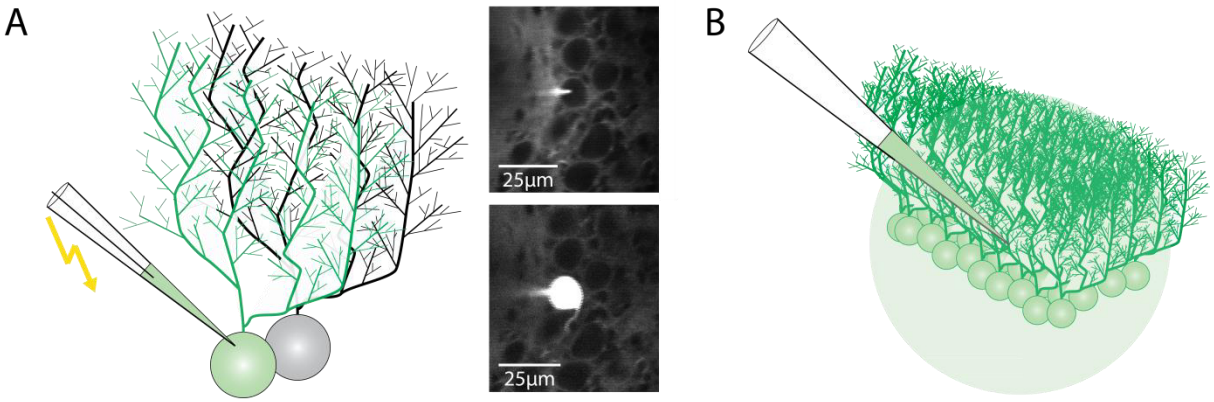

Figure 12: Illustration of the methods used for calcium-indicator loading (after Grienberger and Konnerth 2012). (A) Left: Illustration of single-cell electroporation of a Purkinje neuron. Right: Images taken from calcium-sensitive fluorescent microscopy during single-cell electroporation of a Purkinje neuron. Upper: Before electroporation. Lower: After electroporation. (B) Illustration of multi-cell bolus loading of a Purkinje neuron population.

3.6.5 Experimental protocol

1.5h after loading of the calcium-sensitive indicator Cal520AM and reduction of anaesthesia, mice were exposed to continuous background noise of 60dB for acclimation 10min prior to the respective experiment. Acoustic startle stimulation was delivered by white noise of 95dB and 100ms on continuous 60dB background white noise (see also 3.6.2).

In case of experiments on ASR suppression, control recordings (n=3-4) with inter-stimulus-intervals (ISI) of ≥15s were acquired within a maximum of 2min. After a 1Hz-stimulation period of 1min without data acquisition for startle suppression and animal calming, multiple recordings were taken during another 4-5min of 1Hz-stimulation. Finally, recordings (n=4-6) at an ISI of ≥15s were acquired during recovery (5min). Figure 22 in section 4.7 illustrates the protocol. Basis was the respective protocol from behavioural testing (see 3.3.4).

In case of experiments on the ASR under harmaline, control recordings (n=2-4) were taken within 2min with an ISI ≥15s. These were followed by immediate harmaline administration at 3mg/kgBW under short isoflurane anaesthesia. After a 30min break, recordings (n=4-8) were taken within a period of 5 to 30min during harmaline-tremor and at an ISI ≥15s. The protocol based on previous findings (section 4.9) and is illustrated in figure 30 in section 4.11.

Another set of experiments after single-cell electroporation with OGB-1 6k was performed together with *in-vivo* single-cell electrophysiology. Besides spontaneous recordings, these were combined on one condition with harmaline application intraperitoneally (3mg/kgBW) See section 3.5 for the protocol, more information on *in-vivo* electrophysiology and figure 28 in section 4.10 for an illustration of the protocol.

Calcium-sensitive microscopy of Purkinje cell dendrites was performed in the upper third of the molecular layer of the vermis in the stained area given by the coordinates of the craniotomy (see 3.4.2 for the exact coordinates and the surgical procedure).

3.7 Data acquisition, processing and analysis

Raw data of behavioural experiments was acquired from the piezoelectric sensor as changes in voltage over time via the analogue-digital converter using the recording software LabChart (Version 8, ADInstruments) either at 1kHz in case of mere behavioural experiments, or at 12kHz in case of combined behavioural experiments and calcium-sensitive fluorescent microscopy. For offline data processing and analysis, files were subsequently exported to MATLAB (R2014b, Version 8, 64-bit, MathWorks). The absolute startle response amplitude was determined as the maximum of the absolute voltage value within a 100ms time window after auditory stimulation using a self-written script in MATLAB. Frequency spectra were calculated using MATLAB's fast Fourier transform function.

For electrophysiology, raw data was acquired from the microelectrode as changes in current over time via the recording amplifier using the recording software PatchMaster (Version 2x42, HEKA Elektronik) at 12kHz. Files were transferred into MATLAB (R2014b, Version 8, 64-bit, MathWorks) for offline data processing and analysis. In MATLAB, a self-written script allowed for complex spike detection by their characteristic shape (i.e. their spikelets) and, subsequently, the calculation of their frequency and the frequency of simple spikes.

Raw data of calcium-sensitive fluorescent microscopy experiments was acquired from the photomultiplier tube and via the modular electronic unit using a costume-designed recording software based on LabView (Version 14, 64-bit, National Instruments), reconstructing images from the scanning process at a frame rate of either 40 or 80Hz in case of population imaging after multi cell bolus loading, or at 240Hz in case of single-cell imaging after electroporation.

Subsequently, dendritic trees of Purkinje neurons were identified offline in computed time lapse videos of raw images and set as regions of interest (ROIs) for further calculation in a costume-written analysis software based on LabView (Version 14, 64-bit, National Instruments). Raw calcium signals were calculated as the spatial average of all pixels in a ROI. For subtraction of background fluorescence, ROIs were set on unstained regions (e.g. blood vessels). Briefly, relative changes in fluorescence of ROIs, used to display changes in calcium concentration, were subsequently calculated as follows (Jia, Rochefort et al. 2011):

$$R(t) = \frac{F(t) - F0(t)}{F0(t)} = \frac{\Delta F(t)}{F0(t)}$$

Where R(t) is the relative change in fluorescence of one pixel in the ROI at time t, F(t) is the fluorescence of that pixel at time t and F0(t) is the ground level fluorescence of the pixel, immediately before time t. Some data was filtered with an exponentially weighted moving average filter. For more details on the calculation and filtering see Jia et al. 2011.

Files of relative fluorescence change over time of a ROI were subsequently imported in MATLAB (R2014b, Version 8, 64-bit, MathWorks) for data analysis with self-written scripts. In MATLAB, calcium transients were identified by their shape and time course (i.e. steep rise time in the millisecond-range and at least three fold the standard deviation of the ground level fluorescence of the recording). Single exponential fits to determine decay times were applied using MATLAB's curve fitting tool. Amplitudes were calculated as the difference of the calcium transient peak to its minimal base within 50ms before rising. Synchronicity of cell activity in population recordings was defined as the presence of a calcium transient peak in a time window of respectively 25ms before and after a calcium transient peak of the reference cell.

In case of auditory stimulation, a calcium transient was considered responsive only if both its beginning was within a 100ms time window after stimulation and with no precedent transient onset at the time of stimulation

Adobe Illustrator (CS5, Version 15, Adobe Systems Incorporated) was used for generation of figures. For more details on the experimental instrumentation, kindly consult the respective section on the experimental setup and devices of each method.

3.8 Statistical analysis

Statistical analysis and visualisation were performed in MATLAB (R2014b, Version 8, 64-bit, MathWorks). Statistical tests deployed were the Kolmogorov-Smirnov-Lilliefors-test on normal distribution and the paired-sample t-test. A p-value of <0.05 was considered significant.

4. Results

The first part of the results will focus on experimental findings concerning the acoustic startle response, its habituation upon repetitive stimulation and associated *in-vivo* signals in Purkinje neurons evoked by acoustic startle stimulation. In the second part of the results, behavioural and neurophysiological findings in context of harmaline-induced cerebella tremor are presented. Minor aspects of the present findings will be reviewed directly in this chapter. For the general discussion, however, consider chapter 5.

4.1 Acoustic startle response – general appearance and responses to repetitive stimulation

Under the specified stimulus parameters of 100ms of 95dB white noise for stimulation presented over a continuous 60dB white noise background, every stimulus was able to reliably elicit an acoustic startle response (ASR). For the ASR had a clear appearance in the whole-body accelerometer measurements, that is, a high signal-to-noise ratio, it was easily identifiable. In figure 13A an example trace of a series of four ASRs is shown together with the magnification of a single ASR. As abundantly described (Landis and Hunt 1939, Horlington 1968, Koch 1999, Valsamis and Schmid 2011), the present data affirmed that the ASR is a short latency response, having an onset in the millisecond range, and consisted of an initial steep incline to a peak (startle response proper) and a variable oscillation fluctuating back to the baseline.

Also visible in figure 13A, the startle response amplitude had some degree of variation in magnitude within an individual animal. Hence, for general statements on the time course and temporal progression of the ASR, averaged recordings of a larger sample were preferable. This is a standard routine (Davis 1970, Koch 1999, Simons-Weidenmaier, Weber et al. 2006, Davis, Antoniadis et al. 2008, Valsamis and Schmid 2011).

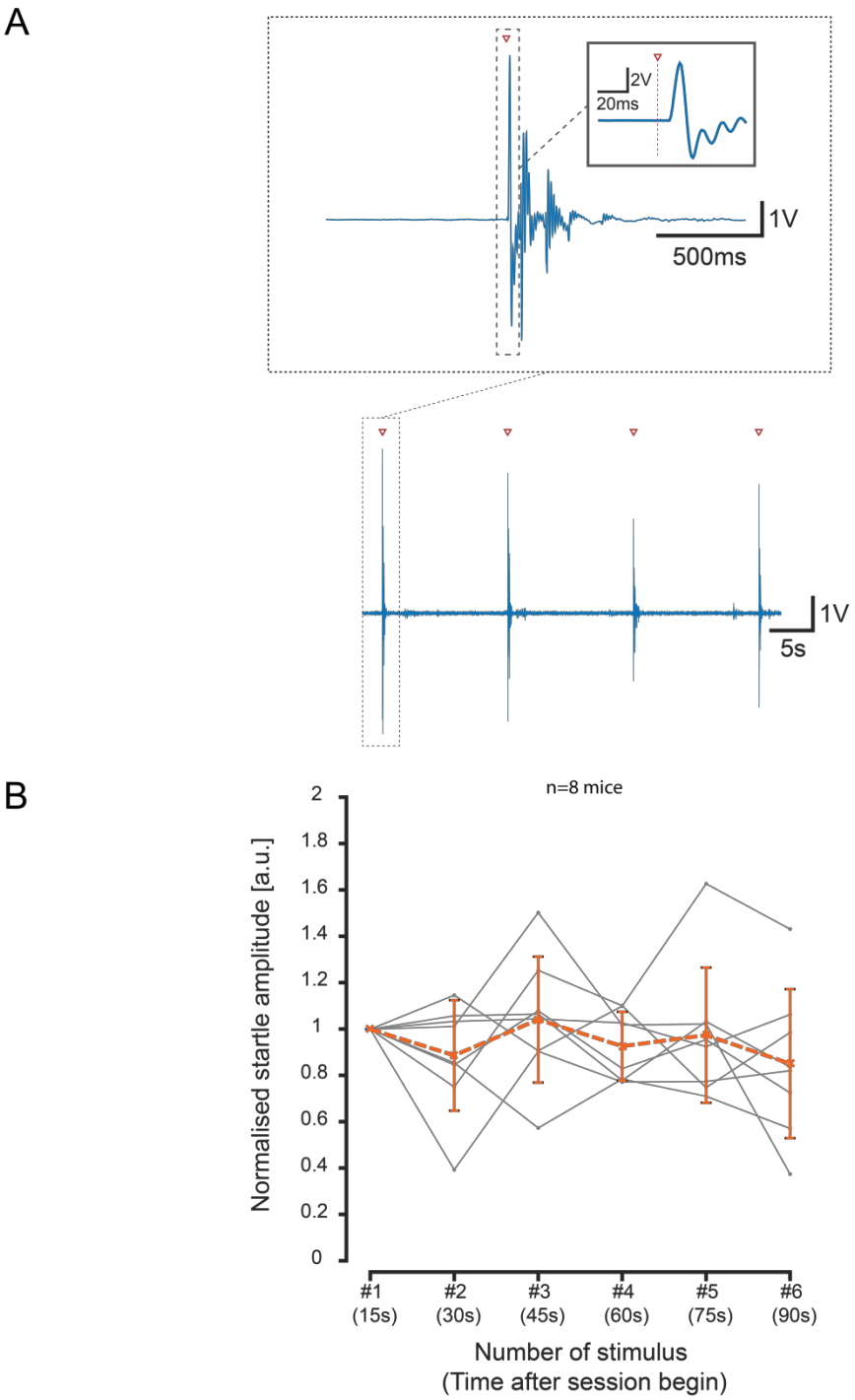

Figure 13: The acoustic startle response - general appearance and response signals upon repetitive stimulation. (A) Upper: Magnification of a startle response from the example trace below as indicated by dotted box. Inset: Extension of the startle response initiation and peak (startle response proper). Lower: Example trace of a series of four startle responses elicited at a 15s inter-stimulus-interval. Red triangles and red dotted line indicate acoustic stimuli. (B) Normalised startle amplitudes over a time course of six stimuli (session time: 90s) from 8 mice (grey lines) and their group average (orange line). Error bars represent standard deviation.

Absolute startle amplitudes differed considerably among animals. Besides, the magnitude depended, for instance, highly on the animal's positioning relative to the sensor underneath the startle chamber. Therefore, startle amplitudes were normalised to an animal's first startle, a common procedure which allows comparison of calculated ratios across animals and plotting of a time course of the mean from several animals (Davis 1970, Simons-Weidenmaier, Weber et al. 2006, Valsamis and Schmid 2011).

Figure 13B shows normalised startle amplitudes from eight mice (grey lines) and their mean (orange line) over the time course of six stimuli. Again, one notices variation in responses of each mouse and variability across animals. Repetitive stimulation at 15s inter-stimulus-intervals (ISI) was accompanied by a tendency of the mean to decline to approximately 85% of the initial startle at the last stimulus. A progressive decrease is referred to as startle habituation. Comparable values of startle habituation to 15-20s ISIs in mice have been reported (Dirks, Groenink et al. 2002, Valsamis and Schmid 2011, Typlt, Mirkowski et al. 2013). Since the plotted means in figure 13B displayed relative temporal stability within the given conditions, they were used as control in subsequent experiments (4.2 and 4.9).

4.2 Stimulation frequency-dependent suppression of the acoustic startle response

In order to provoke maximisation of the phenomenological appearance of acoustic startle response (ASR) reduction, the stimulation frequency was increased to 1Hz. Furthermore, this high-frequency stimulation was integrated in a protocol consisting of a sequence of different stimulation frequencies which allowed for comparison of three controlled stages: An initial stage of 15s inter-stimulus-intervals (ISI), defined as control, was followed by an interventional stage of 1Hz high-frequency stimulation and eventually concluded by another stage of 15s ISIs. The precise protocol may be found in figure 14A.

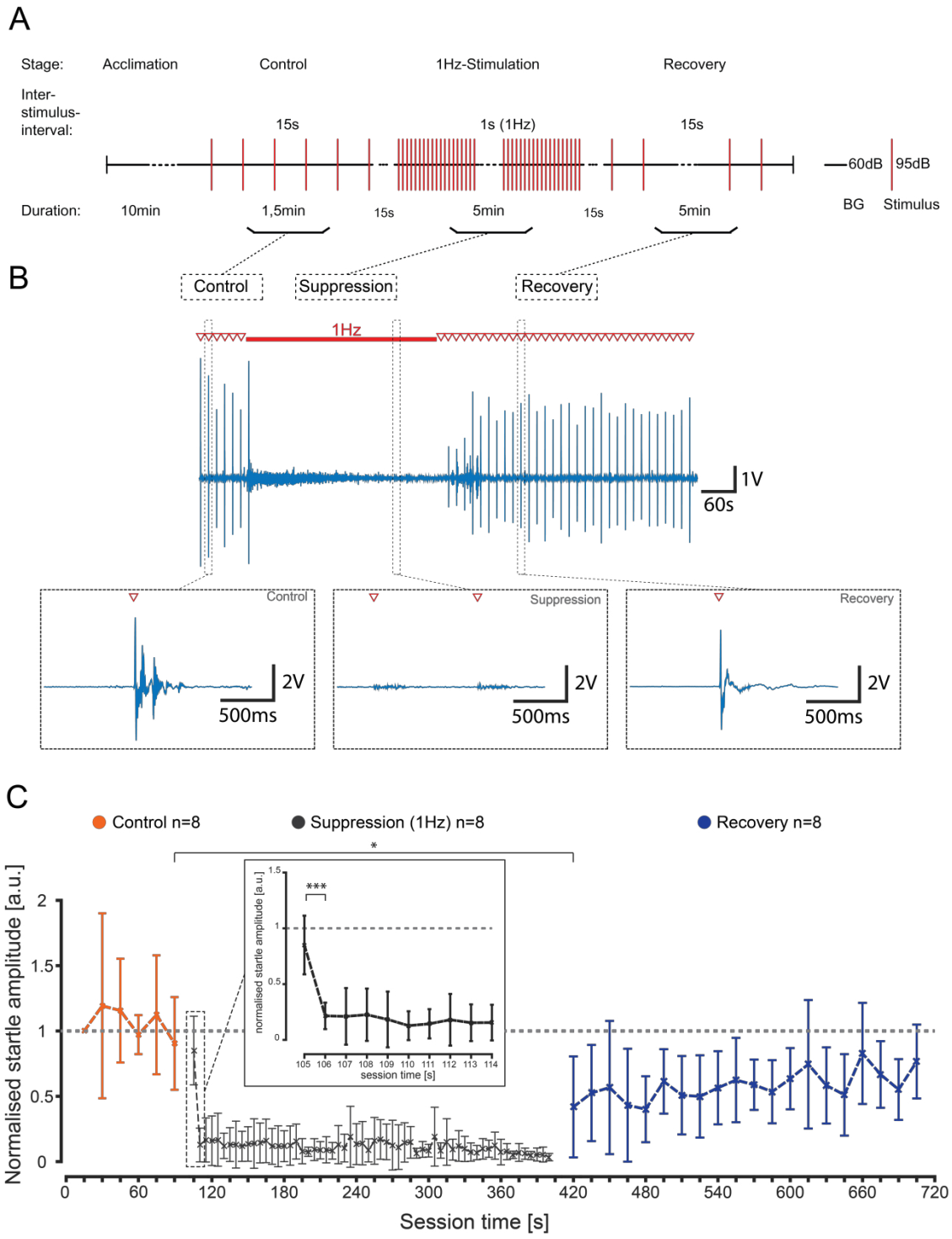

Figure 14: Stimulus frequency-dependent suppression of the acoustic startle response.
(A) Experimental protocol. Background noise (BG). (B) Upper: Example trace of a session according to protocol. Lower: Magnifications of startle responses taken from the different stages of the example trace as indicated by dotted boxes. Red triangles indicate acoustic stimuli. (C) Course of the mean normalised startle amplitude of 8 mice. Colours indicate different stages as indicated. For the suppression stage every fifth mean is shown. Inset: Magnification of inital 10 stimuli during 1Hz-stimulation. Error bars represent standard deviation.

Figure 14B shows an example trace of a single trial according to this protocol and 14C the time course of the mean normalised startle amplitudes from a sample of eight mice. Under control conditions, the mean normalised ASR amplitude remained relatively stable with only a subtle decline in amplitude of the last startle to approximately 90% of the initial startle, which was comparable to the decline already seen in 4.1. Remarkably, the subsequent 1Hz stimulation resulted in a highly-significant, nearly-complete suppression of the ASR within the first stimuli (t-test, p=0.00012). During the course of high-frequency stimulation, the startle amplitude decreased further from initially 22±12% (mean±s.d.) after the first 1s ISI to approximately 3±3% (mean±s.d.) at the end of the stage. Additionally, the set amplitude seemingly lessened in variation. At recovery, the amplitude immediately increased to 42± 39% (mean±s.d.) after the first 15s ISI, nonetheless, remaining significantly reduced to control conditions (t-test, p=0.0125). The mean then gradually recovered to 77%.

The intervention was, thus, able to induce both a reduction occurring directly during high-frequency stimulation as well as a temporally-sustained reduction during the 5min observational period after intervention. The 1Hz-intervention led, moreover, to a subtotal suppression of the ASR. Especially compared to the low reduction apparent under initial control conditions, this demonstrated the stimulus frequency-dependence of ASR-reduction. Whereas at control and recovery the stereotypic appearance of the ASR remained, at high-frequency suppression the response was admittedly still present, however, only visible as a noise-band lacking the typical ASR-shape (see magnifications in figure 14B).

Due to its critical reduction of the ASR, the protocol was termed “startle suppression”. It was used, henceforth, to unambiguously reduce the ASR in subsequent behavioural experiments in head-fixed animals during calcium-sensitive microscopy experiments and allowed for controlled and distinct experimental stages.

4.3 Spontaneous synaptically-evoked somatic electric responses of Purkinje neurons

In the first step towards the connection of behavioural tests on the acoustic startle response and experiments on cerebellar neurophysiology, *in-vivo* single-cell electrophysiology of Purkinje cells (PCs) was established in anaesthetised mice. By characterising spontaneous signals recorded extracellularly-attached at PCs somata, electrophysiology set the foundation for subsequent interpretation of signals and hypothetic signal changes observed in calcium-sensitive fluorescent microscopy. Calcium imaging was selected the method of choice regarding a combination with behavioural testing since stable somatic electrical recordings under conditions of repetitive whole-body startling in awake, alert mice did not seem feasible at this point.

After the formation of loose-patch cell-attached somatic recordings, spontaneous neuronal activity of single PCs could be observed. Due to the high signal-to-noise ratio of the recordings, action potentials reflecting the neuronal output of a PC were clearly identified. Furthermore, two distinctive types of signals were discernible – firstly, the so-called simple spike (SS) representing supra-threshold activation as a computational result of synaptic parallel fibre-input transmission and, secondly, the so-called complex spike (CS) reflecting climbing fibre synapse-mediated supra-threshold activation (see section 1.2 for basic cerebellar neuroanatomy and neurophysiology). SSs resembled the stereotypic course of an action potential. In contrast, the typical shape of a CS was characterised by the strong climbing fibre synapse-mediated depolarisation followed by a prolonged after-depolarisation period. As a result, this activation caused formation of additional wavelets, so-called spikelets, after the initial action potential. A sample trace of the spiking activity of a Purkinje neuron *in-vivo* as well as depictions of the two characteristic types of signals – the CS and SS - are shown in figure 15A.

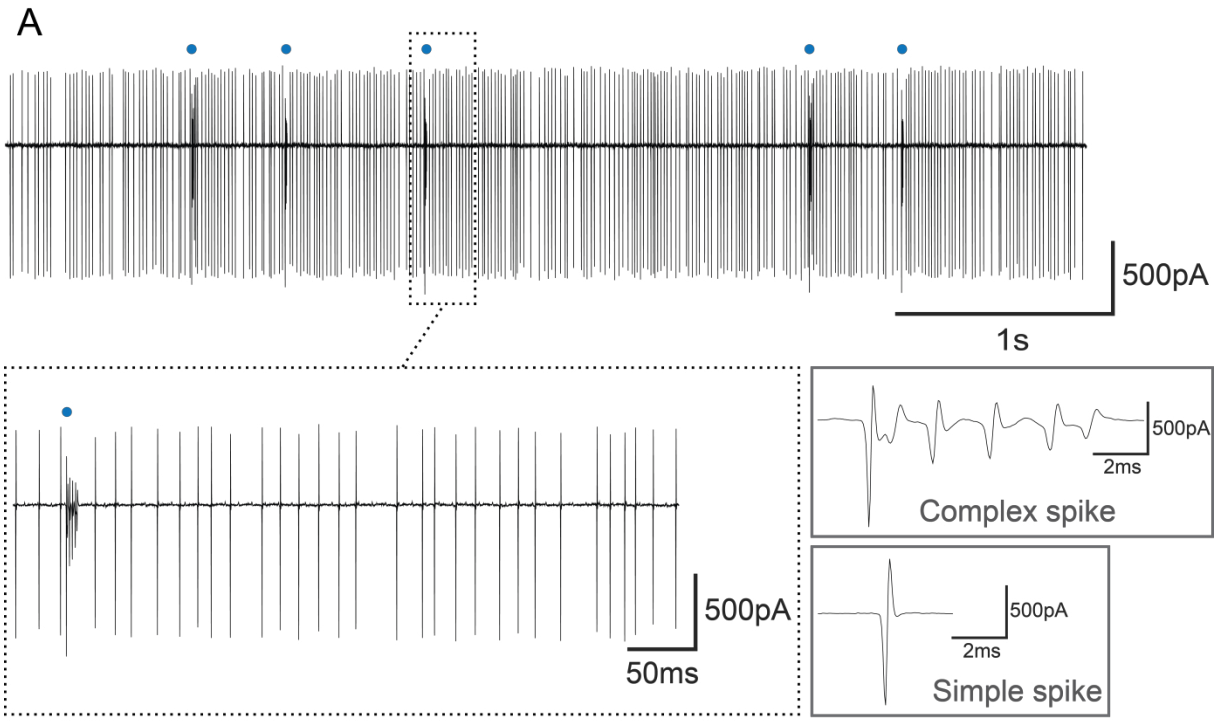

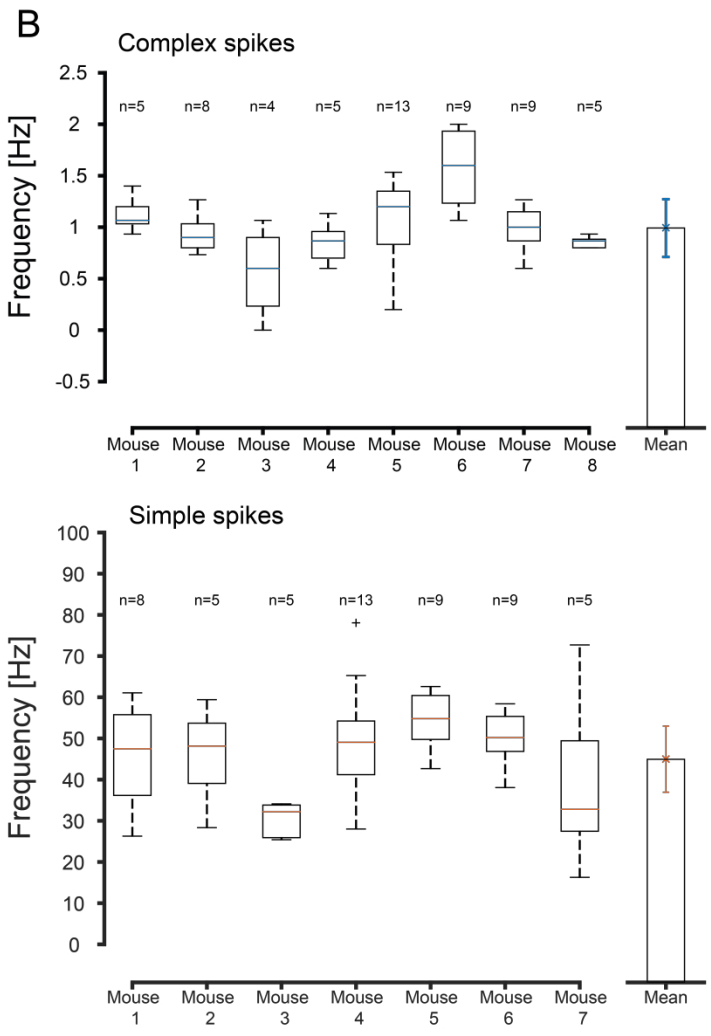

Figure 15: Synaptically-evoked somatic electric responses of Purkinje neurons *in-vivo* - frequency ranges of complex and simple spikes.
(A) Upper: Example trace of spontaneous electrophysiological responses recorded in the cell-attached configuration at the soma of a Purkinje neuron *in-vivo*. Lower: Left box: Magnification taken from the example trace as indicated by the dotted box. Right boxes: Extensions of the two characteristic response signals, i.e., the complex spike (upper-right box) upon climbing fibre synapse-input and the simple spike (lower-right box) reflecting suprathreshold parallel fibre synapse-transmission. Blue dots indicate complex spikes. (B) Upper: Frequency ranges of complex spikes from 8 cells in 8 mice and their mean. Lower: Frequency ranges of simple spikes from 7 cells in 7 mice and their mean. Number of recordings indicated by n (15s/recording). Box plots represent quartile points with whiskers indicating range of extremes, crosses indicating outliers and blue/orange lines indicating median. Orange/Blue error bars show standard deviation of the mean.

CS and SS differed considerably in frequency, with CS occurring at a mean rate of 0.99± 0.28Hz (mean±s.d., n=8 cells in 8 mice) and SS occurring at a mean rate of 44.97±8.02Hz (mean±s.d., n=7 cells in 7 mice). Moreover, CS and SS, respectively, showed a dynamic range of frequencies over the course of time in a given cell. In this respect, complex spike frequencies reached a maximum of 2Hz and a minimum of 0Hz, whereas simple spike frequencies ranged between 72.7Hz and 16.3Hz in the present recordings. In figure 15B, frequency ranges of complex spikes (upper graph, 8 cells in 8 mice, n indicates number of 15s-recodings in a cell) as well as of simple spikes (lower graph, 7 cells in 7 mice, n indicates number of 15s-recodings in a cell) across different mice are compared.

4.4 Spontaneous synaptically-evoked global dendritic calcium signals of Purkinje neurons

After establishing *in-vivo* single-cell electrophysiology, in the second step, electric somatic responses were correlated with simultaneous recordings of global dendritic calcium signals from single-cell electroporated neurons with OGB-1 6k. Complex spikes (CS) and simple spikes (SS) were present in electroporated Purkinje neurons (PCs) at equal frequencies as in previous experiments. Recorded signals in calcium-sensitive microscopy resembled the stereotypic course of calcium transients. A representative global dendritic calcium transient is depicted in figure 16C (lower trace), once unfiltered (black line) and once filtered (smooth grey line, standard for subsequent figures). Notably, all detected calcium transients co-occurred to CSs from somatic recordings and vice versa. As such, they appeared at the known mean frequency of approximately 1Hz. This suggested that these global dendritic calcium transients originated from synaptic climbing fibre input. Global dendritic calcium transients and their co-occurrence to somatic complex spikes recorded simultaneously in *in-vivo* electrophysiology and calcium-sensitive microscopy are demonstrated in figure 16.

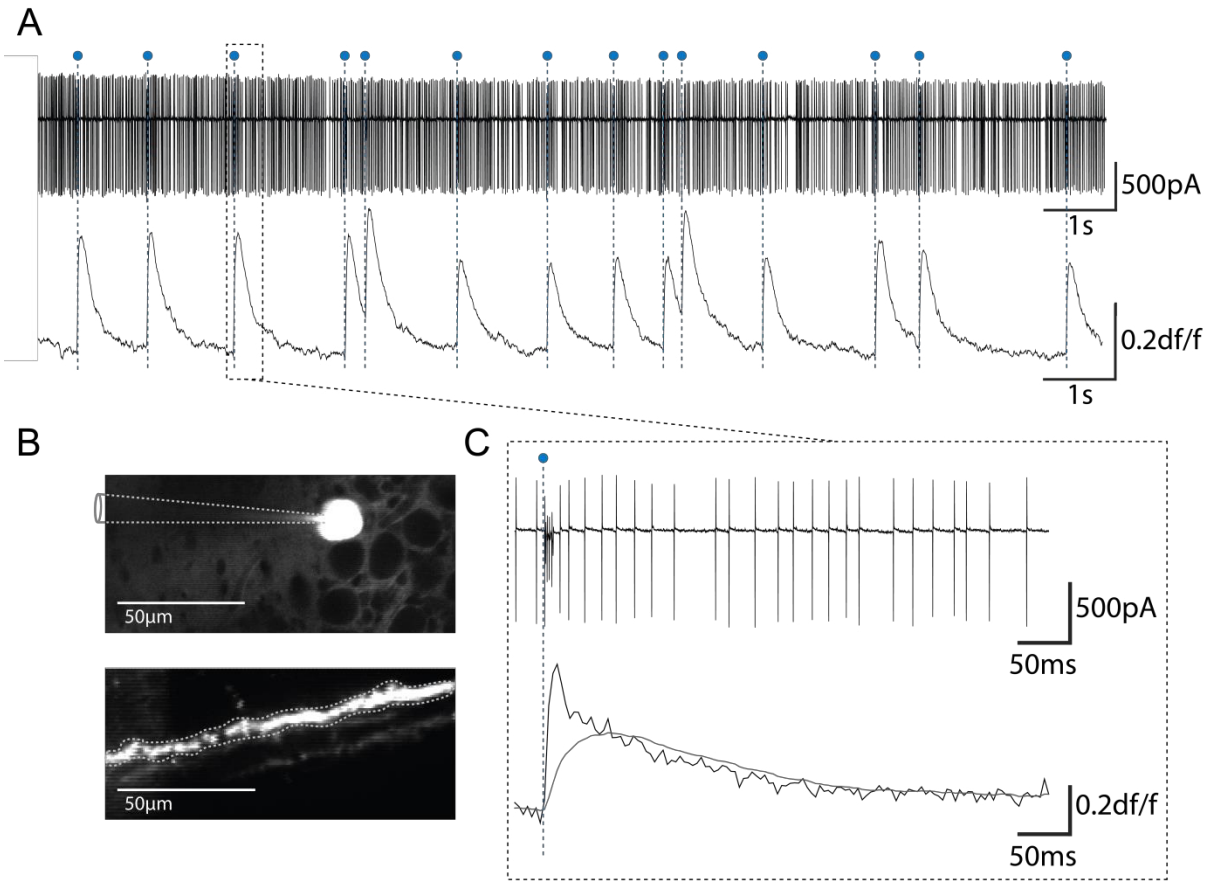

Figure 16: Synaptically-evoked global dendritic calcium transients in a single-cell electroporated Purkinje neuron with OGB-1 6k *in-vivo*. (A) Simultaneous single-cell electrophysiology and calcium-sensitive fluorescent microscopy of a Purkinje neuron *in-vivo*. Upper: Example trace of spontaneous electrophysiological responses recorded extracellularly-attached to the soma. Lower: Corresponding trace of spontaneous global dendritic calcium signals recorded in the upper third of the cerebellar molecular layer. (B) Images (xy-plane) taken from calcium-sensitive fluorescent microscopy. Upper: Patch-pipette (indicated by dotted lines) at the calcium indicator-filled soma of the recorded Purkinje neuron. Lower: Calcium-indicator filled dendritic tree of the Purkinje neuron in the upper third of the cerebellar molecular layer. Region of interest for calculation of calcium signal as indicated by dotted line. (C): Magnification of a single calcium transient (lower trace, black line: unfiltered, grey/smooth line: filtered) co-occuring to a complex spike response in somatic electrical recordings (upper trace) taken from the example trace in (A) as shown by the dotted box. Blue dots indicate complex spikes. Blue lines illustrate complex spike-global dendritic calcium transient co-occurrence.

Indeed, there are multiple studies which assign global dendritic calcium transients to climbing fibre-mediated synaptic input (Konnerth, Dreessen et al. 1992, Miyakawa, Lev-Ram et al. 1992, Kitamura and Hausser 2011, Kitamura and Kano 2013). As such, somatic CSs and global dendritic calcium transients reliably served as indicators for presence of synaptic climbing fibre-input and cross-validate each other.

As mentioned above, recorded calcium signals comprised of the typical structure of a calcium transient. After an initial steep rise to its peak, the signal declined by an exponential decay. For a more detailed characterisation, transients were compared regarding peak amplitudes and decay time constants both in a given PC and across PCs. Figure 17A superimposes 14 calcium transients (grey traces) exemplarily taken from a single recording of an OGB-1 6k-stained PC. Additionally, their average (black trace) and the single exponential fitting curve to its decay (blue line) are illustrated. The fitting curve served for calculation of the decay time constant (τ=136ms).

In figure 17B, ranges of calcium transient amplitudes from different cells are compared (6 cells in 6 mice, n=10 transients/cell). Although peak amplitudes differed considerably among cells, the extent of amplitude range was comparable between them. Considering the inaccuracy of the loading procedure, differences in peak amplitudes among cells, on the one hand, could be explained by uneven intracellular indicator quantity resulting in disparity of generated fluorescent signals. On the other hand, similarity of amplitude ranges was in accord with the shared common origin of the signals. Amplitude variations in global dendritic calcium transients have been reported in other studies (Kitamura and Hausser 2011, Kitamura and Kano 2013, Najafi, Giovannucci et al. 2014, Roome and Kuhn 2018) and will be discussed in section 5.2.2.

Decay time constants of mean calcium transients of different PCs are compared in figure 17C (6 cells in 6 mice, n=10 transients/cell). The average signal decay had a time constant of 155±30ms (mean±s.d.). The similarity of the decay time constants pointed again to the shared common physiology of the signals. Additionally, it confirmed the stability of the method. Comparable values for decay time constants of global dendritic calcium signals in Purkinje cells electroporated with OGB-1 have been reported (Kitamura and Hausser 2011).

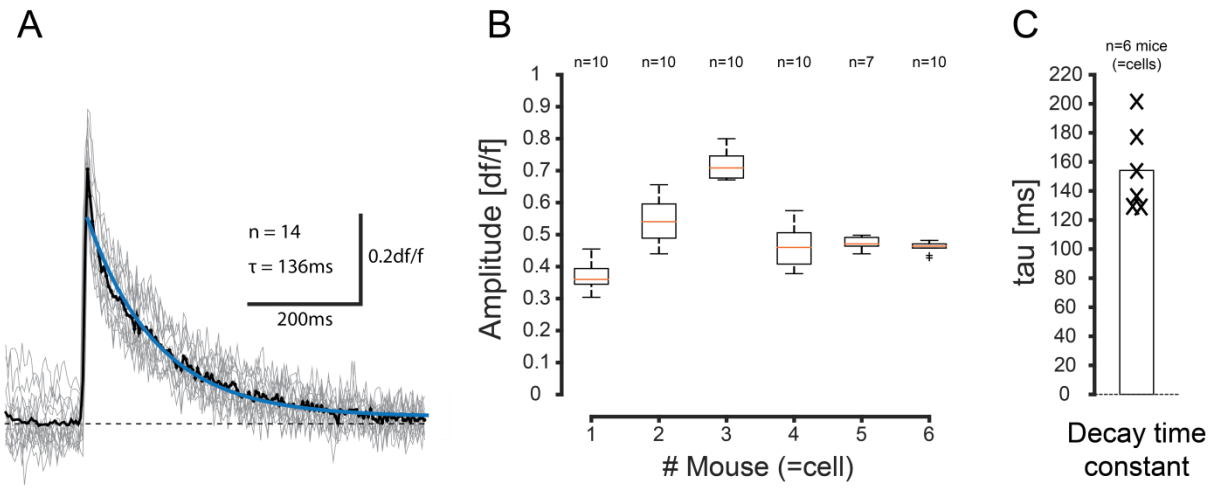

Figure 17: Characterisation of synaptically-evoked global dendritic calcium transients in single-cell electroporated Purkinje neurons with OGB-1 6k *in-vivo*. (A) Superposition of 14 global dendritic calcium transients (grey lines) taken from one recording of a Purkinje cell, their mean (black line) and its approximated single exponential fit to the decay (blue line). Decay time constant (τ). (B) Ranges of calcium transient amplitudes from 6 cells in 6 mice (n=number of calcium transients/cell). Box plots defined as in fig. 15. (C) Decay time constants of mean calcium transients (10 calcium transients/cell for mean) from 6 cells in 6 mice. Bar indicates group average.

Taken together, comparable ranges of calcium transient amplitudes and similar values of decay time constants lent support to conformity of recorded calcium signals. In this respect, somatic electrical recordings revealed that a shared common origin of global dendritic calcium transients was to be found solely or at least primarily in synaptic climbing fibre-input.

4.5 Spontaneous global dendritic calcium signals in Purkinje cell populations of awake mice

In the final preparatory step before combining behavioural experiments with calcium-sensitive microscopy, spontaneous global dendritic calcium signals of Purkinje neurons (PCs) were recorded in awake animals, for these mice could be subsequently exposed to acoustic startle stimulation and undergo behavioural testing. Furthermore, instead of sparse and restricted single-cell labelling, larger populations of PCs were stained using the multi-cell bolus loading approach. Besides statements on spatial relationships among neighbouring

PCs, this allowed for a drastically higher yield of observable cells for analysis. For this purpose the membrane-permeable indicator Cal520AM was used. Figure 18 displays spontaneous global dendritic calcium activity of four neighbouring PCs simultaneously recorded in an awake mouse. Due to the high signal-to-noise-ratio, calcium transients were readily identified. Spontaneous transients occurred at a frequency of 1.21±0.14Hz (mean± s.d., n=15 cells in 5 mice), consistent with prior experiments. Notably, additional, smaller signals could be observed, potentially reflecting distinct calcium signals, which, however, were not rated transients under the parameters of the transient identification algorithm.

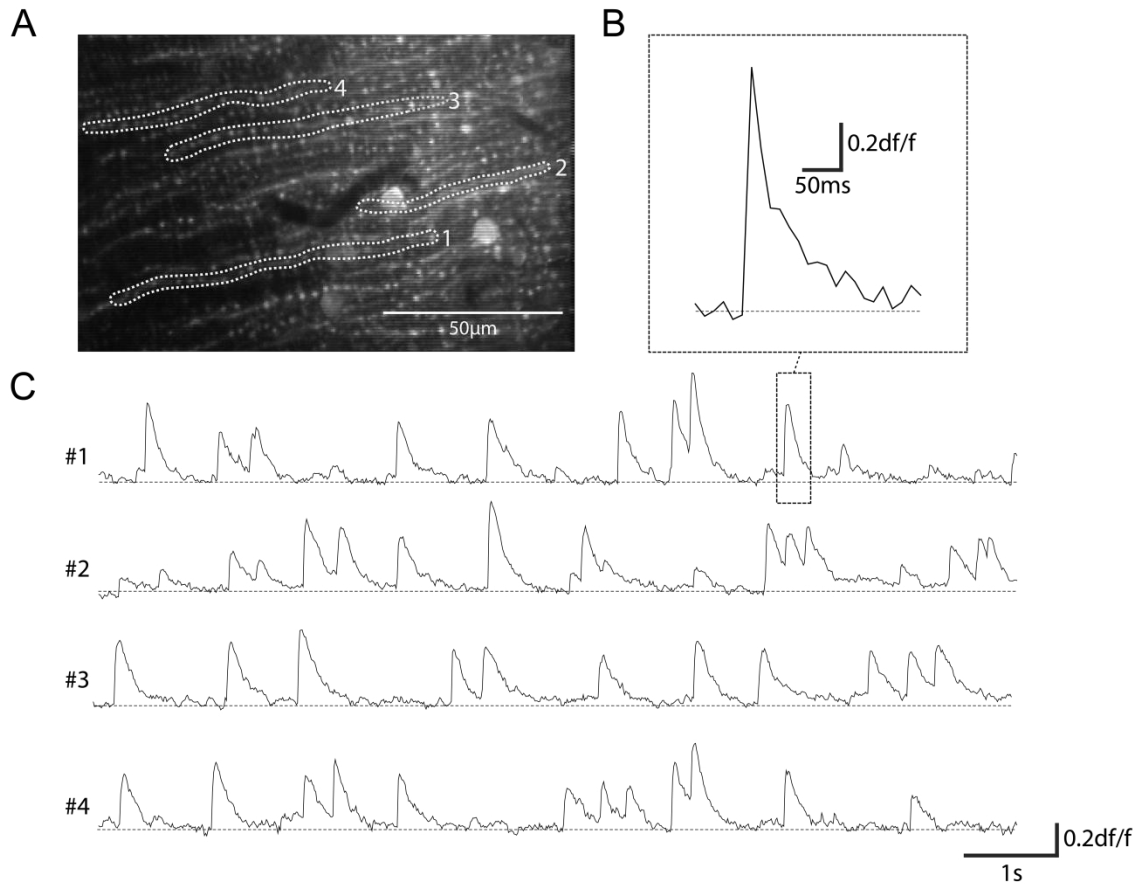

Figure 18: Spontaneous global dendritic calcium signals in a population of neighbouring Purkinje neurons multi-cell bolus stained with Cal520AM *in-vivo*. (A) Image (xy-plane) taken from *in-vivo* calcium-sensitive microscopy. Dotted lines indicate regions of interest on dendrites of different Purkinje neurons used for calculation of the calcium signals in (C). Adjoining numbers correspond to the numbers of calcium traces in (C). (B) Magnification of a single calcium transient taken from (C) as shown by the dotted box. (C) Simultaneous recording of spontaneous global dendritic calcium signals from a population of 4 neighbouring Purkinje neurons *in-vivo*.

In figure 19A, ten calcium transients from a single recording of a Cal520AM-stained PC are superimposed (grey traces), together with their group average (black trace) and the single exponential fitting curve to its decay (blue trace, decay time constant τ=95ms). Peak amplitude ranges of different Cal520AM-stained PCs are shown in figure 19B (5 cells in 5 mice, n=10 transients/cell). As previously seen in electroporated cells with OGB-1, the peak amplitude in a given cell displayed some degree of variation. Likewise, the detected calcium transients showed again considerable differences in peak amplitudes in-between cells, with their amplitude ranges, yet, being once more comparable. The similarity in extent of amplitude ranges across PCs is once again demonstrated in figure 19C, in which both amplitude ranges from OGB-1 6k-electroporated PCs and amplitude ranges from Cal520AM-stained PCs are contrasted after normalisation of each range to its maximum amplitude.

Non-normalised peak amplitudes of calcium transients were generally higher in Cal520AM-stained PCs than in OGB-1 6k-electroporated cells (compare figures 17B and 19B). Besides, decay time constants of calcium transients in Cal520AM-stained cells were shorter (figure 19D). The average decay had a time constant of 79±10ms (mean±s.d., n=5 cells in 5 mice, 10 transients/cell). Comparable findings concerning shorter time constants as well as higher amplitudes of Cal520AM compared to OGB-1 have been reported (Tada, Takeuchi et al. 2014).

Analysis of synchronism of calcium transients among four neighbouring PCs revealed both asynchronicity (48% of reference events) and intermittent but variable synchronicity (52% of reference events). Notably however, there was no instance in which all cells were entirely in synchronism (figure 19E, observation time: t=18s, transients as reference events: n=21). As such, the presence of asynchronous stages validated the capability of the methodology to identify individual dendritic trees of distinct PCs in multi-cell staining approach.

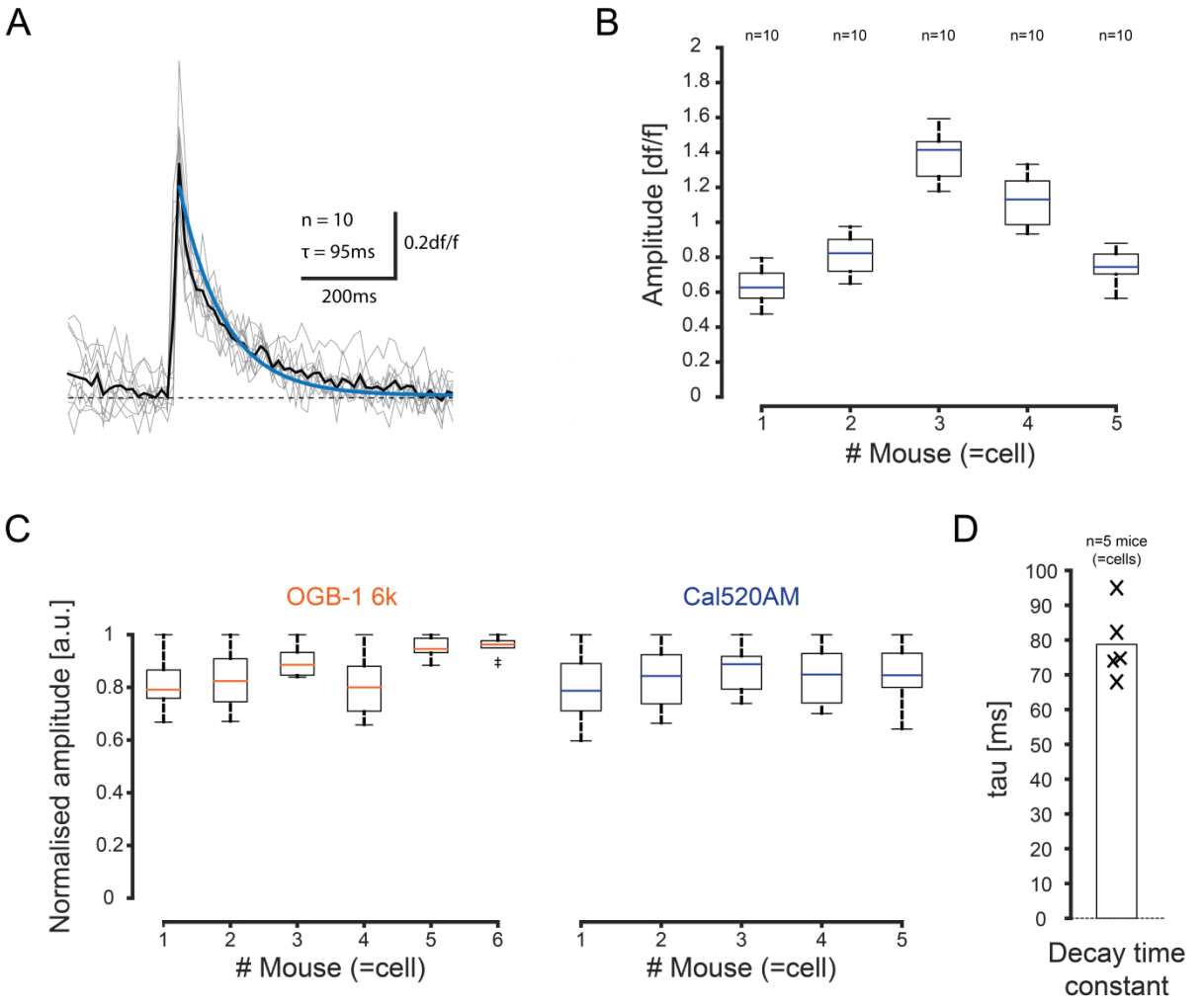

Figure 19: Characterisation of spontaneous global dendritic calcium transients in neighbouring Purkinje neurons multi-cell bolus stained with Cal520AM *in-vivo*.
(A) Superposition of 10 consecutive global dendritic calcium transients (grey lines) taken from one recording of a Purkinje cell, their mean (black line) and its approximated single exponential fit to the decay (blue line). Decay time constant (τ). (B) Ranges of calcium transient amplitudes from 5 cells in 5 mice (n=10 transients/cell). (C) Comparison of normalised calcium transient amplitudes from Purkinje neurons electroporated with OGB-1 6k (left) or mulit-cell bolus stained with Cal520AM (right). Box plots defined as in fig. 15. (D) Decay time constants of mean calcium transients (n=10 transients/cell for mean) from 5 cells in 5 mice. Bar indicates group average. (E) Synchronism of spontaneous global dendritic calcium transients in a population of 4 neighbouring Purkinje neurons.

Together conformity in normalised amplitude ranges across the two types of staining together with consistency of the signal frequency suggested that detected global dendritic calcium transients from population imaging in awake mice were identical to global dendritic calcium transients from prior single-cell electroporation. As such, they served again for identification of synaptic climbing fibre-input despite the amplitude variations. Additional deviations, e.g., in signal kinetics (decay time constants, non-normalised peak amplitudes), by contrast, most likely based on the distinct properties of the two different indicators.

4.6 Sound-evoked global dendritic calcium transients in Purkinje neurons of awake mice

At this stage of experimentation, calcium-sensitive microscopy was combined with auditory stimulation in awake animals. After multi-cell bolus staining, global dendritic calcium transients were clearly identifiable and occurred spontaneously at the known frequency of approximately 1Hz. Spontaneous calcium signals resembled the overall appearance from previous experiments. The presence of synchronous and asynchronous periods in spontaneous recordings confirmed distinctness of selected dendrites for analysis, as previously reviewed in 4.5. Auditory stimulation was conducted under the same parameters as in previous mere behavioural experiments, that is, parameters for acoustic startle stimulation (see materials and methods or 4.1). A representative trial of calcium signals before, during and after acoustic stimulation is displayed in figure 20.

Remarkably, acoustic startle stimulation was able to effectively elicit global dendritic calcium responses. As side of that, calcium signalling exhibited no obvious alterations after auditory stimulation and returned to spontaneous activity. Signal characteristics of acoustic startle stimulus-induced calcium responses detected by the transient identification algorithm were comparable to characteristics of previously described spontaneous calcium transients.

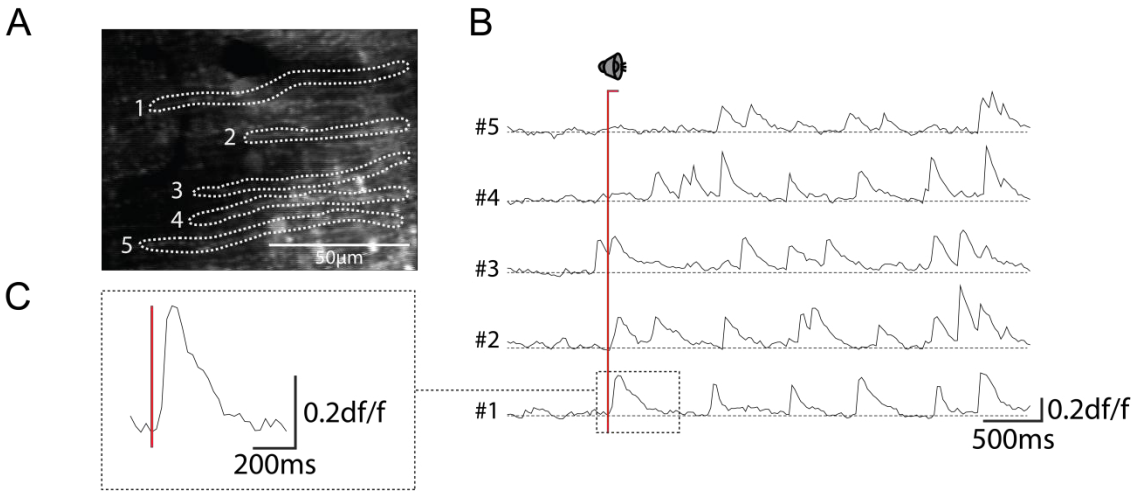

Figure 20: Acoustic startle stimulus-evoked global dendritic calcium responses of Purkinje neurons in an awake mouse. (A) Image (xy-plane) taken from *in-vivo* calcium-sensitive microscopy in an awake mouse. Dotted lines indicate regions of interest on dendrites of different Purkinje neurons used for calculation of the calcium signals in (B). Adjoining numbers correspond to the numbers of calcium traces in (B). (B) Simultaneous recording of global dendritic calcium signals from the population of 5 neighbouring Purkinje neurons in (A) during sound stimulation. Stimulus indicated by speaker symbol and red line. (C) Magnification of a single sound-evoked global dendritic calcium response taken from (B) as shown by the dotted box.

Figure 21A displays representative acoustic startle stimulation-evoked calcium transients (grey traces) of a Purkinje neuron (PC) from three consecutive trials of stimulation and their group average (black trace). The range of normalised amplitudes from stimulation-evoked calcium transients was consistent to normalised amplitude ranges of spontaneous calcium transients from prior experiments (compare figures 21B and 19C). Therefore, a shared common signal origin could be assumed, i.e., synaptic climbing fibre-input. As a side note, acoustic startle stimulation seemingly also led to synchronicity of calcium responses at a higher rate as under spontaneous activity (figure 21C in comparison to figure 19E). This is in line with other studies reporting stimulus-induced increased synchronicity of climbing fibre input (Ozden, Sullivan et al. 2009, Schultz, Kitamura et al. 2009, Wise, Cerminara et al. 2010). As earlier in 4.5, additional calcium signals could be observed in response to stimulation undetected by the algorithm.

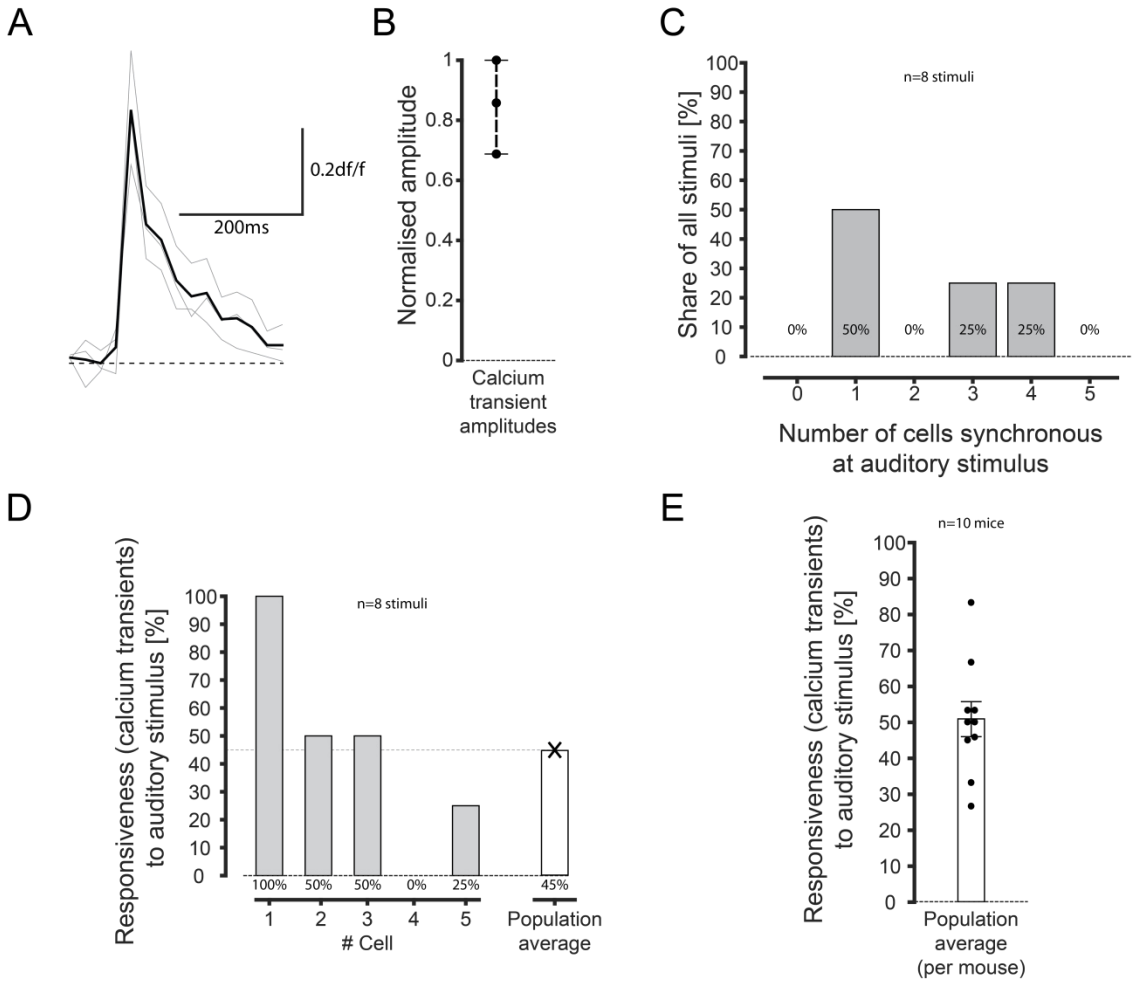

Figure 21: Characterisation of acoustic startle stimulus-evoked global dendritic calcium transients in Purkinje neurons of awake mice. (A) Superposition of acoustic startle stimulation-evoked global dendritic calcium transients (grey lines) and their mean (black line) taken from the same cell in three consecutive trials. (B) Normalised calcium amplitudes of acoustic startle stimulation-evoked global dendritic calcium transients from (A). Whiskers indicate range. (C) Synchronism of global dendritic calcium transients to acoustic startle stimulation in a population of neighbouring Purkinje neurons (5 cells, n=8 stimuli/cell). (D) Responsiveness (defined as the ratio of stimuli with a related calcium transient response to all stimuli) of individual Purkinje neurons from the population in (C) and their population average (5 cells, n=8 stimuli/cell). (E) Population averages of responsiveness to acoustic startle stimulation from 10 mice (total of 135 stimuli in 30 cells). Bar indicates mean. Error bars illustrate standard error for uncertainty of the mean.

Figure 21D illustrates responsiveness of a PC-population in a mouse to multiple acoustic startle stimulation (5 cells, n=8 stimuli, responsiveness defined as the ratio of stimuli with positive detection of a responsive calcium transient to all stimuli).

As becomes apparent, responsiveness was highly diverse across individual cells and a given cell was not necessarily responsive to every stimulus. This observation was made in all animals tested (n=10 mice). As such, there were PCs with a strong relation of calcium transient to acoustic startle stimulation (e.g. cell #1 in figure 21D), PCs with a less well relation (e.g. cell #5 in figure 21D) and non-responsive PCs (e.g. cell #4 in figure 21D). To estimate overall responsiveness, population averages were calculated. The average responsiveness of the example population in figure 21D was 45 ± 37% (mean ± s.d). Population averages of responsiveness from a group of mice are displayed in figure 21E (n=10 mice, total of 135 stimuli in 30 cells). Their overall mean population responsiveness was 51±16% (mean±s.d.). It has to be remembered, however, that individual populations and underlying single PCs could show considerable higher or lower responsiveness (figure 21E). The probability of ongoing spontaneous activity to confound at a given stimulus, in contrast, is much lower (approximately 10%) given a mean spontaneous signal frequency of 1Hz and an event detection window of 100ms for signal onset. Moreover, similar response probabilities have been found for other stimulation modalities (see 5.2.3).

In summary, the data demonstrated for the first time that acoustic startle stimulation was effective in reliably evoking climbing fibre-associated global dendritic calcium responses in Purkinje neurons of the vermis in awake mice. The detected responses resembled global dendritic calcium transients suggestible for synaptic climbing fibre-input.

4.7 Persistence of sound-evoked dendritic calcium transients despite startle suppression

At this stage, single auditory stimulation was extended to behavioural testing on acoustic startle response habituation and was combined with simultaneous calcium-sensitive microscopy. The experimental protocol was a slightly-modified version of the established startle suppression protocol (see section 4.2) and integrated all parts of it (figure 22A).

Figure 22C displays a representative trial according to this protocol. The startle amplitude changed as anticipated from previous behavioural experiments throughout the course of the trial. As seen in freely-moving animals (section 4.2), 1Hz-high-frequency stimulation was also able to induce a direct and marked reduction of the startle response with subtotal suppression in head-fixed animals. Likewise, the startle amplitude reappeared gradually during the stage of spontaneous recovery.

In figure 23A, the experimental course of normalised startle amplitudes from a set of three mice confirmed this finding. Under control conditions, the expected subtle decline according to low-frequency-induced habituation could be observed in all three mice. During 1Hz-high-frequency-stimulation, the startle response was suppressed to values ranging from 17% to 4% of the initial startle amplitude of the control, as such, being equally pronounced as in freely-moving animals. The prolonged reduction of the amplitude with gradual recovery during subsequent 15s inter-stimulus-intervals was also present in all mice.

Interestingly, shape of acoustic startle responses in head-fixed animals slightly differed from the shape previously seen in feely-moving animals. As visible in figure 22D, the initial peak of a startle (startle response proper) was attenuated and a second peak of similar magnitude was present. Presumably, attenuation of the initial startle peak was due to head-fixation in the holder. Quantification of differences in startle response amplitude, however, remained feasible (figure 23A).

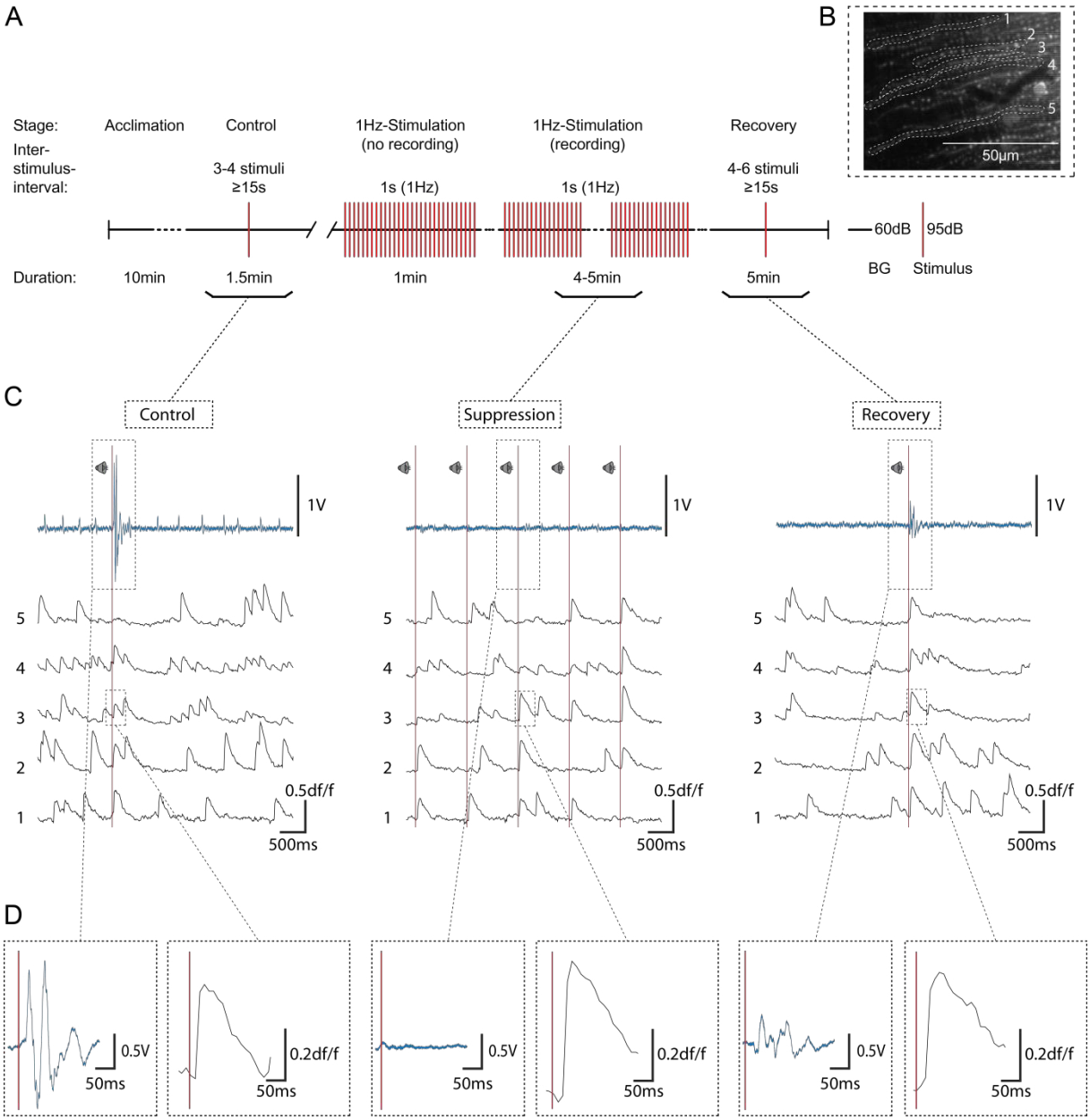

Figure 22: Persistence of acoustic startle stimulation-evoked global dendritic calcium transients despite startle suppression. (A) Experimental protocol. Background noise (BG). (B) Image (xy-plane) of the recording site taken from *in-vivo* calcium-sensitive microscopy. Dotted lines indicate regions of interest on dendrites of 5 different Purkinje neurons for calculation of calcium signals in (C). Adjoining numbers correspond to the numbers of calcium traces in (C). (C) Simultaneous recordings of startle behaviour and global dendritic calcium responses in 5 neighbouring Purkinje neurons of a mouse during the different stages of acoustic startle stimulation. Blue traces: Startle measurements. Black traces: Global dendritic calcium signals. Left column: Control condition. Middle column: 1Hz-high-frequency stimulation. Right column: Recovery stage. Red lines and speaker symbols indicate auditory stimuli. (D) Magnifications of individual startle responses and global dendritic calcium transients from the different stages in (C) as indicated by dotted boxes.

Remarkably, and in contrast to the manifest startle response reduction, acoustic startle stimulation-evoked global dendritic calcium responses persisted throughout all stages of the startle suppression protocol (figure 22C). In this context, global dendritic calcium transients (e.g. in figure 22D) found by the detection algorithm resembled transients from prior experiments (e.g. in figures 18 and 20). Unexpectedly however, responsive transients in PCs appeared seemingly at similar rates during control conditions, 1Hz-high-frequency stimulation and recovery.

Figure 23B depicts the responsiveness from a set of Purkinje neurons (PCs) to acoustic startle stimulation at the three different experimental stages (n=15 cells in 3 mice, 5 cells/mouse). Again, responsiveness differed notably across individual neurons. Their population means, however, remained comparable at all experimental stages, with 39±17% for control conditions, 38±12% for startle suppression and 53±28% for recovery (mean±s.d. respectively). As such, population differences were not significant (t-test, control/1Hz: p=0.8259, control/recovery: p=0.1535, 1Hz/recovery: p=0.0841). Their responsiveness was, moreover, in line with response-probabilities found in prior single acoustic startle stimulation experiments (compare figure 21E). Noteworthy, the data suggested even a mild, yet, non-significant trend towards an incline in responsiveness at the stage of recovery.

Together, whereas the acoustic startle response changed markedly in respect to the different inter-stimulus-intervals over the course of time, correlated acoustic startle stimulation-elicited global dendritic calcium transients persisted at all stages. Other than expected, it had not come to an obvious change in underlying climbing fibre (CF) input.

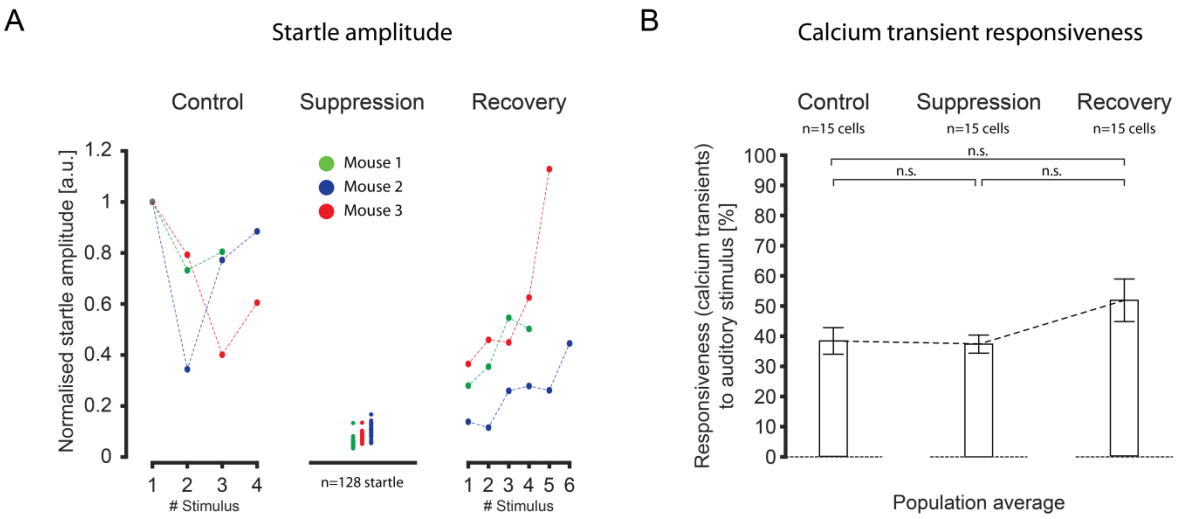

Figure 23: Persistence of acoustic startle stimulation-evoked global dendritic calcium transients despite acoustic startle suppression - quantification. (A) Course of normalised startle amplitudes of 3 mice at the different experimental stages. Individual stimuli are not shown for suppression stage (total of stimuli for control: n=11, for suppression: n=138 and for recovery: n=15). Colours indicate different mice as specified. (B) Population averages of responsiveness (defined as the ratio of stimuli with a related calcium transient response to all stimuli) to acoustic startle stimulation at the different experimental stages of Purkinje neurons from mice in (A) (n=15 cells in 3 mice, 5 cells/mouse). Bars show population averages at the different experimental stages and dotted lines their temporal course. Error bars illustrate standard error for uncertainty of the mean. For the experimental protocol see fig. 22A.

As a consequence of these findings, previously identified neurophysiological correlates in context of the acoustic startle response ought to be manipulated in the second part of the project agenda (see chapter 2). In section 4.4, it was demonstrated that global dendritic calcium transients in Purkinje neurons indicated underlying synaptic CF-input. Moreover, persistence of acoustic startle stimulus-evoked global dendritic calcium transient during startle habituation suggested that climbing fibre-input might reflect part of a distinct cerebellar mechanism affecting the acoustic startle response (see more in discussion). Therefore, subsequent experiments intended to disrupt reliability of stimulus-evoked CF-input and, hence, its hypothetical function. In this regard, the pharmaceutical harmaline was used as an experimental intervention. It is known to elicit a rather specific effect on neurons of the inferior olivary body and, thus, on the climbing fibre-input onto Purkinje neurons (see section 1.3 for a review on harmaline).

4.8 Transient induction of harmaline-induced cerebellar tremor

Harmaline is known to induce cerebellar tremor (see section 1.4). Therefore, alterations of spontaneous behaviour following harmaline administration were characterised at first. In the process, a dosage of harmaline was determined (3mg/kgBW) allowing for the transient induction of tremor. This was used to create controlled experimental stages in subsequent experiments. Figure 24 illustrates a representative experiment of transiently induced cerebellar tremor by harmaline application.

Shortly upon administration (usually the onset was under 10 minutes, yet, no dedicated analysis was undertaken), harmaline-characteristic whole-body tremor was clearly visible. Recordings were taken approximately 30min after injection, once tremor was fully and continuously established reproducibly across all animals. As depicted in figure 24B/C (middle panel), harmaline induced a periodic, rhythmic, sinusoidal tremor with subtle-undulating amplitude fluctuations. Recordings for wash-out conditions were taken once tremor had visibly clearly ceased. In this context, however, it has to be mentioned that no precise ending of tremor existed but rather a transition stage. After precedent continuous tremor, this stage presented with tremor offs and re-onsets as well as residual tremor subsisting at marginal magnitudes which could outlast for longer periods of time. Since no distinct delineation between tremor and post-tremor was present, recordings for post-tremor were taken once tremor had ceased continuously for at least 10min. This feature defined the post-tremor stage. Temporal range of onset of this post-tremor stage was approximately 90-120min. In this regard, non-steady tapering-off of the systemically (intraperitoneally) applied harmaline has to be considered as the possible cause.

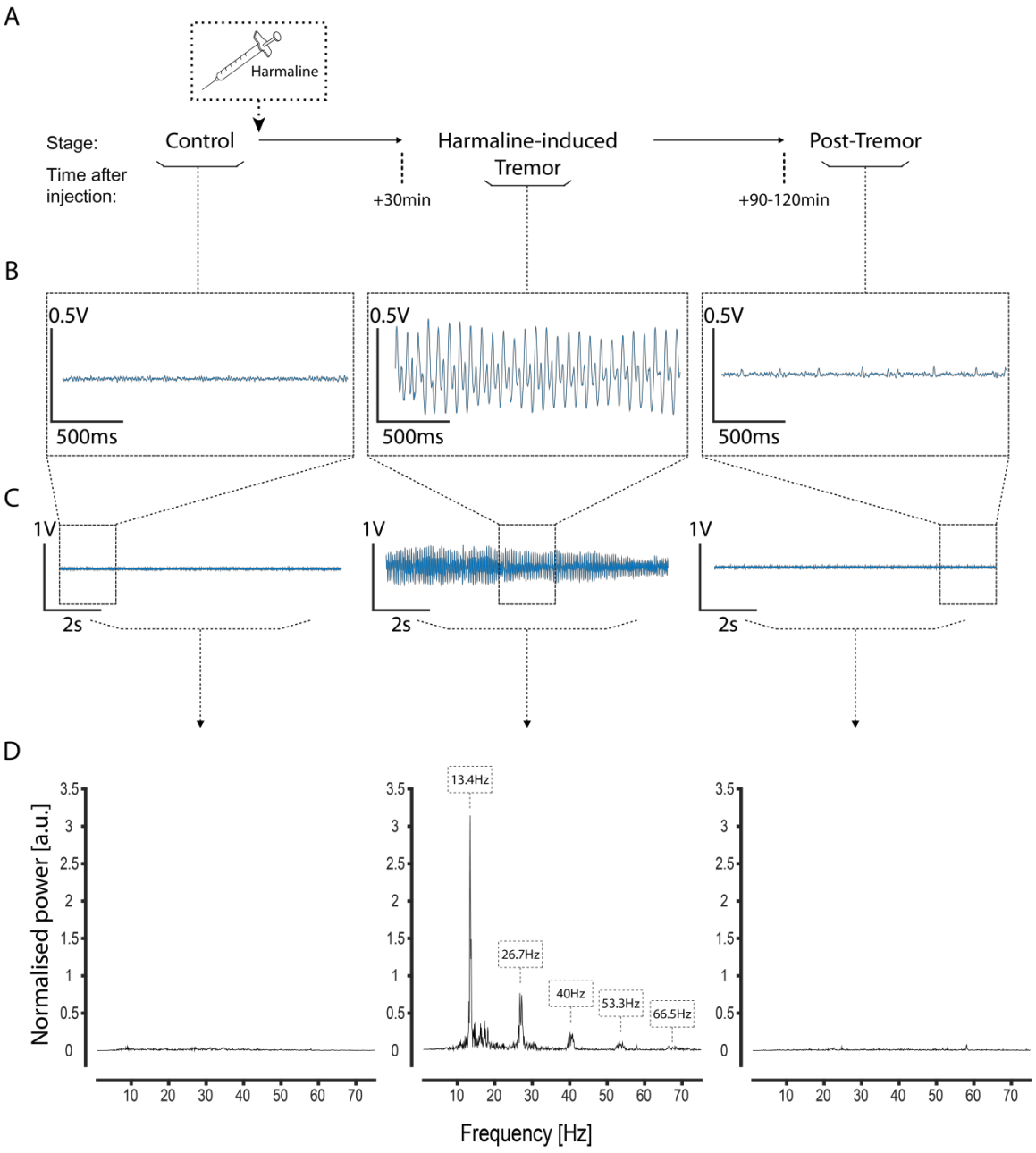

Figure 24: Transient induction of harmaline-induced cerebellar tremor. (A) Experimental protocol. Dotted box indicates harmaline-application. (B) Magnifications taken from the example traces at the different experimental stages in (C) as indicated by dotted boxes. (C) Example traces of the different experimental stages taken from the same trial of one mouse. Left: Control. Middle: Harmaline-induced cerebellar tremor. Right: Post-tremor. (D) Corresponding frequency power spectra of the example traces in (C). Power was normalised to the group minimum. Left: Control. Middle: Harmaline-induced cerebellar tremor. Boxes state frequencies of individual normalised power peaks as indicated. Right: Post-tremor.

To determine if tremor was indeed absent in the post-tremor stage, a spectral analysis of the traces was performed. Spectral analysis revealed a characteristic composition of the tremor in terms of its frequency power spectrum. In figure 24D, the spectral power analysis to the corresponding experiment in figure 24B/C is shown. Power was normalised to the respective recording minimum for easier comparison. Both in control and wash-out conditions no predominant frequency was detectable, but the frequency band had rather a constant power spectral density across all frequencies. Harmaline-induced cerebellar tremor, by contrast, had a major frequency in terms of a normalised power peak at 13.4Hz. Additionally, the tremor frequency spectrum displayed further peaks at approximated integer multiples of the major frequency in decreasing power. As such, the tremor frequency spectrum was suggestive for a harmonic series with equidistant frequency peaks. In figure 24D (middle), frequencies from the individual peaks of the tremor frequency spectrum are stated in dotted boxes.

The tremor frequency spectra of 4 additional mice are illustrated in figure 25A. As can be seen, in some cases the power peak of the main frequency is distorted to a narrow-band spectrum. Besides, the higher order harmonic frequencies may appear less pronounced or of comparable magnitude as the initial power peak of the lowest frequency. In figure 25B, major tremor frequencies from a set of six mice are compared. The mean major tremor frequency was at 13.5±1.8Hz (mean±s.d.). This is in accordance with other reports on the major tremor frequency of harmaline-induced cerebellar tremor in mice (Ahmed and Taylor 1959, Milner, Cadoret et al. 1995, Miwa 2007).

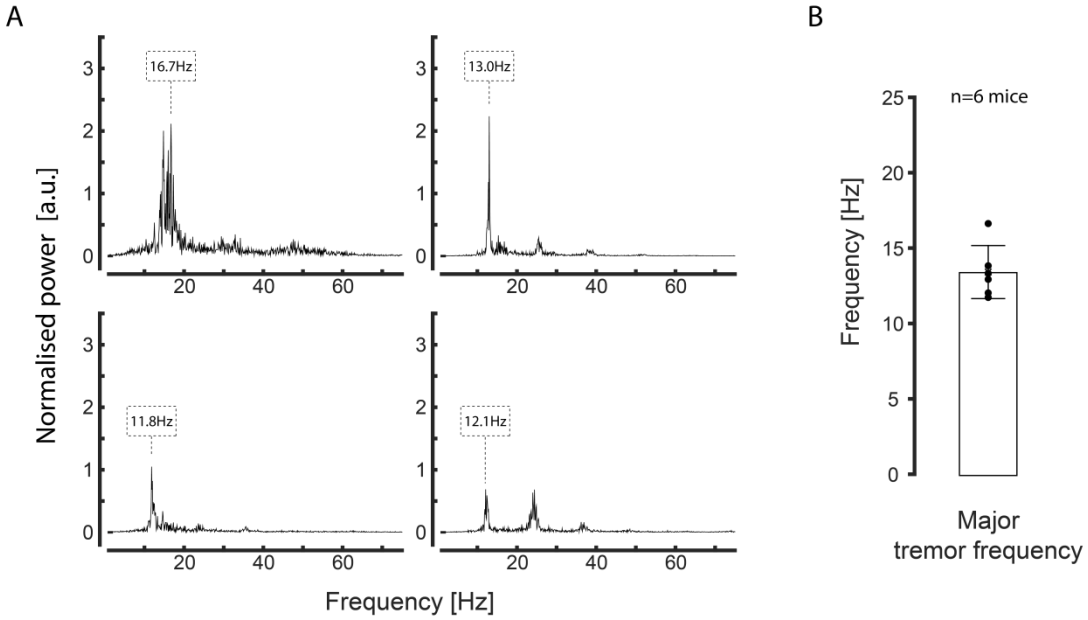

Figure 25: Frequency power spectra of harmaline-induced cerebellar tremor and the major tremor frequency. (A) Frequency power spectra of harmaline-induced cerebellar tremor in 4 mice. Power was normalised to the group minimum. (B) Major tremor frequencies from a set of 6 mice (10s-recordings from tremor/frequency analysis). Bar indicates group mean and error bars standard deviation.

In conclusion, harmaline could be used to transiently induce a cerebellar tremor. Spectral analysis identified a characteristic composition of the tremor frequency power spectrum which was not present at control or the post-tremor stages.

4.9 Suppression of the acoustic startle response by harmaline-induced cerebellar tremor

Subsequently, acoustic startle response (ASR) behaviour under harmaline-induced cerebellar tremor was investigated. In this regard, a protocol was designed creating three distinct experimental stages (see section 3.6.5 and figure 26A). Figure 26B depicts a representative trial of ASR behaviour according to this protocol.

Control conditions provided reliable and relatively stable startle responses as previously seen in behavioural experiments on frequency-dependent suppression of the acoustic startle response (see 4.2). Remarkably, under conditions of harmaline-induced cerebellar tremor, startle responses were markedly suppressed. Startle responses, nevertheless, could still be reliably evoked and remained clearly discernible from the tremor band. Furthermore, startle responses remained reduced even after tremor had ceased at the post-tremor stage. The magnitude of startle reduction, however, seemed less pronounced compared to the tremor stage. Importantly, apart from the startle amplitude, the general shape of the acoustic startle response remained alike at all experimental stages (figure 26C, upper boxes), that is, it persisted to resemble the typical shape of an ASR as seen in prior experiments (e.g. see figure 13A). Analysis of frequency power spectra confirmed that only during the stage of harmaline-induced cerebellar tremor the characteristic tremor frequency spectrum was present (figure 26C, lower boxes).

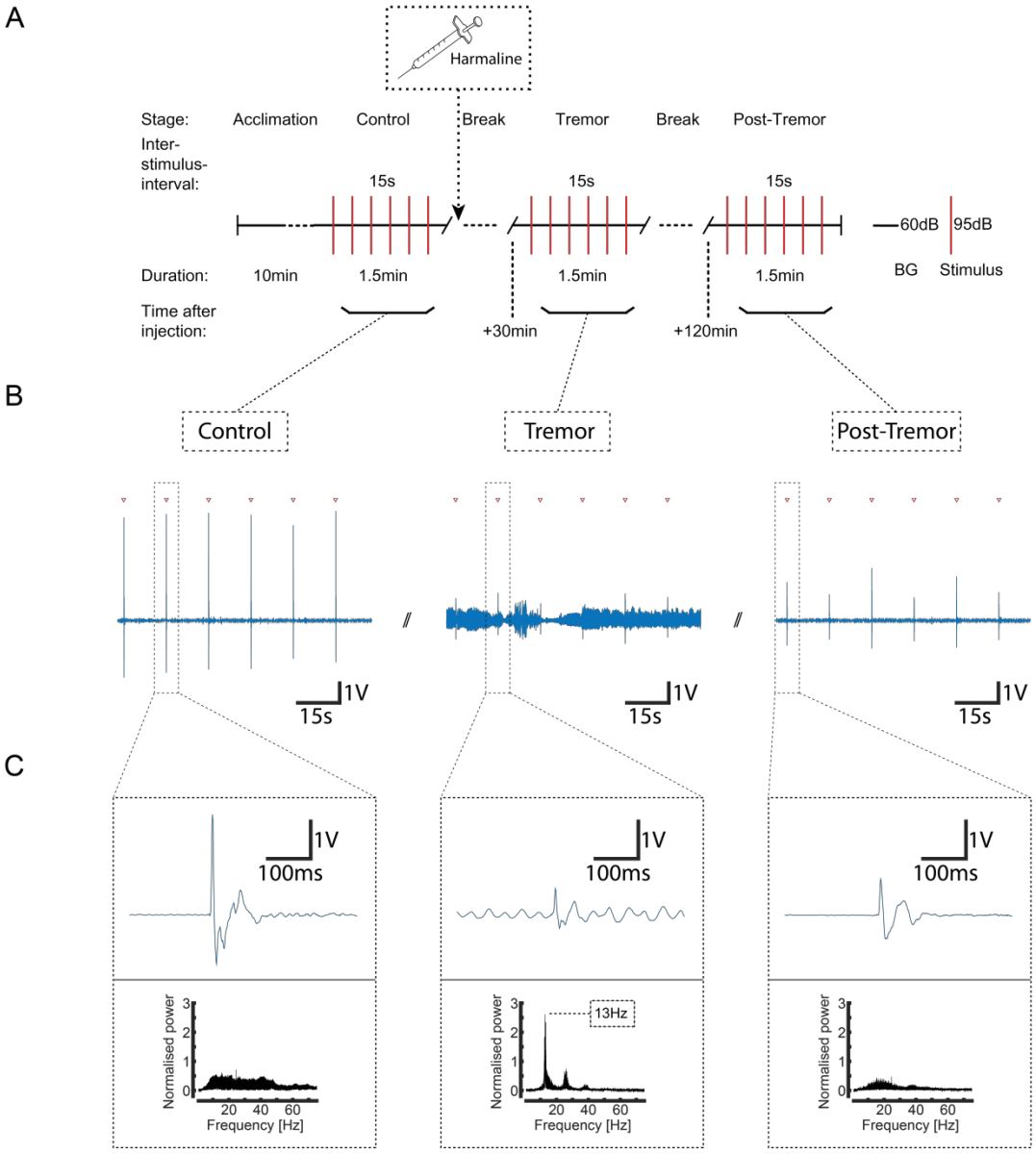

Figure 26: Suppression of the acoustic startle response by harmaline-induced cerebellar tremor.
(A) Experimental protocol. Dotted box indicates harmaline-application. Background noise (BG). (B) Example traces of acoustic startle responses at the different experimental stages taken from the same trial of one mouse. Left: Control. Middle: Harmaline-induced cerebellar tremor. Right: Post-tremor. Red triangles indicate acoustic stimuli. (C) Magnifications of representative acoustic startle responses (upper boxes) taken from the example traces in (B) as indicated by dotted boxes and frequency power spectra (lower boxes) of the example traces in (B). Power was normalised to the group minimum. Left boxes: Control. Middle boxes: Harmaline-induced cerebellar tremor. Inset box indicates frequency of normalised power peak. Right boxes: Post-tremor.

Equal findings were manifest in the entire tested set of mice shown in figure 27. An expected subtle decline of the mean normalised startle amplitude under control conditions to 86±28% (mean±s.d., n=10mice) of the initial startle is succeeded by a significantly pronounced reduction of the ASR during harmaline tremor (t-test, p<0.00001). As such, the mean normalised amplitude triggered by the last stimulus at the tremor stage was at 16±9% (mean ±s.d., n=10 mice). Again, the reduction persisted well beyond tremor termination at the post-tremor stage. The final startle at the post-tremor stage remained with a mean of 36±11% (mean ± s.d., n=6 mice) significantly reduced to control conditions (t-test, p=0.00028). Compared to the tremor stage the difference was also significant, however, less pronounced (t-test, p=0.0107).

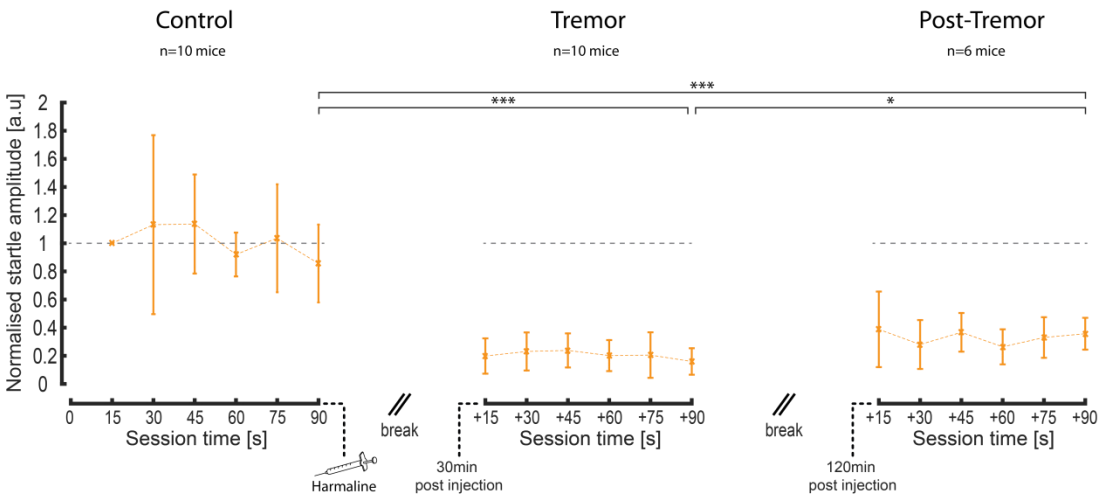

Figure 27: Suppression of the acoustic startle response by harmaline-induced cerebellar tremor - quantification. Course of the mean normalised startle amplitudes from a set of mice at the different experimental stages according to protocol (see fig. 26A). Left: Control (n=10 mice). Middle: Harmaline-induced cerebellar tremor (n=10 mice). Right: Post-tremor (n=6 mice). Error bars indicate standard deviation. Session time is depicted in reference to the end of the prior break. Harmaline-application and time after injection illustrated by black dotted lines.

In this context, however, it should be mentioned again that extinction of tremor, that is, the limit between tremor and post-tremor, was not always sharply delineated. As described in 4.8, this was due to relapsing re-onset of tremor and due to residual tremor subsisting at marginal magnitudes, as such, outlasting for longer periods of time. From the observations made in 4.8, recordings for the post-tremor stage were, thus, taken once tremor had ceased for at least 10min and 120min after harmaline-injection. Noteworthy, auditory stimulation during this transition stage could evoke re-onset of tremor (not shown). Additionally, long-lasting recordings were challenging due to confounding animal behaviour like grooming or sleepiness which had to be accounted to acquire high-quality recordings.

Together, the data suggested that the acoustic startle response is suppressed under conditions of transient harmaline-induced cerebellar tremor. Moreover, the reduction persisted once tremor had ceased.

4.10 Harmaline-induced suppression of simple spike responses of Purkinje neurons

After evaluation of the global behavioural impact of harmaline on the acoustic startle response, the effects of harmaline on Purkinje cell neurophysiology ought to be investigated at this stage. This was done by combing once more *in-vivo* single-cell electrophysiology and calcium-sensitive microscopy. A protocol was created (figure 28A) which based on the acquired knowledge of the temporal dynamics from harmaline-tremor (4.8 and 4.9). Under anaesthesia no tremor occurred and formation of single-cell somatic recordings was possible under stable conditions. Onset of the harmaline effect was confirmed by presence of tremor when anaesthesia was briefly reduced. Figure 28C displays a representative experiment on harmaline-induced neurophysiological changes recorded in the same Purkinje neuron.

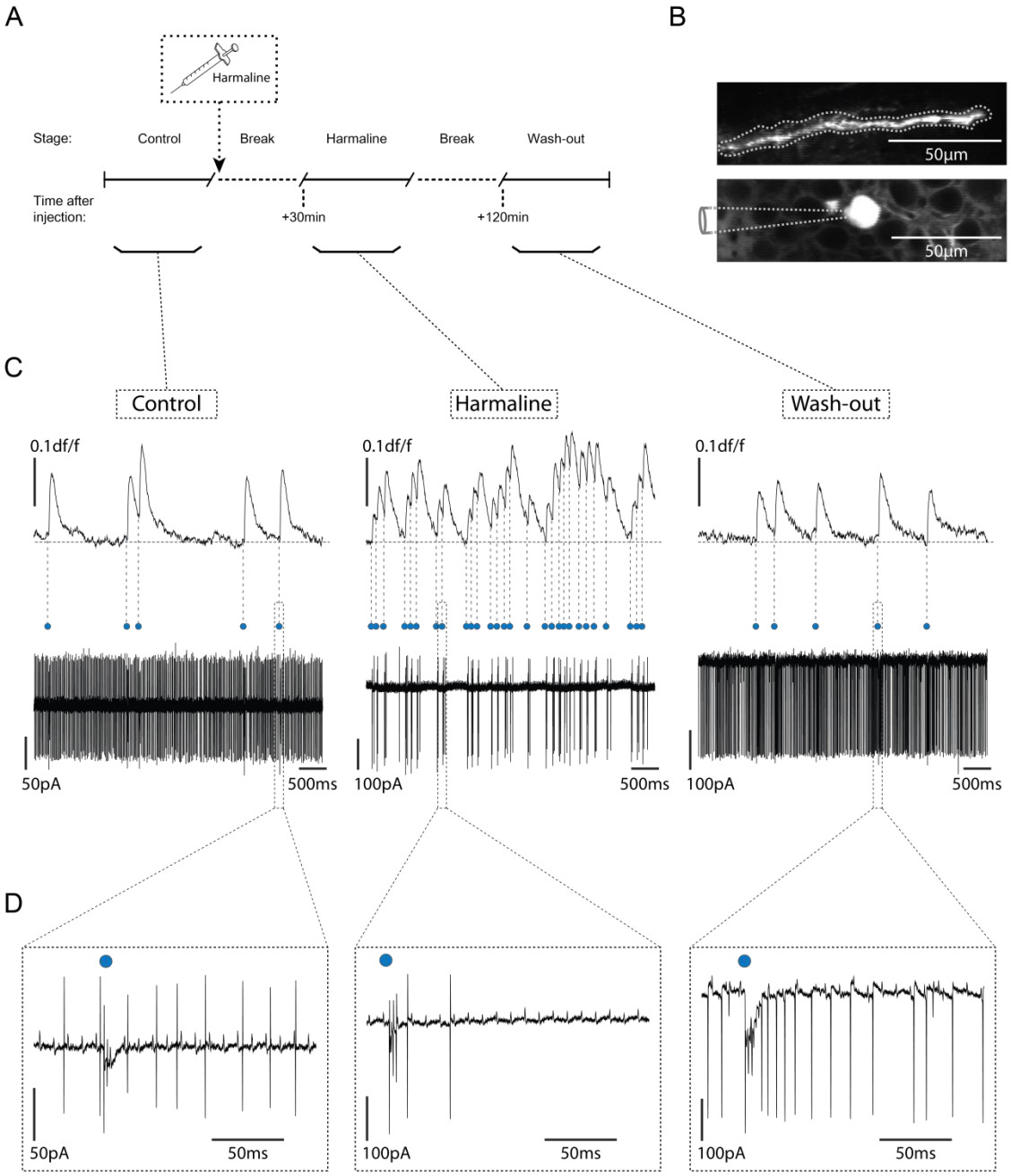

Figure 28: Harmaline-induced increase in complex spike activity with simultaneous suppression of simple spike responses. (A) Experimental protocol. (B) Images (xy-plane) taken from *in-vivo* calcium-sensitive microscopy. Upper: Calcium-indicator filled dendritic tree of the recorded Purkinje neuron in the upper third of the cerebellar molecular layer. Dotted lines indicate region of interest for the calculation of global dendritic calcium signals in (C). Lower: Recording pipette at the corresponding Purkinje neuron soma. Shape of the pipette depicted by dotted lines. (C) Simultaneous *in-vivo* single-cell electrophysiology and calcium-sensitive microscopy of the Purkinje neuron in (B) at the different experimental stages. Upper traces: Global dendritic calcium signals. Lower traces: Somatic electrophysiological recordings. Blue dots indicate complex spikes. Blue lines illustrate complex spike-dendritic calcium transient co-occurence. Left: Control. Middle: Harmaline. Right: Wash-out. (D) Magnifications of complex spikes taken from the three different experimental stages as shown by the dotted boxes in (C). Blue dots indicate complex spike.

Under control conditions, spontaneous somatic electric responses and calcium signals presented themselves as in previous experiments. Complex spikes (CSs), respectively, their matching calcium transients appeared at the anticipated frequency of approximately 1Hz. Likewise, simple spike (SS) activity showed expected high frequency firing rates (figure 28C, left). Remarkably, harmaline provoked a complete change in activity at the interventional stage. While inducing an increase in CS activity, SSs were strongly suppressed at the same time. Related to the elevated CS count, calcium imaging revealed a pronounced increase in calcium transients causing long-lasting periods of elevated dendritic calcium (figure 28C, middle). In this context, both CSs and calcium transients showed burst-like appearance (figure 28C, middle). Bursts differed considerably in length ranging from short-lasting bursts of 2-3 CSs/transients up to continuous bursting of several seconds. Also at this stage, dynamic transitions between periods of elevated and unelevated CS count as well as respective suppressed and unsuppressed SS count were possible which could last for several seconds (not shown). SSs frequently reappeared shortly after CS count intermittently normalised or stopped, whereas SSs decreased when CSs increased once again. For the most part, however, CSs were constantly increased and SSs drastically suppressed. At the wash-out stage, CS- as well as calcium transient-activity normalised. Besides, SS count recovered (figure 28C, right). In some trials, paralleled increase of CSs and recovered SS count was observed shortly before CS-normalisation. Similar to tremor in behavioural experiments, there were offs and re-onsets of increased CS activity before definite recovery. In the same style as for behavioural experiments, the wash-out stage was, thus, defined as of the time CS-/calcium transient-activity had normalised for 10min. Noteworthy, the CS shape remained comparable throughout all stages (figure 28D).

Figure 29 opposes the inverse effects of harmaline on CS- and SS-frequencies over the experimental course in a group of mice. Mean CS frequencies changed significantly from initially 1.05±0.22Hz (mean±s.d., n=8 cells in 8 mice) at control conditions to 3.72±0.82Hz (mean±s.d., n= 8 cells in 8 mice) following harmaline-application (t-test, p=0.000027). At wash-out, CS frequencies returned to 1.1±0.21Hz (mean±s.d., n=6 cells in 6 mice) which was not significantly different form control conditions (t-test, p=0.8811) but to the interventional stage (t-test, p=0.00046).

In contrast, mean SS frequencies had a spontaneous rate of 44.97±8.02Hz (mean±s.d., n= 7 cells in 7 mice). Harmaline induced a highly significant suppression to 6.71±5.09Hz (mean± s.d., n=7 cells in 7 mice, t-test, p=0.0000036). At wash-out, the SS frequency had a mean of 62.03±16.45Hz (mean±s.d., n=4 cells in 4 mice). Although having no significant difference to control (t-test, p=0.1752), the data might even suggest a trend to higher SS frequencies after wash-out compared to control conditions. To the stage of the harmaline-intervention, however, the difference was again significant (t-test, p=0.0067).

In conclusion, harmaline-application caused fundamental changes in Purkinje cell neurophysiology. On the one hand, the number of CSs and global dendritic calcium transients were markedly elevated under harmaline. As such, they indicated increased synaptic climbing fibre-input from the inferior olive. On the other hand, SSs reflecting synaptic parallel fibre-activity were drastically suppressed at the same time.

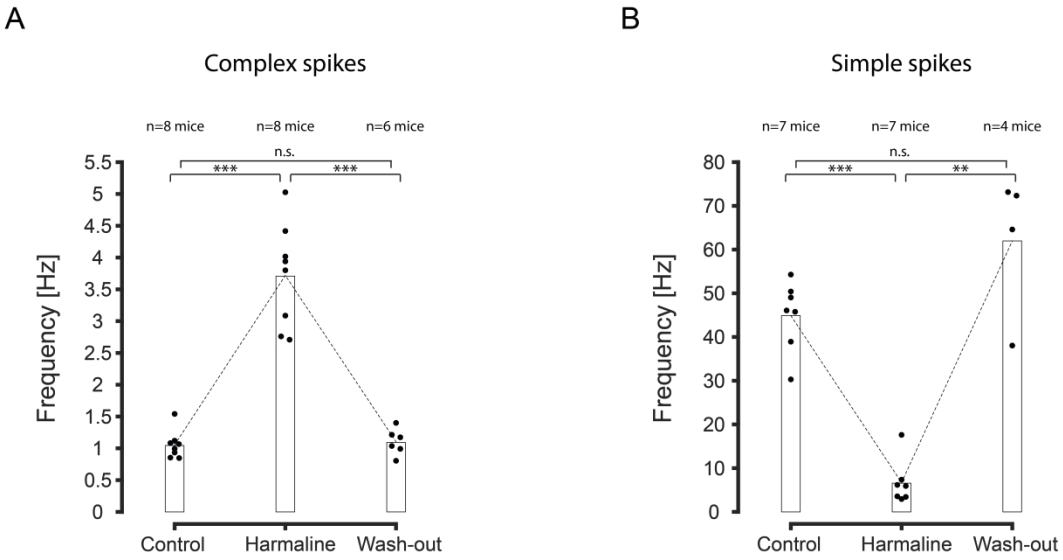

Figure 29: Harmaline-induced increase of complex spikes with simultaenous suppression of simple spikes. (A) Complex spike frequencies at the different experimental stages (n=8 Purkinje neurons in 8 mice. Except wash-out: n=6 cells in 6 mice). (B) Simple spike frequencies at the different experimental stages (n=7 Purkinje neurons in 7 mice. Except wash-out: n=4 cells in 4 mice). Bars indicate group means at the different experimental stages and dotted lines their temporal course. For the experimental protocol see fig. 28A.

4.11 Persistence of sound-evoked calcium responses during harmaline-induced tremor

At the final stage of experimentation, the question was addressed of how acoustic startle stimulation-evoked global dendritic responses of Purkinje neurons (PC) were affected during harmaline-induced changes of PC neurophysiology. The respective experimental protocol may be found in figure 30A. The time course of the experimental protocol based on observations on the temporal dynamics of the harmaline-effect made in prior behavioural studies (see section 4.8 and 4.9). An exemplary trial of simultaneously recorded acoustic stimulus-evoked startle and calcium responses before and after harmaline-application is depicted in figure 30C.

Under control conditions (figure 30C, left), startle and calcium responses evoked by auditory stimulation resembled the overall pattern seen in previous experiments. The startle response fluctuated in an anticipated range which was comparable to prior findings of startling to 15s-inter-stimulus-intervals (figure 30D, upper panel). Besides, startle responses presented themselves with the previously observed distorted shape in head-fixated animals (figure 30C, left, blue trace). Likewise, responsiveness of the simultaneously recorded PC-population was with a mean of 53±30% (mean±s.d., 5 cells, n=3 stimuli/cell, figure 30D, lower panel) comparable to previous findings (e.g. see section 4.6).

Under harmaline, startle responses were markedly reduced and partly not discernible from the tremor band (figure 30C, right, blue trace). Absence of discernible startles was most likely due to the previously described startle attenuation in head-fixed animals (see section 4.7). Minor stimulus-evoked responses in the traces were, nonetheless, present. Despite their presence, the startle peak detection algorithm was left unchanged to avoid bias. Thus, quantified responses frequently reflected post-stimuli tremor peaks usually being larger than response signals proper. Reduced response amplitudes during tremor are illustrated in figure 30E (upper panel). The reduction corresponded to prior behavioural results (section 4.9).

As seen in figure 30C (right, black traces), harmaline induced increased and burst-like activity of global dendritic calcium transients, equally to the harmaline-effect seen in prior experiment (figure 28C, middle). Unexpectedly, acoustic stimulation persisted to evoke calcium responses, however, usually in terms of induced calcium transient-bursting (figure 30C, right, black traces). Besides, stimuli frequently hit on pre-existent calcium bursting (not shown). In some cases, single calcium transients were elicited (not shown), equally to previous experiments (see 4.6 and 4.7). As a result, responsiveness remained surprisingly at 57±19% (mean±s.d., 5 cells, n=6 stimuli/cell, figure 30E, lower panel).

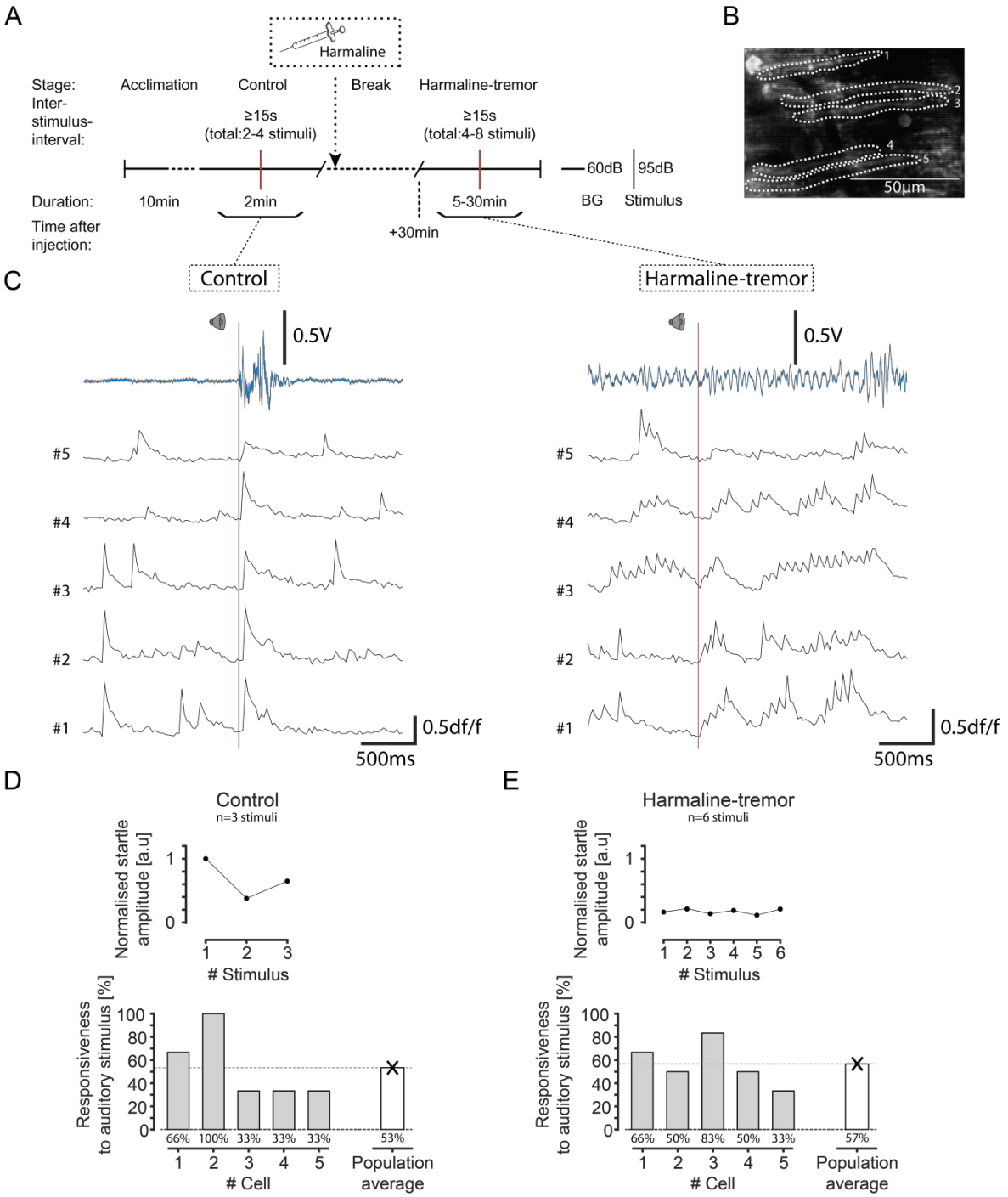

Figure 30: Persistence of sound-evoked calcium responses during harmaline-induced cerebellar tremor. (A) Experimental protocol. Background (BG). (B) Image (xy-plane) of the recording site taken from *in-vivo* calcium-sensitive microscopy. Dotted lines indicate regions of interest on dendrites of 5 different Purkinje neurons for calculation of calcium signals in (C). Adjoining numbers correspond to the numbers of calcium traces in (C). (C) Simultaneous recordings of startle behaviour and global dendritic calcium responses of 5 neighbouring Purkinje neurons in a mouse during control conditions and harmaline-induced cerebellar tremor. Blue traces: Startle measurements. Black traces: Global dendritic calcium signals. Left column: Control. Right column: Harmaline-induced cerebellar tremor. Red lines and speaker symbols indicate auditory stimuli. (D) Upper: Course of the normalised startle amplitude from the mouse during control (n=3 stimuli). Lower: Responsiveness to auditory stimulation in the Purkinje neuron population from (B) and their group average during control (5 cells, n=3 stimuli/cell). (E) Upper: Course of the normalised startle amplitude from the mouse during tremor (n=6 stimuli). Lower: Responsiveness to auditory stimulation and the group average during tremor (5 cells, n=6 stimuli/cell).

Quantifications from a larger set of mice confirmed these findings (figure 31). Normalised mean startle amplitudes were markedly reduced during harmaline-induced tremor compared to control (n=6 mice, figure 31A). Thus, results of prior behavioural testing were reproducible in head-fixed animals. As previously seen (4.6 and 4.7), average responsiveness of PC-populations varied across mice both in control and under harmaline-tremor. Remarkably, they were, nevertheless, not significantly different (figure 31B, control: 49±21%, harmaline-tremor: 51±8% [mean±s.d. respectively], n=32 cell in 8 mice, t-test, p=0.8097).

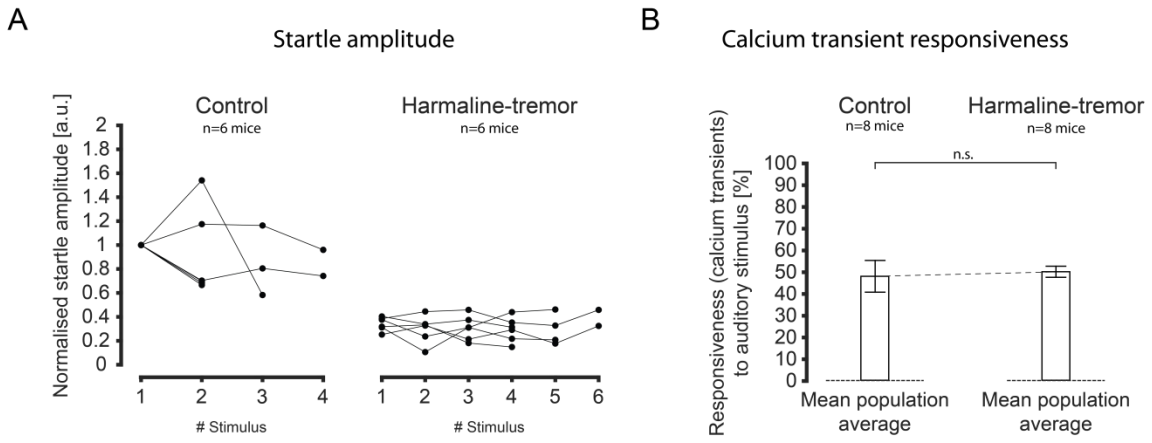

Figure 31: Persistence of sound-evoked calcium responses during harmaline-induced suppression of the acoustic startle response. (A) Course of the normalised startle amplitudes from a set fo 6 mice at the different experimental stages. Left: Control. Right: Harmaline-induced cerebellar tremor. (B) Mean population averages of responsiveness (defined as the ratio of stimuli with a related calcium transient response to all stimuli) to acoustic startle stimulation at the different experimental stages from a set of 8 mice. Recordings of 6 mice in parallel to behavioural testing depicted in (A). Left: Control (total of 94 stimuli in 32 cells). Right: Harmaline-induced cerebellar tremor (total of 205 stimuli in 32 cells). Bars show mean population averages at the different experimental stages and dotted lines their temporal course. Error bars illustrate standard error for uncertainty of the mean. For the experimental protocol see fig. 30A.

Noteworthy, in a few experiments dendritic calcium bursting could be observed sporadically without detectable tremor, yet, never vice versa (not shown). In these cases, acoustic stimulation could induce both calcium transient-bursting and re-onset of tremor.

Together, harmaline-induced tremor was associated with increased burst-like activity of global dendritic calcium transients in PCs reflecting elevated synaptic climbing fibre-input from the inferior olive. Whereas acoustic startle responses were drastically suppressed under these conditions, acoustic startle stimulation unexpectedly remained effective in evoking climbing fibre-input despite ongoing harmaline-induced changes in background activity. This indicates that the acoustic startle stimulus-evoked synaptic climbing fibre-input is highly preserved.

5. Discussion

This chapter will discuss the results in view of the theoretical foundations introduced in chapter 1 and the current state of literature. The first section is an appreciation of all major findings. In the subsequent sections, major focus will be given to acoustic startle response (ASR) habituation and associated signals in Purkinje neurons. Subsequently, the implication of a causal relation between changes in Purkinje cell physiology and ASR-modulation inferred from harmaline-interventions is discussed. Additionally, a potential circuit and synaptic mechanism of ASR-modulation is proposed based on the processes observed during harmaline-interventions. Finally, limitations will be addressed before closing with the significance of the present findings and conclusive remarks. Minor findings have been discussed directly in their respective sections within the results.

5.1 Résumé of experimental findings

Initial behavioural studies on the habituation of the acoustic startle response demonstrated frequency-dependence of startle reduction. Responses could be subtotally suppressed during 1Hz-high-frequency stimulation and presented with a prolonged reduction after stimulus termination together with gradual spontaneous recovery.

Characteristic complex and simple spikes were observed in Purkinje neurons *in-vivo* and identified as responses to synaptic climbing fibre-input and transmission of parallel fibre-input, respectively. Combined *in-vivo* single-cell somatic electric recordings and calcium-sensitive microscopy revealed consistent co-occurrence of climbing fibre synapse-driven complex spikes with global dendritic calcium transients despite subtle calcium signal variation. Similar calcium transients were observed in Purkinje neuron populations of awake, alert mice. These signals could be reliably ascribed to single cells.

Acoustic startle stimulation effectively evoked global dendritic calcium responses in Purkinje neuron populations of awake, alert mice. In behavioural experiments on startle habituation combined with simultaneous calcium imaging, persistence of acoustic startle stimulation-evoked global dendritic calcium responses could be observed throughout the entire habituation protocol, even during 1-Hz-stimulation-induced startle suppression.

Systemic injection of harmaline reliably induced a characteristic transient cerebellar tremor. In behavioural testing, the acoustic startle response was markedly suppressed by harmaline-induced cerebellar tremor. The harmaline-induced reduction persisted beyond tremor. In Purkinje neurons, harmaline-application increases climbing fibre-mediated complex spike responses and simultaneously suppressed parallel fibre-associated simple spike responses. Nonetheless, acoustic startle stimulation-evoked global dendritic calcium responses of Purkinje neurons persisted despite startle suppression by harmaline-induced cerebellar tremor.

5.2 The acoustic startle response and associated sound-evoked signals in Purkinje neurons

5.2.1 Different manifestations of acoustic startle response habituation

In line with present findings, the acoustic startle response (ASR) has been abundantly described as a reliable reaction upon acoustic stimulation which, nonetheless, may express variation across individuals and within a given individual (Landis and Hunt 1939, Koch and Schnitzler 1997, Koch 1999, Valsamis and Schmid 2011). Prerequisite is the adequacy of the stimulus in terms of sound intensity, frequency, duration and rise time (Shnerson and Willott 1980, Parham and Willott 1988, Valsamis and Schmid 2011). This was accounted for in the present thesis. Repetitive stimulation leads to a pronounced reduction of the amplitude (Prosser and Hunter 1936), a process referred to as startle habituation (Harris 1943,

Thompson and Spencer 1966, Koch 1999, Rankin, Abrams et al. 2009). According to the dual-process theory, habituation has to be considered as a net result of the parallel process of habituation and sensitisation (Groves and Thompson 1970, Ornitz and Guthrie 1989).

Anyway, reduction due to habituation resembles a progressive decrease which, by approximation, plateaus at an asymptotic level (Rankin, Abrams et al. 2009). It has been demonstrated both for habituation in general (Rankin and Broster 1992, Rankin, Abrams et al. 2009) and for habituation of the ASR in particular (Davis 1970), that the degree of reduction depends on the stimulus frequency, i.e., the shorter the inter-stimulus-interval (ISI) the more responses are reduced. After startle decrement, stimulus termination leads to spontaneous (partial) recovery (Prosser and Hunter 1936, Thompson and Spencer 1966, Davis 1970, Rankin and Broster 1992, Rankin, Abrams et al. 2009).

The results of behavioural testing from the present thesis are in accord with this. ISIs of 1s opposed to ISIs of 15s induced habituation at markedly different levels (see 4.2). The observations are comparable to results from a study in rats (Davis 1970). Likewise, the startle response expressed prolonged reduction with spontaneous gradual (partial) recovery after stimulus termination. Additionally, it could be shown that ASR testing is feasible also in head-fixed mice (see 4.7). Limitations from the ASR-shape deviations, however, have to be considered. In accord with a report from Davis (Davis 1970), major part of the habituation effect was present already after the first ISI at 1Hz-stimulation (see 4.2).

In this context, Davis further reported that the amplitude reduction identified upon a belated test stimulus (during the stage of spontaneous recovery) depends on the prior ISI during inductive habituation training (Davis 1970). Importantly, the reduction was inverse proportional to the stimulus frequency, i.e., the longer the ISI, the more reduced the startle remained (Davis 1970). This contrasts the proportional dependency of startle reduction to

stimulus frequency during initial repetitive stimulation (see above). However, equal findings were made in other models of habituation (Rankin and Broster 1992, Rankin, Abrams et al. 2009).

The discovery of these two opposing phenomena led to the distinction of two manifestations of habituation. Firstly, there is short-term habituation (STH) at the interventional stage which is more pronounced to shorter ISIs (Davis 1970, Rankin and Broster 1992). Secondly, there is long-term habituation (LTH) present at the post-interventional stage which is more pronounced after longer ISIs (Davis 1970, Rankin and Broster 1992). Both phenomena are suggested to occur at the same time and thus their effects might run parallel or overlap (Davis 1970, Christoffersen 1997). Importantly, exact differentiation of these two types of habituation is not clear, for they base on phenomenological definitions in relation to one another (Davis 1970). Definitions based on distinct parametric values have not yet been established (Ornitz and Guthrie 1989). Therefore, a common pragmatic, yet, rough definition approximates that STH accounts mainly for the reduction at the level of seconds to minutes as seen at the interventional stage within one test-session (Leaton 1976, Ornitz and Guthrie 1989, Koch 1999). In contrast, LTH occurs deferred at the level of days, weeks up to months and over the course of multiple sessions (Leaton 1976, Leaton and Supple 1986, Ornitz and Guthrie 1989, Koch 1999). Moreover, it is suggested that there are even more components which may be found after precise analysis of the temporal course of habituation as well as of its spontaneous recovery (Christoffersen 1997). The gradual decline of the amplitude during 1Hz-high-frequency stimulation might be in accord with such an assumption. Notably, the contrasting entities STH and LTH have been postulated to be suggestive for different neuronal processes in distinct brain structures (Groves, Wilson et al. 1974, Jordan and Leaton 1983, Leaton and Supple 1986, Leaton and Supple 1991).

Together, this means that both manifestations of habituation might be found in the present results of behavioural testing. They might run in parallel and at the stage of spontaneous recovery LTH unmasks only at later stages when STH is completely recovered. Additionally, both processes might have further components and underlying processes are not necessarily congruent with phenomenological appearances. Finally, another limitation which is inherent in the method of behavioural ASR testing has to be taken into account at the stage of spontaneous recovery. Every test stimulus is at the same time a confounding training stimulus inducing habituation. (Davis 1970, Christoffersen 1997)

5.2.2 Global dendritic calcium signals of Purkinje neurons in-vivo

Spontaneous complex (CS) and simple spike (SS) frequencies of Purkinje neurons (PCs) from *in-vivo* single-cell electrophysiology are in accord with earlier studies (Eccles, Llinas et al. 1966, Armstrong and Rawson 1979, Kitamura and Hausser 2011, Roome and Kuhn 2018). Likewise, the consistent co-occurrence of global dendritic calcium transients to somatic CS responses without failure is in line with previous reports (Tank, Sugimori et al. 1988, Davie, Clark et al. 2008, Kitamura and Hausser 2011, Kitamura and Kano 2013, Roome and Kuhn 2018). Thus, global dendritic calcium transients reliably indicated synaptic climbing fibre (CF) input. In PCs, voltage-gated P-type channels are the primary source for this global calcium influx (Usowicz, Sugimori et al. 1992, Westenbroek, Sakurai et al. 1995).
As seen in 4.4, 4.5 and 4.6, the recorded calcium signals, however, displayed amplitude variations. In this context, it has to be remembered that the recorded calcium signal reflects a global spatial average from a transversal cross-section of a PC dendritic tree. Besides, recordings were taken in the upper third of the cerebellar molecular layer where spiny distal dendrites may be found representing parallel fibre-PC-synapses (Eilers, Augustine et al.

1995). Therefore, respective recording-sections may include neighbouring branches, processes and possibly spines from a single PC dendritic tree. Several studies demonstrated that amplitudes of such global dendritic calcium transients may present variability (Tank, Sugimori et al. 1988, Miyakawa, Lev-Ram et al. 1992, Davie, Clark et al. 2008, Kitamura and Hausser 2011, Kitamura and Kano 2013, Najafi and Medina 2013, Najafi, Giovannucci et al. 2014, Najafi, Giovannucci et al. 2014, Roome and Kuhn 2018). Multiple underlying reasons may be considered.

Firstly, various intrinsic morphological factors of a PC need to be taken into account. These include dendrite geometry, dendritic location (distance from the soma) and inhomogeneous distribution of ion channel as well as their intrinsic activity and stochasticity (Miyakawa, Lev-Ram et al. 1992, Anwar, Hepburn et al. 2013, Kitamura and Kano 2013, Roome and Kuhn 2018). Moreover, firing state of a PC and its membrane potential up and down states are able to affect climbing fibre-mediated global calcium responses (Kitamura and Hausser 2011, Kitamura and Kano 2013).

Secondly, there might be variation in the presynaptic climbing fibre action potential burst which is able to form the postsynaptic response (Maruta, Hensbroek et al. 2007, Bazzigaluppi, De Gruijl et al. 2012). Besides, influence of neuromodulatory afferents has to be taken into account (Schweighofer, Doya et al. 2004).

Thirdly, the dynamic and diverse spatiotemporal map of dendritic voltage due to local background synaptic activity is reported to account for global signal variation (Callaway, Lasser-Ross et al. 1995, Davie, Clark et al. 2008, Kitamura and Hausser 2011, Kitamura and Kano 2013, Najafi and Medina 2013, Roome and Kuhn 2018). As such, dendritic voltage differences are suggested to locally modify and direct CF-mediated calcium influx which, in turn, sums up to temporally variable global dendritic calcium amplitudes. Various processes

may contribute to this phenomenon. Inhibitory GABAergic-input from molecular layer interneurons (MLIs), for instance, is reported to effectively modulate local calcium signals (Callaway, Lasser-Ross et al. 1995). Similarly, localised excitatory parallel fibre (PF)-input may influence CF-driven calcium influx (Kitamura and Hausser 2011, Kitamura and Kano 2013).

Fourthly, it has been suggested that PF-synaptic activity can additionally contribute calcium to a mainly CF-derived calcium signal (Najafi, Giovannucci et al. 2014). These events may also appear sensory-driven, as such, encoding sensory information (Najafi, Giovannucci et al. 2014). Notably, it has been moreover proposed that there are distinct elevations of dendritic calcium which derive solely from synaptic PF-input in absence of climbing fibre-activity, however, being subtle and with different kinetics (Miyakawa, Lev-Ram et al. 1992, Najafi, Giovannucci et al. 2014). In line with this proposition, it has been reported that sharp rises in activity of so-called localised voltage hotspots in spiny dendrites may cause small increases in dendritic calcium without an expected correlated somatic response (Roome and Kuhn 2018).

Finally, it has been demonstrated *in-vitro* that there is also calcium release from internal storages upon PF-synapse input, for example, via metabotropic glutamate-receptors in spines (Eilers, Augustine et al. 1995, Wang, Denk et al. 2000). For in-vivo recordings, however, this has not yet been shown and in regard of globally averaged dendritic responses their contribution is probably negligible. Similarly, calcium influx mediated by AMPA-receptors at PF- and CF-synapses may be considered insignificant for global dendritic calcium signals due to its very low calcium permeability (Konnerth, Llano et al. 1990, Tempia, Kano et al. 1996).

Together, global dendritic calcium transients reliably indicated synaptic CF-input. Additionally, their calcium amplitudes might have been modified by spatiotemporally-dynamic background processes at PF- and/or MLI-synapses (Najafi and Medina 2013, Roome and Kuhn 2018). Besides the CF-mediated bulk of calcium, minor contributions to the signal possibly have been made by localised PF-input (Roome and Kuhn 2018). These inputs could appear sensory-driven (Kitamura and Hausser 2011, Najafi and Medina 2013, Najafi, Giovannucci et al. 2014, Najafi, Giovannucci et al. 2014). Nevertheless, it also has to be carefully taken into account that calcium signal variations are either due to intrinsic properties (Kitamura and Kano 2013, Roome and Kuhn 2018) or confounded by measurement inaccuracies, such as focal plane discrepancies, signal contamination by fluorescence from surrounding structures (e.g. neuropil) or specimen movement (e.g. tissue pulsation). Thus, dedicated assignment of calcium to distinct synaptic input other than climbing fibres is not viable under the given experimental parameters.

5.2.3 Acoustic startle stimulus-evoked responses and their persistence during habituation

Multiple studies across different animal species using auditory-evoked potentials as well as single unit recordings demonstrated that the cerebellar vermis receives auditory input (Snider and Stowell 1944, Altman, Bechterev et al. 1976, Huang and Liu 1985). Additionally, morphological tracing studies confirmed direct anatomical connections from auditory sites to the cerebellar vermis in cats (Huang, Liu et al. 1982). Similarly, anatomical studies in cat and opossum showed that there are projections from accessory nuclei of the inferior olive onto congruent parts of the vermis (Armstrong 1974, Brodal, Walberg et al. 1975, Linauts and Martin 1978). Electrophysiological experiments have confirmed these olivo-cerebellar connections in cats (De Montigny and Lamarre 1975).

Notably, respective accessory nuclei of the inferior olive have been reported to receive once more input from auditory and basic startle pathway-related sites as shown in rhesus monkey and opossum (Frankfurter, Weber et al. 1976, Harting 1977, Martin, Beattie et al. 1977, Linauts and Martin 1978). Also in humans, auditory-task associated activation of the cerebellum has been demonstrated in functional studies (Petacchi, Laird et al. 2005, Pastor, Vidaurre et al. 2008, Baumann and Mattingley 2010).

There are electrophysiological studies in monkey which explicitly used acoustic startle stimulation while recording electric somatic responses of Purkinje neurons (PCs) and cerebellar nuclear cells (Mortimer 1973, Mortimer 1975). Stimulation could evoke complex spike responses in approximately 50% of the recorded PCs (Mortimer 1973, Mortimer 1975). In responsive cells, complex spikes occurred at a fixed temporal relation to the stimulus but at variable rates of responsiveness ranging from less than 30% to near-complete responsiveness across trials (Mortimer 1975). Unfortunately, no detailed statistics on response rates are given. This, nonetheless, confirms the finding that acoustic startle stimulation is effective in evoking climbing fibre-derived responses in PCs and that there is variability in responsiveness across PCs.

Other modalities of sensory-stimulation have been shown to evoke climbing fibre-responses in PCs at comparable levels, such as, tactile (Kitamura and Hausser 2011, Najafi, Giovannucci et al. 2014, Najafi, Giovannucci et al. 2014) or visual (Mortimer 1975). Notably, adequate tactile (Simons-Weidenmaier, Weber et al. 2006, Pilz, Arnold et al. 2014) and visual (Mortimer 1975, Koch 1999) stimuli have to be considered effective startle stimuli at the same time. In this regard, visual and acoustic startle stimuli are reported to evoke responses both in the same and in mutually exclusive PCs (Mortimer 1975), as such, supporting the view that these responses do not reflect sole sensorimotor feedback.

Furthermore, it has been shown that, besides the CF-input, acoustic startle stimulation additionally affects parallel fibre (PF) input (Mortimer 1973, Mortimer 1975). In line with this, several studies reported that auditory-stimulation reliably induces synaptic mossy fibre-input to granule cells (Ishikawa, Shimuta et al. 2015) and synaptic PF-input-related activity in PCs (Freeman 1970, Aitkin and Boyd 1975, Supple, Sebastiani et al. 1993). Therefore, one may assume that acoustic startle stimulus-evoked CF- and PF-input responses are present in PCs at the same time.

The present study moreover contrasted for the first time effects of repetitive acoustic startle stimulation on the acoustic startle response (ASR) habituation with effects on responsiveness of evoked global dendritic calcium responses in a correlative experiment. The results suggested that signals persist at similar rates of responsiveness throughout the entire process of startle habituation. Additionally, they seem to appear at comparable rates independent of the inter-stimulus-interval used and even despite startle suppression. Likewise, they remain present at equal rates during the stage of spontaneous recovery.

Together, potential anatomic connections from auditory sites to the cerebellar vermis are present in form of its two major afferents – the mossy and climbing fibre inputs. Moreover, sound-elicited responses have been demonstrated in PCs in terms of sound-evoked synaptic CF- and PF-input responses. This is also true for acoustic startle stimulation. The present results are in line with these observations showing additionally relevant presence of acoustic startle stimulation-evoked dendritic calcium signals in PCs of awake mice during single acoustic startle stimulation, startle habituation as well as startle recovery for the first time.

The data suggests that these signals persist at comparable response rates despite different inter-stimulus-intervals as well as despite different stages of correlated ASR habituation. However, the experiments give no direct indication on which function these ASR-habituation correlated signals might represent and what their relation to the ASR generally is, if at all.

In this respect, do they reflect primary auditory input from auditory-/startle pathway-related sites or second-order responses to secondary auditory-associated input from subordinate processes following ASR stimulation? Are they in this sense relevant for the ASR at all or do they merely mediate associated processes like autonomic responses, for example? If they are relevant, do they modulate the startle response proper (i.e. primary parameters like amplitude) or secondary parameters, such as for sensorimotor coordination and correction of startle movement? In this context, the persistence of stimulus-evoked responses despite startle suppression might suggest that the input is more than mere sensorimotor feedback for coordination. However, on a temporal scale, would this be immediate and restricted modulatory action and/or include persistent modulatory effects, for instance, in the context of habituation? Finally, if sound-evoked signals of vermal PCs are relevant for habituation, can they be ascribed to short-term habituation, long-term habituation or any other component of habituation?

Insights on the role of observed cerebellar processes regarding the ASR were expected to derive from harmaline-interventions which were conducted to disrupt intact olivary CF-input to PCs and, as such, also to disrupt the preserved acoustic stimulation-evoked CF-input. Respective results are discussed in the following sections. In section 5.4.3, questions of cerebellar function regarding ASR-modulation are re-addressed.

5.3 Suggested cerebellar modulation of startle by harmaline-induced startle suppression

5.3.1 Prolonged harmaline-induced suppression of acoustic startle responses

Harmaline-application was potent in reliably eliciting a transient tremor in all mice. The tremor had a characteristic rhythmic appearance with a major tremor frequency power at around 13.5Hz. The tremorgenic effect of harmaline on mice has been described extensively in earlier reports (Ahmed and Taylor 1959, Lamarre and Mercier 1971, Llinas and Volkind 1973, Miwa 2007, Handforth 2012). This effect is generally attributed to its action on neurons of the inferior olive (IO) (Lamarre and Mercier 1971, Llinas and Volkind 1973). In section 1.4, the effect of harmaline on olivary neurons has been introduced. Briefly recapitulated, by facilitating their pacemaking rhythmic subthreshold oscillations, frequency and extent of olivary climbing fibre (CF) input to the cerebellum is increased (Llinas and Volkind 1973, Llinas, Baker et al. 1974, Llinas and Yarom 1981, Llinas and Yarom 1986). This, in turn, leads to amplified cerebellar output on different motor structures, as such, mediating the phenotypic tremor (Llinas and Volkind 1973). Tremor is interrupted by dissection of olivo-cerebellar fibres in the inferior peduncle (Llinas and Volkind 1973) or by lesion of the IO (Simantov, Snyder et al. 1976), however, not by elimination of Purkinje neurons (Llinas and Volkind 1973, Milner, Cadoret et al. 1995). Likewise, complex spike activity remains unchanged after direct application of harmaline on the cerebellar cortex (Chen, Kovalchuk et al. 2010). Together, this points to deep cerebellar nuclei being key mediators of tremor, although PCs are as much affected by increased CF-input. The resulting tremor has been reported to have a frequency of around 14Hz (Ahmed and Taylor 1959, Milner, Cadoret et al. 1995, Miwa 2007), as such, being in line with the present findings (see 4.8).

Testing of the acoustic startle response (ASR) during harmaline-induced cerebellar tremor revealed a pronounced reduction of the startle amplitude during tremor. This reduction was present throughout the stage of manifest tremor and, notably, persisted even after tremor had ceased. An earlier study on guinea-pigs which used electromyography of nuchal muscles for recordings of the ASR head-jerk-component found a significantly depressed amplitude after harmaline-injection (Pellet, Weiss et al. 1983). Interestingly, some data presented in this study indicated moreover a sustained effect of startle reduction over hours. This would be in line with the present results, however, was not deliberately discussed by the author.

Regarding the persistent ASR-reduction after tremor possible confounders must be considered nonetheless. On the one hand, spectral power analysis of accelerometric traces confirmed that tremor was indeed absent (see 4.9). On the other hand, climbing fibre-mediated busting-alike calcium activity had been observed sporadically in absence of detectable tremor (see 4.11). Challenged delineation of tremor and post-tremor stages due to re-onset and residual tremor has to be bared in mind as well, although particular precaution was taken in terms of strict protocol routines (see 4.8 and 4.9). Together, it cannot be excluded to the last that the ASR reduction at the post-tremor stage in behavioural experiments was at least partially due to persistent harmaline-induced increase of climbing fibre-input, for no simultaneous neurophysiological recordings of PCs were made. Accepting that the prolonged ASR-reduction was not confounded by residual CF-activity, the question arises which mechanism allows for persistence of the effect. Potential mechanisms for the induction of a prolonged ASR-reduction are discussed in section 5.4.2.

5.3.2 Validity of conclusions derived from harmaline experiments

Harmaline was used to demonstrate effective modulation of the acoustic startle response (ASR) by Purkinje neurons in the cerebellar vermis. However, to what extent are conducted interventions valid to reveal such a causal relation? In this context it must be considered that the proposed harmaline-induced and cerebellar-mediated effect might be confounded. Since harmaline was administered intraperitoneally, systemic effects cannot be excluded. Generally, two types of confounders may be distinguished in this respect. On the one hand, confounders may trouble the assumed cause, i.e., increased climbing fibre (CF) input from the inferior olive (IO). On the other hand, confounders may trouble the assumed effect, i.e., effective ASR-modulation by cerebellar interference with the basic startle pathway. As a consequence, several alternatives must be reflected.

Firstly, harmaline could act directly on a structure within the basic startle pathway including the sensor and effector systems. Secondly, harmaline could act directly or indirectly on a structure other than the IO or the basic startle pathway which confounds ASR-modulation. Similarly, another IO-targeted structure extrinsic to the olivo-cerebellar circuit could be a mediator. Such structures might actually modulate the ASR by interfering with the basic startle pathway. Else, they could imitate ASR-modulation by confounding the effective ASR, respectively, the readout. Thirdly, harmaline-induced tremor and/or disrupted cerebellar function due to increased CF-input might confound the effective ASR, respectively, its readout. As such, it solely mimics ASR-modification. Finally, a combination of the above is conceivable.

Several observations mitigate above concerns. This is especially true for the concern that tremor or disrupted cerebellar neurophysiology due to increased CF-input confound general elicitation of the ASR. Despite tremor, startle could be triggered and remained demarcated

from the tremor-band. The ASR remained reduced in brief tremor-pauses and in particular even after tremor had ceased, indicating that the ASR is not merely reduced because of ongoing tremor movement. Even compensating for the tremor amplitude, startle was reduced compared to control. Since stereotypic appearance of the ASR was preserved and undistorted during tremor despite reduced startle amplitudes, motor execution, control and coordination appeared to be intact. Moreover, aforementioned study on guinea-pigs (see section 5.3.1) demonstrated startle reduction after harmaline-application without tremor-corrupted recordings by using electromyography of nuchal muscles and low harmaline doses (Pellet, Weiss et al. 1983). It has to be considered that tremor might have led to impaired strength or muscle fatigue which imitated ASR amplitude-reduction. Mice showed no apparent behavioural abnormalities during and after tremor that would indicate weakness or fatigue. Studies on rats showed impaired strength during harmaline-induced tremor (Tariq, Arshaduddin et al. 2002, Vaziri, Abbassian et al. 2015), however, not to a degree which would be expected to suppress startle responses representing a highly-conserved primitive reflex. Likewise, patients with essential tremor do not generally exhibit impaired muscle strength (Solbach, Mumm et al. 2016, Ozer, Kirmaci et al. 2018). Designated experiments demonstrating preserved strength during and particularly after harmaline-tremor, e.g. a grip force test after tremor, have not been conducted. Together, although it cannot be rejected to the last, several lines of evidence suggest that significant readout-confounding effects of harmaline-disrupted cerebellar physiology are not present.

On the one hand, studies demonstrating that harmaline fails to induce tremor after selective lesions of the IO (Simantov, Snyder et al. 1976) and studies showing intact cerebellar neurophysiology after dissection of CF-fibres (Llinas and Volkind 1973) lend support to the specificity of the harmaline-effect on the IO regarding the olivo-cerebellar circuit.

On the other hand, effects of harmaline on structures extrinsic to the olivo-cerebellar circuit cannot be excluded. As introduced in section 1.4, effects and sites of action of harmaline are diverse. Consequently, the lack of specificity after systemic harmaline-application could allow for confounders regarding the assumed cause and/or the assumed effect. Thus, in order to accept a causal relation it is necessary to assume that the harmaline-induced ASR-modulatory effect is mediated specifically by the olivo-cerebellar circuit.

5.3.3 Further evidence suggesting cerebellar modulation of the acoustic startle response

Several lines of evidence support the proposed cerebellar role in acoustic startle response (ASR) modulation. Manifest anatomical connections have been reported between cerebellar nuclei and startle pathway-related sites which could serve for transmission of modulatory cerebellar function (Ito, Udo et al. 1970, Brodal, Destombes et al. 1972, Asanuma, Thach et al. 1983, Teune, van der Burg et al. 2000). Although ASR is generally possible after cerebellectomy (Wright and Barnes 1972), stimulation of the anterior lobe has been shown to cause amplitude reduction (Misrahy, Spradley et al. 1961). Multiple lesion studies (Leaton and Supple 1986, Lopiano, de'Sperati et al. 1990, Leaton and Supple 1991) and studies using artificial spreading depression (Storozeva and Pletnicov 1994) of the vermis reported impaired amplitude reduction, particularly, in context of long-term habituation (LTH) of the ASR. Moreover, functional imaging studies confirmed the involvement of the medial cerebellum in LTH in humans (Timmann, Musso et al. 1998, Maschke, Drepper et al. 2000, Frings, Awad et al. 2006). Patients with schizophrenia spectrum disorder which is known for cerebellar involvement display impaired ASR habituation (Ludewig, Geyer et al. 2003). Interestingly, also cerebellar-mediated associative learning may be disrupted by harmaline (Welsh 1998) and in patients with essential tremor (Kronenbuerger, Gerwig et al. 2007).

In view of this evidence, results from harmaline-interventions are strongly supported in suggesting that cerebellar neurophysiology effectively modulates the startle amplitude. In doing so, harmaline-induced ASR-reduction appears to be a prolonged phenomenon.

5.4 A potential circuit and synaptic mechanism of acoustic startle response-modulation

5.4.1 A potential cerebellar circuit of acoustic startle response-modulation

This section summarises what can be said regarding a potential acoustic startle response (ASR)-modulatory cerebellar circuit in which Purkinje neurons (PCs) are an integral component. This is only valid accepting the hypothetic causal role of the cerebellar vermis in ASR-modulation in view of the evidence in favour for this assumption (see 5.3.3) and despite the remaining uncertainty of harmaline-specificity (see 5.3.2).

Firstly, acoustic startle stimulus-evoked global dendritic calcium transients were demonstrated to be strongly preserved. On the one hand, this was shown by reliable responsiveness to single acoustic startle stimulation (see 4.6) and by persistence of responses throughout the entire startle suppression experiment (see 4.7). This indicated that responses are preserved at comparable rates despite different stimulation frequencies and different states of startle habituation. On the other hand, acoustic startle stimulus-evoked global dendritic calcium responses were shown to be unexpectedly preserved despite harmaline-disrupted background activity of synaptic climbing fibre (CF) input (see 4.11). As such, sensory stimulation even overcame impaired intrinsic activity in the inferior olive (IO). Altogether, these results underline the importance of sound-evoked global dendritic calcium responses in PCs which were demonstrated to indicate CF-input to the cerebellum.

Secondly, acoustic startle stimulation (Mortimer 1973, Mortimer 1975) and auditory-stimulation (Freeman 1970, Aitkin and Boyd 1975, Supple, Sebastiani et al. 1993) was reported to effectively evoke simultaneous synaptic parallel fibre (PF) input-associated activity (see also 5.2.3). Thirdly, in anatomical studies it has been shown that there are manifest anatomical connections from auditory- and startle pathway-related sites to the cerebellar vermis (see 5.2.3) and from corresponding deep cerebellar nuclei (e.g. the fastigial nucleus) back to startle pathway-associated sites (see 5.3.3).

Therefore, a hypothetic circuit mechanism may be conceptualised as follows. Acoustic startle stimulation is transmitted from auditory-related sites to the cerebellar vermis in terms of both its major afferents – mossy fibre-/PF-input and CF-input. PF- and CF-synaptic input is integrated in vermal PCs and the computational output is relayed via deep cerebellar nuclei (DCN) to startle pathway-associated sites (reconsider figure 2 in section 1.3).

This partly remains a hypothetic and vague circuit but may serve as a working hypothesis for further investigations. In particular, present results do not allow for distinct statements on sound-evoked PF-input and how it changes to repetitive stimulation as in ASR habituation. Inferences on the relevance of PF-input were drawn from earlier reports (Freeman 1970, Mortimer 1973, Mortimer 1975, Supple, Sebastiani et al. 1993) and from insights of harmaline-interventions (see also 5.4.2). Statements on processes up- and downstream of PCs, such as in the IO, granule cells, interneurons or in DCN and their potential startle pathway-related targets, cannot be made. The essential role of PCs is proposed due to the changes in their neurophysiology reported upon repetitive auditory stimulation (Supple, Sebastiani et al. 1993) and observed during harmaline-interventions (see 5.4.2). Additional processes in or mediated by the IO, e.g., in DCN or interneurons were not investigated during harmaline-interventions and thus cannot be excluded.

5.4.2 A potential synaptic mechanism of acoustic startle response-modulation

This section addresses the changes observed in Purkinje cell (PC) neurophysiology upon harmaline-application, especially, since they were associated with acoustic startle response (ASR) reduction. Harmaline provoked a marked increase of climbing fibre (CF) derived complex spikes (CS). Increased CF-input was also indicated by a heightened number of global dendritic calcium transients. As such, both of these read-out markers indirectly reflected the increased activity of neurons from the inferior olive (IO) as expected upon harmaline-application (Llinas and Volkind 1973). Remarkably, harmaline led at the same time to a pronounced suppression of parallel fibre (PF) associated simple spikes (SS). In line with these findings, former studies on cat, wild-type and dystonic rats provide similar evidence on simultaneous harmaline-induced CS increase and SS decrease (De Montigny and Lamarre 1973, Lorden, Stratton et al. 1988, Stratton and Lorden 1991, LeDoux and Lorden 2002).

Together, these results suggest that CF-mediated impaired transmission of synaptic PF-input resulting in depressed output might be a potential synaptic mechanism of ASR-modulation on the level of vermal PCs (see also figure 1A in section 1.2, right panel). Necessary assumption for such a process at PCs is, however, that harmaline acts specifically via the IO and via the olivo-cerebellar circuit (see 5.3.2). As such, it may not act locally on PCs or confound PF-input via direct action on granule cells or pre-cerebellar neurons providing the respective mossy fibre-input. Besides, direct action on interneurons, deep cerebellar nuclei (DCN) or neuromodulatory inputs should be excluded. In line with this, it was demonstrated that systemically-injected harmaline does neither increases CS, nor suppress SSs after dissection of CFs at the level of the inferior cerebellar peduncle (Llinas and Volkind 1973). Similarly, after selective lesion of the IO with subsequent degeneration of CFs, harmaline is

unable to induce any cerebellar tremor at all (Simantov, Snyder et al. 1976). Absence of changes in CS activity of PCs after direct harmaline-application on the cerebellar cortex lends further support for the assumption that harmaline acts specifically via the CF-input (Chen, Kovalchuk et al. 2010). The underlying processes of harmaline-induced SS-suppression at increased CF-input, especially for the phenomenon of sustained SS-suppression, are not clear as for now and are suggested to include among others co-activation of inhibitory interneurons by CFs, CS discharge-induced PC inactivation or possibly more permanent changes (Bloedel and Roberts 1971, Armstrong, Cogdell et al. 1979, Rawson, Wertheimer et al. 1988). Remarkably, PF-input associated activity has been shown to habituate upon repetitive pure-tone stimulation (Supple, Sebastiani et al. 1993), as such, suggesting the presence of the proposed mechanism also at physiological conditions.

Of special interest is which mechanism under physiological conditions could lead to a comparable depression of synaptic PF-input transmission. On the one hand, we have seen that CF-input appeared as a time-locked, acoustic startle stimulus-evoked response. On the other hand, it has been shown that acoustic startle stimulus-evoked PF-input appears at the same time (Mortimer 1973, Mortimer 1975). Considering the co-occurrence of these inputs, two common types of synaptic plasticity at synapses onto PCs may be discussed as potential candidates. Firstly, coinciding input from PF- and CF-afferents may induce a long-term depression of excitatory PF-PC-synapses (Ito and Kano 1982, Ito 2006). This process is called long-term depression. Secondly, postsynaptic depolarisation upon CF-stimulation may induce a long-lasting potentiation of GABAergic inhibition at molecular layer interneuron-PC-synapses (Kano, Rexhausen et al. 1992, Kano, Kano et al. 1996). This process is termed rebound potentiation. Besides, changes on the level of MLIs may be considered.

The cellular processes for both types of synaptic plasticity are mediated by calcium which acts as a second messenger. It either activates cascades including protein kinase C and cyclic guanosine monophosphate-dependent protein kinase in case of long-term depression (Ito 2006) or processes including calcium/calmodulin-dependent protein kinase II in case of rebound potentiation (Kano, Kano et al. 1996). In this context, CF-input provides calcium influx throughout the entire dendritic tree (Konnerth, Dreessen et al. 1992, Miyakawa, Lev-Ram et al. 1992). PF-input additionally provides localised calcium influx which has been demonstrated on the synaptic level *in-vitro* (Eilers, Augustine et al. 1995, Wang, Denk et al. 2000). Comparable global and local processes have been suggested to appear *in-vivo* (see 5.2.2) and acoustic startle stimulation has been demonstrated to be effective in evoking both of these inputs (see 5.2.3).

Mentionable in this respect, it has been proposed that sensory-driven CF-input might serve as an instructive signal for PCs (Marr 1969, Albus 1971). As such, it provides global calcium influx and together with coinciding sensory-driven PF-input providing localised calcium it might be effective in directing plasticity to specific synapses (Konnerth, Dreessen et al. 1992, Wang, Denk et al. 2000, Kitamura and Hausser 2011). Besides these theoretical considerations, there is, nonetheless, also controversy on the role to be assumed for CF-input (De'Sperati, Lopiano et al. 1989, Welsh 1998).

Persistent functional changes due to synaptic plasticity could also explain the prolonged effect in terms of ASR-suppression after harmaline-induced tremor. This would, however, suggest that synaptic plasticity had been induced also in case of harmaline-interventions and, in fact, only after relatively few stimuli or possibly even independent from them. However, the given results do not allow for definite statements on this.

Alternatively, induction of changes in a startle pathway-associated structure which is extrinsic to but targeted by the proposed cerebellar circuit may be considered as the neuroanatomical correlate responsible for prolonged ASR-reduction (Lopiano, de'Sperati et al. 1990). In this case, the identified synaptic mechanism might mediate induction of prolonged changes.

The inferences made on the observed changes in PC activity being a potential mechanism of ASR-modulation are only valid accepting the hypothetic causal role of the cerebellar vermis in ASR-modulation in view of the evidence in favour for this assumption (see 5.3.3) and despite the remaining uncertainty of harmaline-specificity (see 5.3.2). Additionally, the essential role given to PCs in the proposed cerebellar ASR-modulatory circuit is based on observations made during harmaline-intervention. Processes at up- and downstream partners, such as the IO, DCN or interneurons, and their relevance were not investigated. Besides, it has to be remembered that only increased global dendritic calcium transients (reflecting CF-input) were recorded simultaneously to harmaline-induced suppression of the ASR. Statements on depressed SSs during ASR-suppression as well as on recovered PC activity during sustained ASR-reduction base on (temporal) correlations of behavioural testing with electrophysiological experiments. Additionally, there might be the possibility that the prolonged ASR-reduction in this context may have been confounded by residual harmaline-effects (see 5.3.1). Finally, the question remains to what extent processes identified during harmaline-interventions reflect physiological conditions. As mentioned above, similar observations regarding depressed SS activity have been made, however, under more physiological conditions of repetitive pure-tone stimulation (Supple, Sebastiani et al. 1993).

5.4.3 Potential cerebellar function in acoustic startle response-modulation

In section 5.3, the proposed modulatory influence of the cerebellar vermis on the acoustic startle response (ASR) derived from observations during harmaline-interventions has been considered conditionally legitimate. Accepting this type of direct control, nevertheless, uncertainty remains regarding the precise functional role of the cerebellar vermis in ASR-modulation as introduced in section 5.2.3. These include, for instance, whether primary parameters of the ASR, such as response latency and amplitude, or secondary parameters, such as coordination and correction of startle movement, are affected primarily.

Observations made during harmaline-interventions pointed at least towards a role in amplitude control. In contrast, the coordinated startle movement remained unaffected. In line with this proposition, direct electric stimulation of the vermis has been shown to result primarily in ASR-reduction (Misrahy, Spradley et al. 1961). However, is this a type of restricted, immediate amplitude control or is there also a prolonged effect as would be expected for a potential role in habituation?

The persistent effect of ASR-reduction seen after harmaline-tremor at least suggested also a prolonged effect of amplitude control. In support of this observation, lesion studies (Leaton and Supple 1986, Lopiano, de'Sperati et al. 1990, Leaton and Supple 1991) and studies using artificial spreading-depression (Storozeva and Pletnicov 1994) of the cerebellar vermis have advised that the cerebellar vermis is involved in long-term habituation (LTH) of the ASR. Nonetheless, multiple other structures are reported to be relevant in LTH as well. These are, for example, the mesencephalic reticular formation (Jordan and Leaton 1983), the ventral periaqueductal grey (Borszcz, Cranney et al. 1989) and cortical regions (Groves, Wilson et al. 1974). Therefore, the vermis might be one of several key agents in ASR-LTH and/or in general ASR-modulation.

As described in 5.2.1, it has been proposed that there might be additional or synergetic components to the process of habituation (Christoffersen 1997). Both induction of habituation and spontaneous recovery are suggested to consist of such components (Davis 1970, Christoffersen 1997). Thus, the possibility has to be considered that the vermis mediates one of these intermediate components which possibly run in parallel and/or overlapping. An exact assignment of the identified mechanism to a specific type or component of habituation, however, is not possible under the present experimental parameters.

Notably, it has been reported that the vermis is essential only for the acquisition, not for the retention of LTH of the ASR (Lopiano, de'Sperati et al. 1990). Therefore, it needs to be taken into account that cerebellar function is found rather in the induction of a prolonged effect in a structure extrinsic to the vermis but not within the vermis itself. Such an extrinsic site might be found in or involve structures like the mesencephalic reticular formation, since in contrast to the vermis lesions here abolish both LTH acquisition and retention (Jordan and Leaton 1983, Jordan 1989).

Since the cerebellum receives a multitude of sensory information, particularly input related to known startle stimuli like auditory and tactile, it is also an excellent candidate to mediate such an effect in a modality-specific way which is characteristic for startle habituation (Crispino and Bullock 1984, Pilz, Arnold et al. 2014). Despite the focus given to its suggested role in ASR-habituation, the possible involvement in the parallel process of sensitisation has to be kept in mind since reduced sensitisation results as well in a net effect of habituation.

Together, the results provide a potential circuit and synaptic mechanism for ASR-modulation in terms of amplitude control. Moreover, some evidence suggests that these processes might induce a prolonged effect (see also 5.3.1 and 5.4.2). In light of previous studies underlining the importance of the cerebellar vermis in LTH of the ASR, this mechanism could thus reflect a key process in mediating this LTH-specific function. However, it needs to be validated that the identified processes reflect a physiological mechanism at all (see 5.3, 5.4.1 and 5.4.2).

If they do reflect a physiological mechanism, it has to be considered that the process of ASR-reduction seen during harmaline-intervention might mimic a short-term effect by rapid induction of a long-term effect. In order to evaluate the function of the cerebellar vermis more precisely and how this function is eventually mediated, downstream targets of the identified cerebellar circuit, relations to the basic startle pathway and processes under physiological conditions need to be analysed in more detail both anatomically and functionally. Therefore, only future investigations will elucidate the precise role of the cerebellar vermis in ASR-modulation in greater depth.

5.5 Methodological considerations and limitations

In each section of the discussion the respective methodology and its limitations have been critically reflected on. However, major limitations of the present thesis may be summarised. Firstly, insights on a causal relation between changes in Purkinje cell (PC) neurophysiology and acoustic startle response (ASR) modulation might have been confounded by unspecific harmaline-effects (see 5.3.2). Secondly, accepting the assumption of causality in view of additional evidence (see 5.3.3), focus was primarily on harmaline-induced increased climbing fibre (CF) input to PCs. Potential effects on other targets of CF-projections were not addressed (see 5.4.1 and 5.4.2). Thirdly, global dendritic calcium transients allowed for statements on climbing fibre-input but not for distinct statements on parallel fibre-input (PF) (see 5.2.2). Therefore, inference on the role of PF-input regarding a potential circuit and synaptic mechanism of ASR-modulation derived from (temporally) correlated electrophysiology with harmaline-intervention as well as from earlier reports (Mortimer 1973, Mortimer 1975) on acoustic startle stimulus-evoked signals in PCs (see 5.2.3, 5.4.1 and 5.4.2). Fourthly, the sustained effect of startle-reduction by harmaline might have been confounded by residual harmaline-effects (see 5.3.1) and inferences made to propose a potential circuit and synaptic mechanism for sustained ASR-reduction (see 5.4.2) derived once more from (temporally) correlated electrophysiology with harmaline-intervention and previous studies (Mortimer 1973, Mortimer 1975). Finally, it is not clear if the observed processes at harmaline-interventions and the proposed mechanism reflect physiological conditions. Moreover, if they do reflect physiological conditions, precise statements on their relation to ASR-modulation, which is in particular, to manifestations or single components of ASR habituation cannot be made. The experimental parameters of behavioural testing do not allow for a precise differentiation of individual components or manifestations (see 5.2.1).

5.6 Summary, significance and conclusive remarks

The present results suggest that vermal Purkinje neurons (PCs) are part of a distinct cerebellar circuit processing acoustic startle stimulus-evoked signals. Furthermore, changes in PCs neurophysiology have been identified as a potential mechanism for acoustic startle response (ASR) modulation as has been revealed under conditions of harmaline-induced cerebellar tremor. The modulatory effect was primarily found in ASR amplitude reduction. In this regard, highly preserved, instructive-alike, acoustic startle stimulus-evoked synaptic climbing fibre-input and, at the same time, impaired transmission of synaptic parallel fibre-input are given particular attention. Long-lasting ASR-reduction suggests that the mechanism induces prolonged effects. In this context, calcium-dependent synaptic plasticity resulting in depressed parallel fibre synapse transmission-associated PC output and/or distant induction have been proposed to be suitable candidates. Together, objectives and central questions of the present thesis have been successfully addressed (see chapter 2).

These are highly significant novel findings considering the importance of ASR-modulation as a model for sensorimotor integration and habituation in mammals. They contribute and complement to the present knowledge on cerebellar signalling and function, in particular, following acoustic startle stimulation. The view that ASR-modulation, including habituation as one of its manifestations, involves more distributed circuits is supported. Moreover, a potential circuit and synaptic mechanism for the crucial role of the cerebellar vermis in long-term habituation suggested by previous studies has been provided. This also indicates that fundamental behavioural changes in mammals, such as habituation, might be traced back to plastic changes in distinct neural networks.

Additionally, the results are significant regarding the understanding of diseases with cerebellar affection and/or ASR-deviations, such as, schizophrenia spectrum disorder, autism spectrum disorder, post-traumatic stress disorder, essential tremor, cerebellar cognitive and affective syndromes and, as such, might have clinical implications.

Future work ought to confirm the causal relation and elucidate the specific circuit, synaptic and cellular processes in more detail. This could include cell-type specific manipulations, e.g. in (vermal) PCs, for a detailed characterisation of circuit-related functionality as well as cellular physiology of synaptic processes by genetic and pharmaceutical means, such as transgenic animals, channel blockers or enzyme inhibitors. Identification of further up- and downstream partners as well as relevant processes in this restricted cerebellar circuit by similar means could elaborate the relation to the basic startle pathway. In this process, a profound understanding of cerebellar involvement in ASR-modulation may be established, as such, contributing to the ever-growing body of knowledge on diversity of cerebellar functions.

References

Ahmed, A. and N. R. Taylor (1959). "The analysis of drug-induced tremor in mice." Br J Pharmacol Chemother 14: 350-354.

Airaksinen, M. M., V. Saano, E. Steidel, H. Juvonen, A. Huhtikangas and J. Gynther (1984). "Binding of beta-carbolines and tetrahydroisoquinolines by opiate receptors of the delta-type." Acta Pharmacol Toxicol (Copenh) 55(5): 380-385.

Airaksinen, M. M., H. Svensk, J. Tuomisto and H. Komulainen (1980). "Tetrahydro-beta-carbolines and corresponding tryptamines: In vitro inhibition of serotonin and dopamine uptake by human blood platelets." Acta Pharmacol Toxicol (Copenh) 46(4): 308-313.

Aitkin, L. M. and J. Boyd (1975). "Responses of single units in cerebellar vermis of the cat to monaural and binaural stimuli." J Neurophysiol 38(2): 418-429.

Albus, J. S. (1971). "A theory of cerebellar function." Mathematical Biosciences 10(1): 25-61.

Altman, J. A., N. N. Bechterev, E. A. Radionova, G. N. Shmigidina and J. Syka (1976). "Electrical responses of the auditory area of the cerebellar cortex to acoustic stimulation." Exp Brain Res 26(3): 285-298.

Anens, E., B. Kristensen and C. Hager-Ross (2010). "Reactive grip force control in persons with cerebellar stroke: effects on ipsilateral and contralateral hand." Exp Brain Res 203(1): 21-30.

Anwar, H., I. Hepburn, H. Nedelescu, W. Chen and E. De Schutter (2013). "Stochastic calcium mechanisms cause dendritic calcium spike variability." J Neurosci 33(40): 15848-15867.

Armstrong, D. M. (1974). "Functional significance of connections of the inferior olive." Physiol Rev 54(2): 358-417.

Armstrong, D. M., B. Cogdell and R. J. Harvey (1979). "Discharge patterns of Purkinje cells in cats anaesthetized with alpha-chloralose." J Physiol 291: 351-366.

Armstrong, D. M. and J. A. Rawson (1979). "Activity patterns of cerebellar cortical neurones and climbing fibre afferents in the awake cat." J Physiol 289: 425-448.

Asanuma, C., W. T. Thach and E. G. Jones (1983). "Brainstem and spinal projections of the deep cerebellar nuclei in the monkey, with observations on the brainstem projections of the dorsal column nuclei." Brain Res 286(3): 299-322.

Batini, C., C. Buisseret-Delmas and M. Conrath-Verrier (1979). "Olivo-cerebellar activity during harmaline-induced tremor.A 2-[14C]deoxyglucose study." Neurosci Lett 12(2-3): 241-246.

Baumann, O., R. J. Borra, J. M. Bower, K. E. Cullen, C. Habas, R. B. Ivry, M. Leggio, J. B. Mattingley, M. Molinari, E. A. Moulton, M. G. Paulin, M. A. Pavlova, J. D. Schmahmann and A. A. Sokolov (2015). "Consensus paper: the role of the cerebellum in perceptual processes." Cerebellum 14(2): 197-220.

Baumann, O. and J. B. Mattingley (2010). "Scaling of neural responses to visual and auditory motion in the human cerebellum." J Neurosci 30(12): 4489-4495.

Bazzigaluppi, P., J. R. De Gruijl, R. S. van der Giessen, S. Khosrovani, C. I. De Zeeuw and M. T. de Jeu (2012). "Olivary subthreshold oscillations and burst activity revisited." Front Neural Circuits 6: 91.

Benagiano, V., A. Rizzi, L. Lorusso, P. Flace, M. Saccia, R. Cagiano, D. Ribatti, L. Roncali and G. Ambrosi (2018). "The functional anatomy of the cerebrocerebellar circuit: A review and new concepts." J Comp Neurol 526(5): 769-789.

Berridge, M. J. (2006). "Calcium microdomains: organization and function." Cell Calcium 40(5-6): 405-412.

Berridge, M. J., M. D. Bootman and H. L. Roderick (2003). "Calcium signalling: dynamics, homeostasis and remodelling." Nat Rev Mol Cell Biol 4(7): 517-529.

Berridge, M. J. and G. Dupont (1994). "Spatial and temporal signalling by calcium." Curr Opin Cell Biol 6(2): 267-274.

Berridge, M. J., P. Lipp and M. D. Bootman (2000). "The versatility and universality of calcium signalling." Nat Rev Mol Cell Biol 1(1): 11-21.

Bliss, T. V. and G. L. Collingridge (1993). "A synaptic model of memory: long-term potentiation in the hippocampus." Nature 361(6407): 31-39.

Bliss, T. V. and A. R. Gardner-Medwin (1973). "Long-lasting potentiation of synaptic transmission in the dentate area of the unanaestetized rabbit following stimulation of the perforant path." J Physiol 232(2): 357-374.

Bloedel, J. R. and W. J. Roberts (1971). "Action of climbing fibers in cerebellar cortex of the cat." J Neurophysiol 34(1): 17-31.

Bodranghien, F., A. Bastian, C. Casali, M. Hallett, E. D. Louis, M. Manto, P. Marien, D. A. Nowak, J. D. Schmahmann, M. Serrao, K. M. Steiner, M. Strupp, C. Tilikete, D. Timmann and K. van Dun (2016). "Consensus Paper: Revisiting the Symptoms and Signs of Cerebellar Syndrome." Cerebellum 15(3): 369-391.

Bonnet, C., E. Apartis, M. Anheim, A. P. Legrand, J. F. Baizabal-Carvallo, A. M. Bonnet, A. Durr and M. Vidailhet (2012). "Tremor-spectrum in spinocerebellar ataxia type 3." J Neurol 259(11): 2460-2470.

Bootman, M. D., P. Lipp and M. J. Berridge (2001). "The organisation and functions of local Ca(2+) signals." J Cell Sci 114(Pt 12): 2213-2222.

Borszcz, G. S., J. Cranney and R. N. Leaton (1989). "Influence of long-term sensitization on long-term habituation of the acoustic startle response in rats: central gray lesions, preexposure, and extinction." J Exp Psychol Anim Behav Process 15(1): 54-64.

Braff, D. L., C. Grillon and M. A. Geyer (1992). "Gating and habituation of the startle reflex in schizophrenic patients." Arch Gen Psychiatry 49(3): 206-215.

Brochu, G., L. Maler and R. Hawkes (1990). "Zebrin II: a polypeptide antigen expressed selectively by Purkinje cells reveals compartments in rat and fish cerebellum." J Comp Neurol 291(4): 538-552.

Brodal, A., J. Destombes, A. M. Lacerda and P. Angaut (1972). "A cerebellar projection onto the pontine nuclei. An experimental antaomical study in the cat." Exp Brain Res 16(2): 115-139.

Brodal, A., F. Walberg and G. H. Hoddevik (1975). "The olivocerebellar projection in the cat studied with the method of retrograde axonal transport of horseradish peroxidase." J Comp Neurol 164(4): 449-469.

Buckner, R. L. (2013). "The cerebellum and cognitive function: 25 years of insight from anatomy and neuroimaging." Neuron 80(3): 807-815.

Busche, M. A., G. Eichhoff, H. Adelsberger, D. Abramowski, K. H. Wiederhold, C. Haass, M. Staufenbiel, A. Konnerth and O. Garaschuk (2008). "Clusters of hyperactive neurons near amyloid plaques in a mouse model of Alzheimer's disease." Science 321(5896): 1686-1689.

Callaway, J. C., N. Lasser-Ross and W. N. Ross (1995). "IPSPs strongly inhibit climbing fiber-activated [Ca2+]i increases in the dendrites of cerebellar Purkinje neurons." J Neurosci 15(4): 2777-2787.

Cao, R., W. Peng, Z. Wang and A. Xu (2007). "beta-Carboline alkaloids: biochemical and pharmacological functions." Curr Med Chem 14(4): 479-500.

Carlson, S. and J. F. Willott (1998). "Caudal pontine reticular formation of C57BL/6J mice: responses to startle stimuli, inhibition by tones, and plasticity." J Neurophysiol 79(5): 2603-2614.

Castellucci, V., H. Pinsker, I. Kupfermann and E. R. Kandel (1970). "Neuronal mechanisms of habituation and dishabituation of the gill-withdrawal reflex in Aplysia." Science 167(3926): 1745-1748.

Cerminara, N. L., E. J. Lang, R. V. Sillitoe and R. Apps (2015). "Redefining the cerebellar cortex as an assembly of non-uniform Purkinje cell microcircuits." Nat Rev Neurosci 16(2): 79-93.

Chen, X., Y. Kovalchuk, H. Adelsberger, H. A. Henning, M. Sausbier, G. Wietzorrek, P. Ruth, Y. Yarom and A. Konnerth (2010). "Disruption of the olivo-cerebellar circuit by Purkinje neuron-specific ablation of BK channels." Proc Natl Acad Sci U S A 107(27): 12323-12328.

Christoffersen, G. R. (1997). "Habituation: events in the history of its characterization and linkage to synaptic depression. A new proposed kinetic criterion for its identification." Prog Neurobiol 53(1): 45-66.

Cole, K. S. (1949). "Dynamic electrical characteristics of the squid axon membrane." Archives des sciences physiologiques 3(2): 253-258.

Cossart, R., Y. Ikegaya and R. Yuste (2005). "Calcium imaging of cortical networks dynamics." Cell Calcium 37(5): 451-457.

Crispino, L. and T. H. Bullock (1984). "Cerebellum mediates modality-specific modulation of sensory responses of midbrain and forebrain in rat." Proc Natl Acad Sci U S A 81(9): 2917-2920.

Davie, J. T., B. A. Clark and M. Hausser (2008). "The origin of the complex spike in cerebellar Purkinje cells." J Neurosci 28(30): 7599-7609.

Davis, M. (1970). "Effects of interstimulus interval length and variability on startle-response habituation in the rat." J Comp Physiol Psychol 72(2): 177-192.

Davis, M., E. A. Antoniadis, D. G. Amaral and J. T. Winslow (2008). "Acoustic startle reflex in rhesus monkeys: a review." Rev Neurosci 19(2-3): 171-185.

Davis, M., D. S. Gendelman, M. D. Tischler and P. M. Gendelman (1982). "A primary acoustic startle circuit: lesion and stimulation studies." J Neurosci 2(6): 791-805.

De'Sperati, C., L. Lopiano and P. G. Montarolo (1989). "Lesions of the inferior olive do not affect long- or short-term habituation of the acoustic startle response in rats." Neurosci Lett 100(1-3): 164-168.

De Montigny, C. and Y. Lamarre (1973). "Rhythmic activity induced by harmaline in the olivo-cerebello-bulbar system of the cat." Brain Res 53(1): 81-95.

De Montigny, C. and Y. Lamarre (1975). "Effects produced by local applications of harmaline in the inferior olive." Can J Physiol Pharmacol 53(5): 845-849.

De Vry, J., P. Martinez-Martinez, M. Losen, Y. Temel, T. Steckler, H. W. Steinbusch, M. H. De Baets and J. Prickaerts (2010). "In vivo electroporation of the central nervous system: a non-viral approach for targeted gene delivery." Prog Neurobiol 92(3): 227-244.

Deecher, D. C., M. Teitler, D. M. Soderlund, W. G. Bornmann, M. E. Kuehne and S. D. Glick (1992). "Mechanisms of action of ibogaine and harmaline congeners based on radioligand binding studies." Brain Res 571(2): 242-247.

Denk, W. and K. Svoboda (1997). "Photon upmanship: why multiphoton imaging is more than a gimmick." Neuron 18(3): 351-357.

Deuschl, G., P. Bain and M. Brin (1998). "Consensus statement of the Movement Disorder Society on Tremor. Ad Hoc Scientific Committee." Mov Disord 13 Suppl 3: 2-23.

Diaspro, A., P. Bianchini, G. Vicidomini, M. Faretta, P. Ramoino and C. Usai (2006). "Multi-photon excitation microscopy." Biomed Eng Online 5: 36.

Diedrichsen, J., S. E. Criscimagna-Hemminger and R. Shadmehr (2007). "Dissociating timing and coordination as functions of the cerebellum." J Neurosci 27(23): 6291-6301.

Dirks, A., L. Groenink, M. I. Schipholt, J. van der Gugten, T. H. Hijzen, M. A. Geyer and B. Olivier (2002). "Reduced startle reactivity and plasticity in transgenic mice overexpressing corticotropin-releasing hormone." Biol Psychiatry 51(7): 583-590.

Dulhunty, A. F. (2006). "Excitation-contraction coupling from the 1950s into the new millennium." Clin Exp Pharmacol Physiol 33(9): 763-772.

Ebner, T. J., A. L. Hewitt and L. S. Popa (2011). "What features of limb movements are encoded in the discharge of cerebellar neurons?" Cerebellum 10(4): 683-693.

Eccles, J. C., R. Llinas and K. Sasaki (1966). "The excitatory synaptic action of climbing fibres on the Purkinje cells of the cerebellum." J Physiol 182(2): 268-296.

Eccles, J. C., N. H. Sabah, R. F. Schmidt and H. Táboříková (1972). "Integration by Purkyně cells of mossy and climbing fiber inputs from cutaneous mechanoreceptors." Experimental Brain Research 15(5): 498-520.

Eilers, J., G. J. Augustine and A. Konnerth (1995). "Subthreshold synaptic Ca2+ signalling in fine dendrites and spines of cerebellar Purkinje neurons." Nature 373(6510): 155-158.

Ekerot, C. F. and B. Larson (1980). "Termination in overlapping sagittal zones in cerebellar anterior lobe of mossy and climbing fiber paths activated from dorsal funiculus." Exp Brain Res 38(2): 163-172.

Elias, W. J. and B. B. Shah (2014). "Tremor." Jama 311(9): 948-954.

Erturk, O., B. Korkmaz, G. Alev, V. Demirbilek and M. Kiziltan (2016). "Startle and blink reflex in high functioning autism." Neurophysiol Clin 46(3): 189-192.

Fan, G. Y., H. Fujisaki, A. Miyawaki, R. K. Tsay, R. Y. Tsien and M. H. Ellisman (1999). "Video-rate scanning two-photon excitation fluorescence microscopy and ratio imaging with cameleons." Biophys J 76(5): 2412-2420.

Fatemi, S. H., K. A. Aldinger, P. Ashwood, M. L. Bauman, C. D. Blaha, G. J. Blatt, A. Chauhan, V. Chauhan, S. R. Dager, P. E. Dickson, A. M. Estes, D. Goldowitz, D. H. Heck, T. L. Kemper, B. H. King, L. A. Martin, K. J. Millen, G. Mittleman, M. W. Mosconi, A. M. Persico, J. A. Sweeney, S. J. Webb and J. P. Welsh (2012). "Consensus paper: pathological role of the cerebellum in autism." Cerebellum 11(3): 777-807.

Fendt, M., M. Koch and H. U. Schnitzler (1994). "Amygdaloid noradrenaline is involved in the sensitization of the acoustic startle response in rats." Pharmacol Biochem Behav 48(2): 307-314.

Fendt, M., M. Koch and H. U. Schnitzler (1994). "Sensorimotor gating deficit after lesions of the superior colliculus." Neuroreport 5(14): 1725-1728.

Fischer, R. S., Y. Wu, P. Kanchanawong, H. Shroff and C. M. Waterman (2011). "Microscopy in 3D: a biologist's toolbox." Trends Cell Biol 21(12): 682-691.

Frankfurter, A., J. T. Weber, G. J. Royce, N. L. Strominger and J. K. Harting (1976). "An autoradiographic analysis of the tecto-olivary projection in primates." Brain Res 118(2): 245-257.

Freeman, J. A. (1970). "Responses of cat cerebellar Purkinje cells to convergent inputs from cerebral cortex and peripheral sensory systems." J Neurophysiol 33(6): 697-712.

Frings, M., N. Awad, W. Jentzen, A. Dimitrova, F. P. Kolb, H. C. Diener, D. Timmann and M. Maschke (2006). "Involvement of the human cerebellum in short-term and long-term habituation of the acoustic startle response: a serial PET study." Clin Neurophysiol 117(6): 1290-1300.

Gao, Z., B. J. van Beugen and C. I. De Zeeuw (2012). "Distributed synergistic plasticity and cerebellar learning." Nat Rev Neurosci 13(9): 619-635.

Garaschuk, O., R. I. Milos and A. Konnerth (2006). "Targeted bulk-loading of fluorescent indicators for two-photon brain imaging in vivo." Nat Protoc 1(1): 380-386.

Gemba, H., K. Sasaki, Y. Yoneda, S. Hashimoto and N. Mizuno (1980). "Tremor in the monkey with a cerebellar lesion." Exp Neurol 69(1): 173-182.

Glickstein, M., P. Strata and J. Voogd (2009). "Cerebellum: history." Neuroscience 162(3): 549-559.

Glowa, J. R. and C. T. Hansen (1994). "Differences in response to an acoustic startle stimulus among forty-six rat strains." Behav Genet 24(1): 79-84.

Göppert-Mayer, M. (1931). "Über Elementarakte mit zwei Quantensprüngen." Annalen der Physik 401(3): 273-294.

Govert, F. and G. Deuschl (2015). "Tremor entities and their classification: an update." Curr Opin Neurol 28(4): 393-399.

Grienberger, C., X. Chen and A. Konnerth (2015). "Dendritic function in vivo." Trends Neurosci 38(1): 45-54.

Grienberger, C. and A. Konnerth (2012). "Imaging calcium in neurons." Neuron 73(5): 862-885.

Groves, P. M. and R. F. Thompson (1970). "Habituation: a dual-process theory." Psychol Rev 77(5): 419-450.

Groves, P. M., C. J. Wilson and R. D. Boyle (1974). "Brain stem pathways, cortical modulation, and habituation of the acoustic startle response." Behav Biol 10(4): 391-418.

Grynkiewicz, G., M. Poenie and R. Y. Tsien (1985). "A new generation of Ca2+ indicators with greatly improved fluorescence properties." J Biol Chem 260(6): 3440-3450.

Hallett, M. (2014). "Tremor: pathophysiology." Parkinsonism Relat Disord 20 Suppl 1: S118-122.

Hallett, M. and R. M. Dubinsky (1993). "Glucose metabolism in the brain of patients with essential tremor." J Neurol Sci 114(1): 45-48.

Handforth, A. (2012). "Harmaline tremor: underlying mechanisms in a potential animal model of essential tremor." Tremor Other Hyperkinet Mov (N Y) 2.

Harrington, D. L., R. R. Lee, L. A. Boyd, S. Z. Rapcsak and R. T. Knight (2004). "Does the representation of time depend on the cerebellum? Effect of cerebellar stroke." Brain 127(Pt 3): 561-574.

Harris, J. D. (1943). "Habituatory response decrement in the intact organism." Psychological Bulletin 40(6): 385-422.

Harting, J. K. (1977). "Descending pathways from the superior collicullus: an autoradiographic analysis in the rhesus monkey (Macaca mulatta)." J Comp Neurol 173(3): 583-612.

Helmchen, F. and W. Denk (2005). "Deep tissue two-photon microscopy." Nat Methods 2(12): 932-940.

Herraiz, T., D. Gonzalez, C. Ancin-Azpilicueta, V. J. Aran and H. Guillen (2010). "beta-Carboline alkaloids in Peganum harmala and inhibition of human monoamine oxidase (MAO)." Food Chem Toxicol 48(3): 839-845.

Hodgkin, A. L., A. F. Huxley and B. Katz (1952). "Measurement of current-voltage relations in the membrane of the giant axon of Loligo." J Physiol 116(4): 424-448.

Horlington, M. (1968). "A method for measuring acoustic startle response latency and magnitude in rats: Detection of a single stimulus effect using latency measurements." Physiology & Behavior 3(6): 839-844.

Huang, C. M. and G. Liu (1985). "Electrophysiological mapping of the auditory areas in the cerebellum of the cat." Brain Res 335(1): 121-129.

Huang, C. M., G. Liu and R. Huang (1982). "Projections from the cochlear nucleus to the cerebellum." Brain Res 244(1): 1-8.

Humeau, J., J. M. Bravo-San Pedro, I. Vitale, L. Nunez, C. Villalobos, G. Kroemer and L. Senovilla (2018). "Calcium signaling and cell cycle: Progression or death." Cell Calcium 70: 3-15.

Ishikawa, T., M. Shimuta and M. Hausser (2015). "Multimodal sensory integration in single cerebellar granule cells in vivo." Elife 4.

Ito, M. (2006). "Cerebellar circuitry as a neuronal machine." Prog Neurobiol 78(3-5): 272-303.

Ito, M. and M. Kano (1982). "Long-lasting depression of parallel fiber-Purkinje cell transmission induced by conjunctive stimulation of parallel fibers and climbing fibers in the cerebellar cortex." Neurosci Lett 33(3): 253-258.

Ito, M., M. Udo, N. Mano and N. Kawai (1970). "Synaptic action of the fastigiobulbar impulses upon neurones in the medullary reticular formation and vestibular nuclei." Exp Brain Res 11(1): 29-47.

Jackson, R. B. and C. C. Little (1933). "The existence of non-chromosomal influence in the incidence of mammary tumors in mice." Science 78(2029): 465-466.

Jenkins, I. H., P. G. Bain, J. G. Colebatch, P. D. Thompson, L. J. Findley, R. S. Frackowiak, C. D. Marsden and D. J. Brooks (1993). "A positron emission tomography study of essential tremor: evidence for overactivity of cerebellar connections." Ann Neurol 34(1): 82-90.

Jia, H., N. L. Rochefort, X. Chen and A. Konnerth (2010). "Dendritic organization of sensory input to cortical neurons in vivo." Nature 464(7293): 1307-1312.

Jia, H., N. L. Rochefort, X. Chen and A. Konnerth (2011). "In vivo two-photon imaging of sensory-evoked dendritic calcium signals in cortical neurons." Nat Protoc 6(1): 28-35.

Jordan, W. P. (1989). "Mesencephalic reticular formation lesions made after habituation training abolish long-term habituation of the acoustic startle response in rats." Behav Neurosci 103(4): 805-815.

Jordan, W. P. and R. N. Leaton (1983). "Habituation of the acoustic startle response in rats after lesions in the mesencephalic reticular formation or in the inferior colliculus." Behav Neurosci 97(5): 710-724.

Kandel, E. R. (2001). "The molecular biology of memory storage: a dialogue between genes and synapses." Science 294(5544): 1030-1038.

Kano, M., M. Kano, K. Fukunaga and A. Konnerth (1996). "Ca(2+)-induced rebound potentiation of gamma-aminobutyric acid-mediated currents requires activation of Ca2+/calmodulin-dependent kinase II." Proc Natl Acad Sci U S A 93(23): 13351-13356.

Kano, M., U. Rexhausen, J. Dreessen and A. Konnerth (1992). "Synaptic excitation produces a long-lasting rebound potentiation of inhibitory synaptic signals in cerebellar Purkinje cells." Nature 356(6370): 601-604.

Kerr, J. N., D. Greenberg and F. Helmchen (2005). "Imaging input and output of neocortical networks in vivo." Proc Natl Acad Sci U S A 102(39): 14063-14068.

Khan, F. A., A. Maalik, Z. Iqbal and I. Malik (2013). "Recent pharmacological developments in beta-carboline alkaloid "harmaline"." Eur J Pharmacol 721(1-3): 391-394.

Kheradmand, A. and D. S. Zee (2011). "Cerebellum and ocular motor control." Front Neurol 2: 53.

Kim, H., S. O. Sablin and R. R. Ramsay (1997). "Inhibition of monoamine oxidase A by beta-carboline derivatives." Arch Biochem Biophys 337(1): 137-142.

King, J. S., R. H. Ho and R. W. Burry (1984). "The distribution and synaptic organization of serotoninergic elements in the inferior olivary complex of the opossum." J Comp Neurol 227(3): 357-368.

Kitamura, K. and M. Hausser (2011). "Dendritic calcium signaling triggered by spontaneous and sensory-evoked climbing fiber input to cerebellar Purkinje cells in vivo." J Neurosci 31(30): 10847-10858.

Kitamura, K., B. Judkewitz, M. Kano, W. Denk and M. Hausser (2008). "Targeted patch-clamp recordings and single-cell electroporation of unlabeled neurons in vivo." Nat Methods 5(1): 61-67.

Kitamura, K. and M. Kano (2013). "Dendritic calcium signaling in cerebellar Purkinje cell." Neural Netw 47: 11-17.

Koch, M. (1999). "The neurobiology of startle." Prog Neurobiol 59(2): 107-128.

Koch, M. and U. Ebert (1993). "Enhancement of the acoustic startle response by stimulation of an excitatory pathway from the central amygdala/basal nucleus of Meynert to the pontine reticular formation." Exp Brain Res 93(2): 231-241.

Koch, M. and H. U. Schnitzler (1997). "The acoustic startle response in rats--circuits mediating evocation, inhibition and potentiation." Behav Brain Res 89(1-2): 35-49.

Konnerth, A., J. Dreessen and G. J. Augustine (1992). "Brief dendritic calcium signals initiate long-lasting synaptic depression in cerebellar Purkinje cells." Proc Natl Acad Sci U S A 89(15): 7051-7055.

Konnerth, A., I. Llano and C. M. Armstrong (1990). "Synaptic currents in cerebellar Purkinje cells." Proc Natl Acad Sci U S A 87(7): 2662-2665.

Koziol, L. F., D. Budding, N. Andreasen, S. D'Arrigo, S. Bulgheroni, H. Imamizu, M. Ito, M. Manto, C. Marvel, K. Parker, G. Pezzulo, N. Ramnani, D. Riva, J. Schmahmann, L. Vandervert and T. Yamazaki (2014). "Consensus paper: the cerebellum's role in movement and cognition." Cerebellum 13(1): 151-177.

Krauss, G. (2001). Biochemistry of signal transduction and regulation, Wiley-VCH.

Kronenbuerger, M., M. Gerwig, B. Brol, F. Block and D. Timmann (2007). "Eyeblink conditioning is impaired in subjects with essential tremor." Brain 130(Pt 6): 1538-1551.

Kwan, A. C. (2008). "What can population calcium imaging tell us about neural circuits?" J Neurophysiol 100(6): 2977-2980.

Lamarre, Y. and L. A. Mercier (1971). "Neurophysiological studies of harmaline-induced tremor in the cat." Can J Physiol Pharmacol 49(12): 1049-1058.

Landis, C. and W. Hunt (1939). The startle pattern. Oxford, England, Farrar & Rinehart.

Leaton, R. N. (1976). "Long-term retention of the habituation of lick suppression and startle response produced by a single auditory stimulus." J Exp Psychol Anim Behav Process 2(3): 248-259.

Leaton, R. N. and W. F. Supple, Jr. (1986). "Cerebellar vermis: essential for long-term habituation of the acoustic startle response." Science 232(4749): 513-515.

Leaton, R. N. and W. F. Supple, Jr. (1991). "Medial cerebellum and long-term habituation of acoustic startle in rats." Behav Neurosci 105(6): 804-816.

LeDoux, M. S. and J. F. Lorden (2002). "Abnormal spontaneous and harmaline-stimulated Purkinje cell activity in the awake genetically dystonic rat." Exp Brain Res 145(4): 457-467.

Leitner, D. S. and M. E. Cohen (1985). "Role of the inferior colliculus in the inhibition of acoustic startle in the rat." Physiol Behav 34(1): 65-70.

Li, L. and J. S. Yeomans (2000). "Using intracranial electrical stimulation to study the timing of prepulse inhibition of the startle reflex." Brain Res Brain Res Protoc 5(1): 67-74.

Lichtman, J. W. and J. A. Conchello (2005). "Fluorescence microscopy." Nat Methods 2(12): 910-919.

Linauts, M. and G. F. Martin (1978). "The organization of olivo-cerebellar projections in the opossum, Didelphis virginiana, as revealed by the retrograde transport of horseradish peroxidase." J Comp Neurol 179(2): 355-381.

Lingenhohl, K. and E. Friauf (1994). "Giant neurons in the rat reticular formation: a sensorimotor interface in the elementary acoustic startle circuit?" J Neurosci 14(3 Pt 1): 1176-1194.

Llinas, R., R. Baker and C. Sotelo (1974). "Electrotonic coupling between neurons in cat inferior olive." J Neurophysiol 37(3): 560-571.

Llinas, R. and R. A. Volkind (1973). "The olivo-cerebellar system: functional properties as revealed by harmaline-induced tremor." Exp Brain Res 18(1): 69-87.

Llinas, R. and Y. Yarom (1981). "Properties and distribution of ionic conductances generating electroresponsiveness of mammalian inferior olivary neurones in vitro." J Physiol 315: 569-584.

Llinas, R. and Y. Yarom (1986). "Oscillatory properties of guinea-pig inferior olivary neurones and their pharmacological modulation: an in vitro study." J Physiol 376: 163-182.

Lohmann, C., A. Finski and T. Bonhoeffer (2005). "Local calcium transients regulate the spontaneous motility of dendritic filopodia." Nat Neurosci 8(3): 305-312.

Looger, L. L. and O. Griesbeck (2012). "Genetically encoded neural activity indicators." Curr Opin Neurobiol 22(1): 18-23.

Lopiano, L., C. de'Sperati and P. G. Montarolo (1990). "Long-term habituation of the acoustic startle response: role of the cerebellar vermis." Neuroscience 35(1): 79-84.

Lorden, J. F., S. E. Stratton, L. E. Mays and G. A. Oltmans (1988). "Purkinje cell activity in rats following chronic treatment with harmaline." Neuroscience 27(2): 465-472.

Louis, E. D., D. C. Shungu, S. Chan, X. Mao, E. C. Jurewicz and D. Watner (2002). "Metabolic abnormality in the cerebellum in patients with essential tremor: a proton magnetic resonance spectroscopic imaging study." Neurosci Lett 333(1): 17-20.

Ludewig, K., M. A. Geyer and F. X. Vollenweider (2003). "Deficits in prepulse inhibition and habituation in never-medicated, first-episode schizophrenia." Biol Psychiatry 54(2): 121-128.

Lyons, M. R. and A. E. West (2011). "Mechanisms of specificity in neuronal activity-regulated gene transcription." Prog Neurobiol 94(3): 259-295.

Malenka, R. C. and R. A. Nicoll (1993). "NMDA-receptor-dependent synaptic plasticity: multiple forms and mechanisms." Trends Neurosci 16(12): 521-527.

Manto, M., J. M. Bower, A. B. Conforto, J. M. Delgado-Garcia, S. N. da Guarda, M. Gerwig, C. Habas, N. Hagura, R. B. Ivry, P. Marien, M. Molinari, E. Naito, D. A. Nowak, N. Oulad Ben Taib, D. Pelisson, C. D. Tesche, C. Tilikete and D. Timmann (2012). "Consensus paper: roles of the cerebellum in motor control--the diversity of ideas on cerebellar involvement in movement." Cerebellum 11(2): 457-487.

Marr, D. (1969). "A theory of cerebellar cortex." J Physiol 202(2): 437-470.

Martin, G. F., M. S. Beattie, H. C. Hughes, M. Linauts and M. Panneton (1977). "The organization of reticulo-olivo-cerebellar circuits in the North American opossum." Brain Res 137(2): 253-266.

Maruta, J., R. A. Hensbroek and J. I. Simpson (2007). "Intraburst and interburst signaling by climbing fibers." J Neurosci 27(42): 11263-11270.

Maschke, M., J. Drepper, K. Kindsvater, F. P. Kolb, H. C. Diener and D. Timmann (2000). "Involvement of the human medial cerebellum in long-term habituation of the acoustic startle response." Exp Brain Res 133(3): 359-367.

Matilla-Duenas, A., T. Ashizawa, A. Brice, S. Magri, K. N. McFarland, M. Pandolfo, S. M. Pulst, O. Riess, D. C. Rubinsztein, J. Schmidt, T. Schmidt, D. R. Scoles, G. Stevanin, F. Taroni, B. R. Underwood and I. Sanchez (2014). "Consensus paper: pathological mechanisms underlying neurodegeneration in spinocerebellar ataxias." Cerebellum 13(2): 269-302.

Milner, T. E., G. Cadoret, L. Lessard and A. M. Smith (1995). "EMG analysis of harmaline-induced tremor in normal and three strains of mutant mice with Purkinje cell degeneration and the role of the inferior olive." J Neurophysiol 73(6): 2568-2577.

Misrahy, G. A., J. F. Spradley, A. V. Beran and V. P. Garwood (1961). "Acoustic cerebellar pathways in cats." J Neurophysiol 24: 159-166.

Miwa, H. (2007). "Rodent models of tremor." Cerebellum 6(1): 66-72.

Miyakawa, H., V. Lev-Ram, N. Lasser-Ross and W. N. Ross (1992). "Calcium transients evoked by climbing fiber and parallel fiber synaptic inputs in guinea pig cerebellar Purkinje neurons." J Neurophysiol 68(4): 1178-1189.

Mortimer, J. A. (1973). "Temporal sequence of cerebellar Purkinje and nuclear activity in relation to the acoustic startle response." Brain Res 50(2): 457-462.

Mortimer, J. A. (1975). "Cerebellar responses to teleceptive stimuli in alert monkeys." Brain Res 83(3): 369-390.

Murray, W. S. and C. C. Little (1935). "The Genetics of Mammary Tumor Incidence in Mice." Genetics 20(5): 466-496.

Najafi, F., A. Giovannucci, S. S. Wang and J. F. Medina (2014). "Coding of stimulus strength via analog calcium signals in Purkinje cell dendrites of awake mice." Elife 3: e03663.

Najafi, F., A. Giovannucci, S. S. Wang and J. F. Medina (2014). "Sensory-driven enhancement of calcium signals in individual Purkinje cell dendrites of awake mice." Cell Rep 6(5): 792-798.

Najafi, F. and J. F. Medina (2013). "Beyond "all-or-nothing" climbing fibers: graded representation of teaching signals in Purkinje cells." Front Neural Circuits 7: 115.

Neher, E. and T. Sakaba (2008). "Multiple roles of calcium ions in the regulation of neurotransmitter release." Neuron 59(6): 861-872.

Neher, E. and B. Sakmann (1992). "The patch clamp technique." Sci Am 266(3): 44-51.

Nemoto, T., R. Kawakami, T. Hibi, K. Iijima and K. Otomo (2015). "Two-photon excitation fluorescence microscopy and its application in functional connectomics." Microscopy (Oxf) 64(1): 9-15.

Nimmerjahn, A., P. Theer and F. Helmchen (2008). Two-Photon Laser Scanning Microscopy. Ultrashort Laser Pulses in Biology and Medicine. M. Braun, P. Gilch and W. Zinth. Berlin, Heidelberg, Springer Berlin Heidelberg: 29-51.

Numberger, M. and A. Draguhn (1996). Patch-Clamp-Technik, Spektrum Akademischer Verlag.

Ornitz, E. M. and D. Guthrie (1989). "Long-term habituation and sensitization of the acoustic startle response in the normal adult human." Psychophysiology 26(2): 166-173.

Ozden, I., M. R. Sullivan, H. M. Lee and S. S. Wang (2009). "Reliable coding emerges from coactivation of climbing fibers in microbands of cerebellar Purkinje neurons." J Neurosci 29(34): 10463-10473.

Ozer, G., Z. I. K. Kirmaci, H. Adiguzel and N. Ergun (2018). "Correlation of proximal and distal muscle strength with upper limb functional ability in patients with essential tremor." Acta Neurol Belg.

Palmer, L. M., B. A. Clark, J. Grundemann, A. Roth, G. J. Stuart and M. Hausser (2010). "Initiation of simple and complex spikes in cerebellar Purkinje cells." J Physiol 588(Pt 10): 1709-1717.

Paredes, R. M., J. C. Etzler, L. T. Watts, W. Zheng and J. D. Lechleiter (2008). "Chemical calcium indicators." Methods 46(3): 143-151.

Parham, K. and J. F. Willott (1988). "Acoustic startle response in young and aging C57BL/6J and CBA/J mice." Behav Neurosci 102(6): 881-886.

Park, Y. G., H. Y. Park, C. J. Lee, S. Choi, S. Jo, H. Choi, Y. H. Kim, H. S. Shin, R. R. Llinas and D. Kim (2010). "Ca(V)3.1 is a tremor rhythm pacemaker in the inferior olive." Proc Natl Acad Sci U S A 107(23): 10731-10736.

Pastor, M. A., C. Vidaurre, M. A. Fernandez-Seara, A. Villanueva and K. J. Friston (2008). "Frequency-specific coupling in the cortico-cerebellar auditory system." J Neurophysiol 100(4): 1699-1705.

Paxinos, G. and K. B. J. Franklin (2001). The Mouse Brain in Stereotaxic Coordinates. San Diego, Academic Press.

Pazos, A., R. Cortes and J. M. Palacios (1985). "Quantitative autoradiographic mapping of serotonin receptors in the rat brain. II. Serotonin-2 receptors." Brain Res 346(2): 231-249.

Pellet, J., M. Weiss and M. J. Gourdon (1983). "Harmaline effects on the sensory-motor reactivity: modifications of the acoustic startle pattern." Pharmacol Biochem Behav 19(3): 527-534.

Perkins, K. L. (2006). "Cell-attached voltage-clamp and current-clamp recording and stimulation techniques in brain slices." J Neurosci Methods 154(1-2): 1-18.

Petacchi, A., A. R. Laird, P. T. Fox and J. M. Bower (2005). "Cerebellum and auditory function: an ALE meta-analysis of functional neuroimaging studies." Hum Brain Mapp 25(1): 118-128.

Pfeiffer, W. (1962). "The fright reaction of fish." Biol Rev Camb Philos Soc 37: 495-511.

Pilz, P. K., S. W. Arnold, A. T. Rischawy and C. F. Plappert (2014). "Longterm-habituation of the startle response in mice is stimulus modality, but not context specific." Front Integr Neurosci 7: 103.

Pilz, P. K. and H. U. Schnitzler (1996). "Habituation and sensitization of the acoustic startle response in rats: amplitude, threshold, and latency measures." Neurobiol Learn Mem 66(1): 67-79.

Piston, D. W. (1999). "Imaging living cells and tissues by two-photon excitation microscopy." Trends Cell Biol 9(2): 66-69.

Prosser, C. L. and W. S. Hunter (1936). "The extinction of startle responses and spinal reflexes in the white rat." American Journal of Physiology-Legacy Content 117(4): 609-618.

PubChem Compound Database, N. C. f. B. I. Harmaline, CID=3564, last accessed 02.03.2019.

Putney, J., J. , J. Eichberg, A. Estevez, A. Miyawaki, G. Bird, G. Montieth, R. Rizzuto, A. Parekh, V. Flockerzi, K. Strange, K. Cunningham, A. Tepikin, C. Distelhorst, S. Li, M. Poenie, K. Foskett, A. Marks, A. Galione, A. Thomas and L. Missiaen (2006). Calcium Signaling. Boca Raton, CRC Press.

Ramaswami, M. (2014). "Network plasticity in adaptive filtering and behavioral habituation." Neuron 82(6): 1216-1229.

Rankin, C. H., T. Abrams, R. J. Barry, S. Bhatnagar, D. F. Clayton, J. Colombo, G. Coppola, M. A. Geyer, D. L. Glanzman, S. Marsland, F. K. McSweeney, D. A. Wilson, C. F. Wu and R. F. Thompson (2009). "Habituation revisited: an updated and revised description of the behavioral characteristics of habituation." Neurobiol Learn Mem 92(2): 135-138.

Rankin, C. H. and B. S. Broster (1992). "Factors affecting habituation and recovery from habituation in the nematode Caenorhabditis elegans." Behav Neurosci 106(2): 239-249.

Rawson, J. A., S. Wertheimer and S. Rees (1988). "Modification of parallel fibre-Purkinje cell transmission by long-term activation of climbing fibres." Neurosci Lett 91(1): 14-18.

Raymond, J. L. and J. F. Medina (2018). "Computational Principles of Supervised Learning in the Cerebellum." Annu Rev Neurosci 41: 233-253.

Rehberg, M., A. Lepier, B. Solchenberger, P. Osten and R. Blum (2008). "A new non-disruptive strategy to target calcium indicator dyes to the endoplasmic reticulum." Cell Calcium 44(4): 386-399.

Robertson, H. A. (1980). "Harmaline-induced tremor: the benzodiazepine receptor as a site of action." Eur J Pharmacol 67(1): 129-132.

Roome, C. J. and B. Kuhn (2018). "Simultaneous dendritic voltage and calcium imaging and somatic recording from Purkinje neurons in awake mice." Nat Commun 9(1): 3388.

Roostaei, T., A. Nazeri, M. A. Sahraian and A. Minagar (2014). "The human cerebellum: a review of physiologic neuroanatomy." Neurol Clin 32(4): 859-869.

Ruigrok, T. J. (2011). "Ins and outs of cerebellar modules." Cerebellum 10(3): 464-474.

Ruigrok, T. J. H., R. V. Sillitoe and J. Voogd (2015). Chapter 9 - Cerebellum and Cerebellar Connections. The Rat Nervous System (Fourth Edition). G. Paxinos. San Diego, Academic Press: 133-205.

Sakmann, B. and E. Neher (1984). "Patch clamp techniques for studying ionic channels in excitable membranes." Annu Rev Physiol 46: 455-472.

Sanabria-Castro, A., I. Alvarado-Echeverria and C. Monge-Bonilla (2017). "Molecular Pathogenesis of Alzheimer's Disease: An Update." Ann Neurosci 24(1): 46-54.

Schmahmann, J. D. (2004). "Disorders of the cerebellum: ataxia, dysmetria of thought, and the cerebellar cognitive affective syndrome." J Neuropsychiatry Clin Neurosci 16(3): 367-378.

Schultz, S. R., K. Kitamura, A. Post-Uiterweer, J. Krupic and M. Hausser (2009). "Spatial pattern coding of sensory information by climbing fiber-evoked calcium signals in networks of neighboring cerebellar Purkinje cells." J Neurosci 29(25): 8005-8015.

Schweighofer, N., K. Doya and S. Kuroda (2004). "Cerebellar aminergic neuromodulation: towards a functional understanding." Brain Res Brain Res Rev 44(2-3): 103-116.

Shakiba, A. (2014). "The role of the cerebellum in neurobiology of psychiatric disorders." Neurol Clin 32(4): 1105-1115.

Shnerson, A. and J. F. Willott (1980). "Ontogeny of the acoustic startle response in C57BL/6J mouse pups." J Comp Physiol Psychol 94(1): 36-40.

Shoji, H. and T. Miyakawa (2018). "Relationships between the acoustic startle response and prepulse inhibition in C57BL/6J mice: a large-scale meta-analytic study." Molecular Brain 11(1): 42.

Simantov, R., S. H. Snyder and M. L. Oster-Granite (1976). "Harmaline-induced tremor in the rat: abolition by 3-acetylpyridine destruction of cerebellar climbing fibers." Brain Res 114(1): 144-151.

Simons-Weidenmaier, N. S., M. Weber, C. F. Plappert, P. K. Pilz and S. Schmid (2006). "Synaptic depression and short-term habituation are located in the sensory part of the mammalian startle pathway." BMC Neurosci 7: 38.

Smart, L. (1981). "Competitive inhibition of sodium-dependent high affinity choline uptake by harmala alkaloids." Eur J Pharmacol 75(4): 265-269.

Smetters, D., A. Majewska and R. Yuste (1999). "Detecting action potentials in neuronal populations with calcium imaging." Methods 18(2): 215-221.

Snider, R. S. and A. Stowell (1944). "Receiving areas of the tactile, auditory, and visual systems in the cerebellum." Journal of Neurophysiology 7(6): 331-357.

Solbach, K., M. Mumm, B. Brandauer, M. Kronenburger, J. Hermsdorfer and D. Timmann (2016). "Prehension Kinematics, Grasping Forces, and Independent Finger Control in Mildly Affected Patients with Essential Tremor." Cerebellum 15(4): 498-508.

Sotelo, C., T. Gotow and M. Wassef (1986). "Localization of glutamic-acid-decarboxylase-immunoreactive axon terminals in the inferior olive of the rat, with special emphasis on anatomical relations between GABAergic synapses and dendrodendritic gap junctions." J Comp Neurol 252(1): 32-50.

Spencer, K. A. and D. L. Slocomb (2007). "The neural basis of ataxic dysarthria." Cerebellum 6(1): 58-65.

Stephens, D. J. and V. J. Allan (2003). "Light microscopy techniques for live cell imaging." Science 300(5616): 82-86.

Storozeva, Z. I. and M. V. Pletnicov (1994). "Habituation of acoustic startle in rats--a functional ablation study." Neuroreport 5(16): 2065-2068.

Stosiek, C., O. Garaschuk, K. Holthoff and A. Konnerth (2003). "In vivo two-photon calcium imaging of neuronal networks." Proc Natl Acad Sci U S A 100(12): 7319-7324.

Stratton, S. E. and J. F. Lorden (1991). "Effect of harmaline on cells of the inferior olive in the absence of tremor: differential response of genetically dystonic and harmaline-tolerant rats." Neuroscience 41(2-3): 543-549.

Strick, P. L., R. P. Dum and J. A. Fiez (2009). "Cerebellum and nonmotor function." Annu Rev Neurosci 32: 413-434.

Sugihara, I., E. J. Lang and R. Llinas (1995). "Serotonin modulation of inferior olivary oscillations and synchronicity: a multiple-electrode study in the rat cerebellum." Eur J Neurosci 7(4): 521-534.

Supple, W. F., Jr., L. Sebastiani and B. S. Kapp (1993). "Purkinje cell responses in the anterior cerebellar vermis during Pavlovian fear conditioning in the rabbit." Neuroreport 4(7): 975-978.

Svoboda, K. and R. Yasuda (2006). "Principles of two-photon excitation microscopy and its applications to neuroscience." Neuron 50(6): 823-839.

Swain, R. A., A. L. Kerr and R. F. Thompson (2011). "The cerebellum: a neural system for the study of reinforcement learning." Front Behav Neurosci 5: 8.

Tada, M., A. Takeuchi, M. Hashizume, K. Kitamura and M. Kano (2014). "A highly sensitive fluorescent indicator dye for calcium imaging of neural activity in vitro and in vivo." Eur J Neurosci 39(11): 1720-1728.

Tank, D. W., M. Sugimori, J. A. Connor and R. R. Llinas (1988). "Spatially resolved calcium dynamics of mammalian Purkinje cells in cerebellar slice." Science 242(4879): 773-777.

Tariq, M., M. Arshaduddin, N. Biary, K. Al Moutaery and S. Al Deeb (2002). "2-deoxy-D-glucose attenuates harmaline induced tremors in rats." Brain Res 945(2): 212-218.

Tempia, F., M. Kano, R. Schneggenburger, C. Schirra, O. Garaschuk, T. Plant and A. Konnerth (1996). "Fractional calcium current through neuronal AMPA-receptor channels with a low calcium permeability." J Neurosci 16(2): 456-466.

Teune, T. M., J. van der Burg, J. van der Moer, J. Voogd and T. J. Ruigrok (2000). "Topography of cerebellar nuclear projections to the brain stem in the rat." Prog Brain Res 124: 141-172.

Thompson, R. F. and W. A. Spencer (1966). "Habituation: a model phenomenon for the study of neuronal substrates of behavior." Psychol Rev 73(1): 16-43.

Thompson, R. F. and J. E. Steinmetz (2009). "The role of the cerebellum in classical conditioning of discrete behavioral responses." Neuroscience 162(3): 732-755.

Timmann, D., C. Musso, F. P. Kolb, M. Rijntjes, M. Juptner, S. P. Muller, H. C. Diener and C. Weiller (1998). "Involvement of the human cerebellum during habituation of the acoustic startle response: a PET study." J Neurol Neurosurg Psychiatry 65(5): 771-773.

Tsien, R. W. and R. Y. Tsien (1990). "Calcium channels, stores, and oscillations." Annu Rev Cell Biol 6: 715-760.

Tsien, R. Y. (1981). "A non-disruptive technique for loading calcium buffers and indicators into cells." Nature 290(5806): 527-528.

Tsien, R. Y. (1989). "Fluorescent probes of cell signaling." Annu Rev Neurosci 12: 227-253.

Typlt, M., M. Mirkowski, E. Azzopardi, P. Ruth, P. K. Pilz and S. Schmid (2013). "Habituation of reflexive and motivated behavior in mice with deficient BK channel function." Front Integr Neurosci 7: 79.

Usowicz, M. M., M. Sugimori, B. Cherksey and R. Llinas (1992). "P-type calcium channels in the somata and dendrites of adult cerebellar Purkinje cells." Neuron 9(6): 1185-1199.

Valsamis, B. and S. Schmid (2011). "Habituation and prepulse inhibition of acoustic startle in rodents." J Vis Exp(55): e3446.

van den Buuse, M. (2010). "Modeling the positive symptoms of schizophrenia in genetically modified mice: pharmacology and methodology aspects." Schizophr Bull 36(2): 246-270.

Vaziri, Z., H. Abbassian, V. Sheibani, M. Haghani, M. Nazeri, I. Aghaei and M. Shabani (2015). "The therapeutic potential of Berberine chloride hydrate against harmaline-induced motor impairments in a rat model of tremor." Neurosci Lett 590: 84-90.

Verkhratsky, A. (2007). "Calcium and cell death." Subcell Biochem 45: 465-480.

Voogd, J. (2003). "The human cerebellum." J Chem Neuroanat 26(4): 243-252.

Voogd, J. and M. Glickstein (1998). "The anatomy of the cerebellum." Trends Neurosci 21(9): 370-375.

Wang, S. S., W. Denk and M. Hausser (2000). "Coincidence detection in single dendritic spines mediated by calcium release." Nat Neurosci 3(12): 1266-1273.

Weber, M., H. U. Schnitzler and S. Schmid (2002). "Synaptic plasticity in the acoustic startle pathway: the neuronal basis for short-term habituation?" Eur J Neurosci 16(7): 1325-1332.

Weiss, M., S. Buldakova and E. Dutova (1995). "Interaction of the beta-carboline harmaline with a GABA-benzodiazepine mechanism: an electrophysiological investigation on rat hippocampal slices." Brain Res 695(2): 105-109.

Welsh, J. P. (1998). "Systemic harmaline blocks associative and motor learning by the actions of the inferior olive." Eur J Neurosci 10(11): 3307-3320.

Westenbroek, R. E., T. Sakurai, E. M. Elliott, J. W. Hell, T. V. Starr, T. P. Snutch and W. A. Catterall (1995). "Immunochemical identification and subcellular distribution of the alpha 1A subunits of brain calcium channels." J Neurosci 15(10): 6403-6418.

Willott, J. F. and S. Carlson (1995). "Modification of the acoustic startle response in hearing-impaired C57BL/6J mice: prepulse augmentation and prolongation of prepulse inhibition." Behav Neurosci 109(3): 396-403.

Willott, J. F., J. Kulig and T. Satterfield (1984). "The acoustic startle response in DBA/2 and C57BL/6 mice: relationship to auditory neuronal response properties and hearing impairment." Hear Res 16(2): 161-167.

Wise, A. K., N. L. Cerminara, D. E. Marple-Horvat and R. Apps (2010). "Mechanisms of synchronous activity in cerebellar Purkinje cells." J Physiol 588(Pt 13): 2373-2390.

Witter, L. and C. I. De Zeeuw (2015). "Regional functionality of the cerebellum." Curr Opin Neurobiol 33: 150-155.

Wright, C. G. and C. D. Barnes (1972). "Audio-spinal reflex responses in decerebrate and chloralose anesthetized cats." Brain Res 36(2): 307-331.

Yasuda, R. (2017). "Biophysics of Biochemical Signaling in Dendritic Spines: Implications in Synaptic Plasticity." Biophys J 113(10): 2152-2159.

Yeomans, J. S. and P. W. Frankland (1995). "The acoustic startle reflex: neurons and connections." Brain Res Brain Res Rev 21(3): 301-314.

Yeomans, J. S., L. Li, B. W. Scott and P. W. Frankland (2002). "Tactile, acoustic and vestibular systems sum to elicit the startle reflex." Neurosci Biobehav Rev 26(1): 1-11.

Zaman, T., C. De Oliveira, M. Smoka, C. Narla, M. O. Poulter and S. Schmid (2017). "BK Channels Mediate Synaptic Plasticity Underlying Habituation in Rats." J Neurosci 37(17): 4540-4551.

Zheng, J. Q. and M. M. Poo (2007). "Calcium signaling in neuronal motility." Annu Rev Cell Dev Biol 23: 375-404.

Acknowledgements

I would like to thank Prof. Dr. Arthur Konnerth for the opportunity to work in his laboratory, the professional supervision of my doctoral thesis and his scientific support.
I thank Prof. Dr. Helmuth Adelsberger and Prof. Dr. Thomas Misgeld for their professional supervision and their scientific support.

I would like to thank all of my colleagues who supported me during my time at the TUM Institute of Neuroscience, especially, Dr. Carsten Tischbirek and Dr. Valérie Bonfardin. Special thanks as well to the people of the technical and laboratory support, Christine Karrer, Petra Apostolopoulos, Karin Kratz, Felix Beyer, Christian Obermayer and Andreas Fohr.

I would like to thank the Technical University of Munich (Technische Universität München, TUM), the TUM School of Medicine (Fakultät für Medizin) and the TUM Graduate School/TUM Medical Graduate Center for admitting me to the doctoral programme “Translational Medicine” (Promotionsprogramm “Translationale Medizin”) and intermittent scholarship support.

Most of all I would like to thank my friends and my family. In particular, my parents and my brother who give me unconditional support and affection are invaluable to my life. I am more than grateful. To you I would like to dedicate my thesis. Danke von Herzen.

»Im vereinenden Geiste des gemeinsamen Strebens nach Wahrheit mögen zukünftige Generationen hoffentlich gnädig auf unsere heutigen Gewissheiten zurückblicken«

Publications

The results of the present thesis are considered for publication.

Excerpts of this thesis have been published as an abstract in the proceedings of the German Association for Psychiatry, Psychotherapy and Psychosomatics (Deutsche Gesellschaft für Psychiatrie und Psychotherapie, Psychosomatik und Nervenheilkunde, DGPPN) and were presented as a poster at the annual congress in 2018 (DGPPN Kongress 2018) in the session “brain imaging, neurophysiology, neuropsychology and neurobiology”:

Thomas C. Wegehaupt, Charsten Tischbirek, Arthur Konnerth; “Suppression of the acoustic startle response by cerebellar tremor”; DGPPN Kongress 2018.

Besides basic (clinical) neuroscience, additional research interests focus on clinical aspects of neurological disorders, e.g.:

Thomas C. Wegehaupt, Sriram Vundavalli, Sarah Cooper, Maria Leite, Jacqueline Palace, Leonora Fisniku; “Demographic, clinical and paraclinical features in a subgroup of patients with NMOSD”; Association of British Neurologists (ABN) Annual Meeting 2019.